SEMI-AMORPHOUS CARBON NITRIDE FILMS DERIVED FROM SOLUBLE POLYMERIC PRECURSORS: TOWARDS MULTIFUNCTIONAL ELECTROCHEMICAL COATINGS WITH ENHANCED STABILITY

Oleg Dubov

UNIVERSITAT ROVIRA i VIRGILI

Semi-amorphous carbon nitride films derived from soluble polymeric precursors: towards multifunctional electrochemical coatings with enhanced stability

OLEG DUBOV

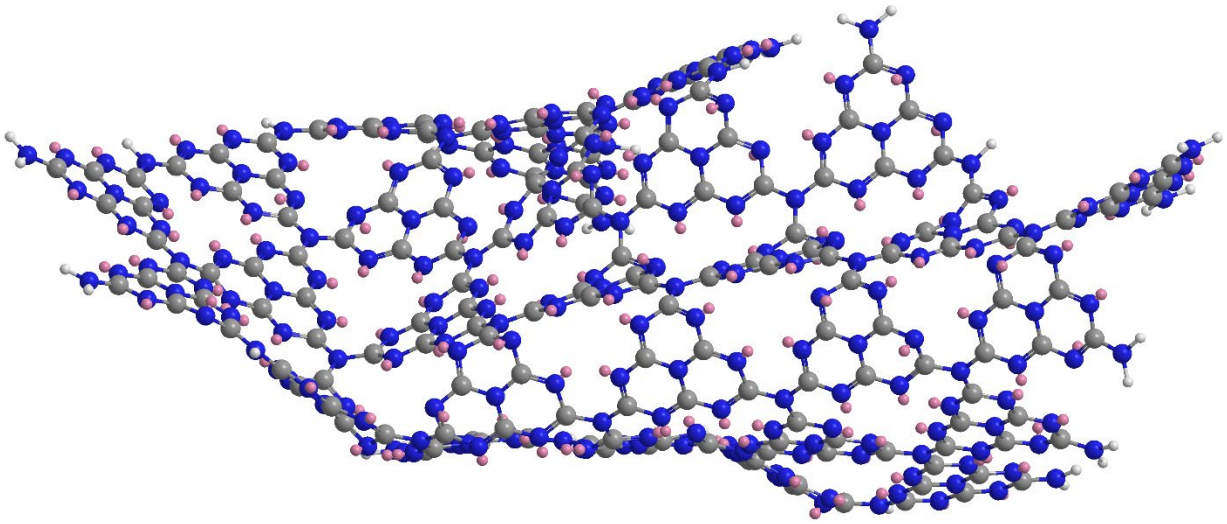

DOCTORAL THESIS

2022

UNIVERSITAT ROVIRA I VIRGILI
SEMI-AMORPHOUS CARBON NITRIDE FILMS DERIVED FROM SOLUBLE POLYMERIC PRECURSORS: TOWARDS MULTIFUNCTIONAL ELECTROCHEMICAL COATINGS WITH ENHANCED STABILITY
Oleg Dubov

DOCTORAL THESIS

Oleg Dubov

Supervised by:
Dr. Josep Font Capafons

Department of Chemical Engineering

UNIVERSITAT ROVIRA i VIRGILI

A Thesis submitted in partial fulfillment of the requirements of the degree of doctor from the Universitat Rovira i Virgili in the Chemical, Environmental and Process Engineering Program

This project has received funding from the European Union's Horizon 2020 research and innovation programme under the Marie Skłodowska-Curie grant agreement No. 713679 and from the Universitat Rovira i Virgili (URV).

Tarragona 2022

UNIVERSITAT ROVIRA I VIRGILI
SEMI-AMORPHOUS CARBON NITRIDE FILMS DERIVED FROM SOLUBLE POLYMERIC PRECURSORS: TOWARDS MULTIFUNCTIONAL ELECTROCHEMICAL COATINGS WITH ENHANCED STABILITY
Oleg Dubov

UNIVERSITAT ROVIRA i VIRGILI

Department of Chemical Engineering
University of Rovira i Virgili,
Avinguda Països Catalans, 26
43007, Tarragona, Spain.
Tel: +34-977-558506
Fax: +34-977-558544

FAIG CONSTAR que el present treball, titulat «Semi-amorphous carbon nitride films derived from soluble polymeric precursors: towards multifunctional electrochemical coatings with enhanced stability», que presenta Oleg Dubov per a l'obtenció del títol de Doctor per la Universitat Rovira i Virgili, ha estat realitzat sota la meva direcció al Departament d'Enginyeria Química i compleix els requeriments per poder optar a Menció Internacional.

HAGO CONSTAR que el presente trabajo, titulado "Semi-amorphous carbon nitride films derived from soluble polymeric precursores: towards multifunctional electrochemical coatings with enhanced stability", que presenta Oleg Dubov para la obtención del título de Doctor por la Universidad Rovira i Virgili, ha sido realizado bajo mi dirección en el Departamento de Ingeniería Química y cumple los requisitos para poder optar a Mención Internacional.

I STATE that the present work, entitled «Semi-amorphous carbon nitride films derived from soluble polymeric precursors: towards multifunctional electrochemical coatings with enhanced stability», presented by Oleg Dubov to obtain the degree of Doctor by the University Rovira i Virgili, has been carried out under my supervision at the Departament of Chemical Engineering.

Tarragona, January 10, 2022

El director / The supervisor

Dr. Josep Font Capafons

DEDICATION

This thesis work is dedicated to my wife, Inna, and my two lovely daughters, Daria and Varvara, who have been a constant source of support, encouragement and enjoyment during all the challenges of these intense years. I am truly thankful for having you in my life. This work is also dedicated to my mother, Lyudmila, who have always loved me unconditionally and whose good examples have taught me to work hard for the things that I aspire to achieve.

UNIVERSITAT ROVIRA I VIRGILI
SEMI-AMORPHOUS CARBON NITRIDE FILMS DERIVED FROM SOLUBLE POLYMERIC PRECURSORS: TOWARDS MULTIFUNCTIONAL ELECTROCHEMICAL COATINGS WITH ENHANCED STABILITY
Oleg Dubov

Acknowledgements

This thesis would not have been possible without the inspiration and support of a number of wonderful individuals — my thanks and appreciation to all of them for being part of this journey and making this thesis possible.

I owe my deepest gratitude to my supervisor Professor Josep Font Capafons. Without his enthusiasm, encouragement, support and continuous optimism this thesis would hardly have been completed. I express my warmest gratitude to Professor Frank Erich Stüber for prolific theoretical discussions on various topics.

I would like to gratefully acknowledge all the members of the PISET research group who support me and give me inestimable advice throughout the Ph.D. project development. It was a pleasure to work with you all. In particular, my special gratitude go to Mohammad Shaiful Alam Amin for fruitful methodological discussions and invaluable practical help.

I´m forever thankful to Dr. Alexey Shavel for introducing me to the world of electrochemistry and his continuous patient and friendly support.

My sincere thanks also go to the URV electronic microscopy team for their vital help, as well as Dr. Ramon Guerrero Grueso and Dr. Francesc Gispert Guirado for their attentive and professional help in materials characterization.

The patenting of the research results would not have been possible without the effective and professional help of the URV Valorization Unit (Fundació URV), with special thanks to Merche Carod Ceperuelo.

I would like to acknowledge the European Union's Horizon 2020 research and innovation program and the Marie Skłodowska-Curie association (grant agreement No. 713679) for the financial support to carry out my Ph.D. thesis. I am also indebted to the Grant TI2018-096467-B-I00 funded by MCIN/AEI/ 10.13039/501100011033 and by “ESF Investing in your future”.

Sumari

A l'electroquímica pràctica moderna, l'estabilitat de les capes superficials als elèctrodes actius és un dels problemes més importants en diversos processos industrials. La inevitable degradació dels elèctrodes és especialment important per a les transformacions catalítiques que tenen lloc a alts potencials d'oxidació, com les reaccions d'evolució d'oxigen i clor, la reacció de reducció d'oxigen, l'electro-oxidació de compostos orgànics en medis aquosos, etc. Les implementacions industrials de processos, que impliquen la formació electroquímica o el consum d'oxidants agressius, sovint es basen en l'ús de metalls nobles com a materials d'elèctrodes.

És important destacar que en molts casos els metalls nobles no es fan servir exclusivament per la seva estabilitat contra l'oxidació, sinó que representen un paper clau en la corresponent transformació com a catalitzadors eficients. Per tant, en els elèctrodes industrials clàssics sovint comparteixen dues funcions, treballant simultàniament com a catalitzadors i matrius d'elèctrodes resistents a l'oxidació. No obstant això, fins i tot en les situacions en què l'ús de metalls nobles es considera raonable a causa de les propietats catalítiques, la quantitat d'aquests materials escassos i costosos en la majoria de casos es podria reduir dràsticament. L'enfocament més actual per assolir aquest objectiu es basa en la implementació del metall catalític corresponent en forma de nanopartícules.

Tanmateix, el sistema catalític basat en nanopartícules sol requerir un suport conductor inert com a matriu estable, sobre la qual es dipositen les nanopartícules, separant així les funcions del material de la matriu i el component actiu. La integració d'aquests sistemes a la pràctica industrial, inclosos els casos d'elevada importància per a la propera transició energètica, com ara la indústria de les piles de combustible i la de producció d'H_2 per descomposició d'aigua, està dràsticament limitada per l'elecció restringida de materials de matriu conductors adequats.

Històricament, els òxids metàl·lics conductors suportats sobre metalls resistents a l'oxidació degut a les seves pròpies capes superficials d'òxid (per exemple, titani) s'han utilitzat típicament per a processos electroquímics en condicions molt oxidatius, com ara la producció d'hipoclorit. Aquests elèctrodes solen ser mecànicament robusts, estan limitats en les possibles formes geomètriques i, en general, no són porosos o tenen una porositat mínima, encara que aquestes limitacions no són crítiques per a les indústries clàssiques a les quals s'utilitzen. Els metalls nobles, en cas de la seva implementació, s'inclouen com a òxids al sistema d'òxids mixtos, i el recobriment de l'ànode TiO_2/RuO_2 (ORTA) és l'exemple més clàssic. També s'han utilitzat àmpliament sistemes d'òxids de metalls catalítics no preciosos, basats en Pb, Co, Ni i molts altres metalls de transició.

En els darrers anys, però, la demanda generada per les indústries electroquímiques nounades relacionades amb l'energia renovable ha conduit a un major interès en elèctrodes flexibles i fàcilment modelables amb una porositat extensa fins al nivell nanomètric i la corresponent superfície operativa alta. Així, les diferents formes de materials amb carboni s'han convertit en un nou punt d'atracció per a la ciència dels elèctrodes. Els suports més estudiats inclouen tela de carboni, feltre de carboni, escumes de carboni i diversos recobriments pirolítics carbonosos. També s'han investigat materials i compostos més sofisticats basats en nanotubs de carboni i fins i tot diamants. La combinació de paràmetres físics, químics i de procés permet que aquests materials superin enormement altres possibles candidats a la majoria de les aplicacions modernes.

Tot i l'atractiva conveniència industrial i econòmica dels materials de suport basats en carboni, la seva estabilitat oxidativa en la majoria dels casos és molt menor en comparació amb la resistència a l'oxidació dels metalls nobles i fins i tot els materials basats en òxids metàl·lics, que per aquesta raó encara es fan servir en processos que inclouen els oxidants més agressius.

Malgrat tot, dos tipus de materials pertanyents al grup de suports carbonosos representen una excepció a aquesta regla general: **els carbonis vitris** i els **nitrurs de carboni**.

Els anomenats **carbonis vitris**, produïts mitjançant piròlisi de polímers carbonosos fàcilment accessibles, tenen una estabilitat oxidativa exclusiva juntament amb una alta conductivitat i inactivitat química. Els elèctrodes de carboni vitri funcionen com a estàndard d'or en la investigació de l'electroquímica a causa de la combinació d'estabilitat i absència de propietats catalítiques pròpies. Tot i això, la seva aplicació industrial es limita a usos en què es prefereixen superfícies catalíticament inactives.

La raó principal d'això rau en el fet que el procés de piròlisi, que condueix a la formació de carboni vitri, requereix temperatures notablement altes (1000-3000 ºC). A més del cost òbviament elevat del material, resulta en la inviabilitat pràctica de la producció de compostos catalíticament actius que se'n deriven, a causa de la inestabilitat demostrada a temperatures elevades per gairebé totes les nanopartícules catalítiques i precursors moleculars dels catalitzadors. D'altra banda, l'aplicació de partícules o compostos moleculars sobre la superfície del suport de carboni vitri fabricat prèviament dóna com a resultat recobriments inestables a causa de l'adhesió feble típica per a la superfície llisa del material. La fragilitat i la dificultat de processament mecànic complica encara més l'ús pràctic. Tot i que s'han realitzat múltiples intents per limitar la temperatura de piròlisi, necessària per a la formació de carbonis vitris, encara es manté molt per sobre del llindar d'estabilitat de la majoria de les nanopartícules, que es troba al rang de 200 a 700 ºC.

Un altre grup de materials de la família del carboni, que es distingeix per la seva alta estabilitat oxidativa, els **nitrurs de carboni**, exhibeix la combinació de propietats que el situen gairebé a l'antípoda del carboni vitri.

Els nitrurs de carboni es produeixen típicament mitjançant piròlisi de melamina, diciandiamida, urea o alguns altres precursors rics en nitrogen. La temperatura de piròlisi, en contrast amb el carbó vitri, és força baixa, situant-se en el rang de 400 a 600 ^{o}C. El material resultant en el cas clàssic és una pols groga amb estructura cristallina imperfecta i superfície rugosa, que no es pot utilitzar directament com a material de matriu de suport.

Com a pedra angular de la present tesi, es va plantejar la hipòtesi de l'existència d'un nou membre de la família dels materials carbonosos, el nitrur de carboni vitri, que es podria produir mitjançant piròlisi de precursors polimèrics rics en nitrogen i retenir un alt contingut de nitrogen en la forma final. També es va suposar que el material així obtingut combinaria els beneficis del carboni vitri i el nitrur de carboni sense experimentar els seus inconvenients. Es va identificar que la formació d'una superfície llisa i mecànicament robusta va ser el resultat de que la matriu de polímer fos el precursor del material pirolític, per la qual cosa s'esperava que el nou material formés aquesta superfície. L'alt contingut de nitrogen, d'altra banda, es va associar amb una temperatura de piròlisi baixa, que es va identificar com a característica del nou material. Com a resultat, s'esperava un producte generador de recobriments amb la capacitat de formar compostos amb nanopartícules i complexos amb ions de metalls de transició catalíticament actius.

La primera publicació, que representa la base de la present tesi, tracta sobre l'obtenció amb èxit d'aquesta nova classe de materials mitjançant la piròlisi de tres nous polímers triazínics, també sintetitzats durant aquest projecte. Aquests tres precursors polimèrics pertanyen a una classe insuficientment estudiada de polímers lineals basats en triazina i demostren una excel·lent solubilitat en diversos dissolvents orgànics, propietats de formació de pel·lícula i una tendència a retenir grans quantitats de nitrogen durant la seva piròlisi. S'han elaborat mètodes eficaços per a la fabricació de revestiments de nitrur de carboni a partir de solucions de N, N-dimetilacetamida dels polímers precursors. Es va demostrar que els materials de recobriment obtinguts així tenen una alta robustesa mecànica i requereixen baixes temperatures de piròlisi, com s'esperava inicialment. Finalment, va demostrar una estabilitat electroquímica extraordinàriament alta de les pel·lícules recollides en polaritzacions anòdiques i catòdiques elevades.

Els resultats han estat patentats i publicats posteriorment al *Journal of Materials Science. E*ls principals resultats obtinguts a la publicació formen part del Capítol 2 del present manuscrit.

La segona línia de recerca dins l'estructura de la tesi es va dedicar a la fabricació de recobriments catalíticament actius a partir de precursors polimèrics prèviament desenvolupats. En primer lloc, es va descobrir que les solucions amb aigua dels precursors podien formasr-se amb èxit en medis alcalins. L'aplicació de solucions de polímer a base d'aigua sobre el substrat de tela de carboni va resultar en deposició de recobriments porosos de nitrur de carboni. L'ús de tintes de polímer precursor que contenen nanopols de carboni va permetre obtenir recobriments compostos amb porositat controlada.

En segon lloc, es va proposar la coordinació de Ni^{2+} al medi aquós amb els polímers precursors com un mètode per a la introducció de centres de metalls de transició catalíticament actius en els recobriments resultants. S'ha demostrat que els recobriments carregats amb Ni sobre elèctrodes de tela de carboni tenen una excel·lent activitat i una estabilitat perllongada com a materials actius per a la reacció de despreniment d'oxigen.

Els resultats estan sota consideració a in *Angewandte Chemie edició internacional*.

L'última part associada al tema de la tesi va sorgir de la necessitat de mesurar els paràmetres electroquímics dels elèctrodes que han estat fabricats en les condicions d'accés intermitent a un potenciòstat adequat a les necessitats, limitat durant un llarg període a causa del confinamentrelacionat amb la pandèmia del COVID-19. É sper això, que es va desenvolupar un esquema de mesura simple, basat en un microxip amplificador operacional, i es va construir el dispositiu corresponent. Juntament amb els programes escrits en llenguatges *Arduino IDE* i *Python*, el sistema va permetre organitzar mesuraments precisos i continus d'acord amb les nostres necessitats.

És interessant que la configuració resultant es pot fer servir de manera eficient també per organitzar les pràctiques d'estudiants amb una experiència d'aprenentatge pràctica més profunda i inversions mínimes. L'article corresponent està sota consideració per a la seva publicació al *Journal of Chemical Education*.

UNIVERSITAT ROVIRA I VIRGILI
SEMI-AMORPHOUS CARBON NITRIDE FILMS DERIVED FROM SOLUBLE POLYMERIC PRECURSORS: TOWARDS MULTIFUNCTIONAL ELECTROCHEMICAL COATINGS WITH ENHANCED STABILITY
Oleg Dubov

Summary

In the modern practical electrochemistry, the stability of active electrode layers is one of the most critical issues in miscellaneous industrial processes. Inevitable degradation of electrodes is especially important for catalytic transformations taking place at high oxidative potentials, such as oxygen and chlorine evolution reaction, oxygen reduction reaction, electrooxidation of organic compounds in aqueous media, etc. Industrial implementations of processes, involving electrochemical formation or consumption of aggressive oxidants, are often based on the use of noble metals as electrode materials.

It is important to emphasize that, in many cases, noble metals are not used exclusively for their oxidative stability, but play a key role in the corresponding transformation as efficient catalysts. Thus, in classical industrial electrodes they often share two roles, working simultaneously as catalysts and oxidation-resistant electrode matrices. However, even in the situations when the use of noble metals seems reasonable due to their catalytic properties, the quantity of these scarce and costly materials can often be drastically reduced. The most contemporary approach to achieve this goal is based on the implementation of the corresponding catalytic metal in the form of nanoparticles.

Nanoparticle-based catalytic systems, however, usually require an inert conducting support as stable matrix, on which the nanoparticles are deposited, thus separating the roles of the matrix material and the active component.

The integration of such systems into industrial practice, including the cases of tremendous importance for the upcoming energy transition – the industry of fuel cells and H_2 production by water splitting, is drastically constrained by limited choice of appropriate conducting matrix materials.

Historically, conducting metal oxides supported over valve metals (e.g. titanium) have typically been used for harsh electrochemical processes, such as hypochlorite production. These electrodes are usually mechanically robust, limited in their possible geometrical shapes and typically are non-porous or have limited porosity – although these limitations are non-critical for the classical industries they are used for. Noble metals, in case of their implementation, are included as oxides in the mixed oxides system, TiO_2/RuO_2 (ORTA) anode coating being the most classical example. Non-precious catalytic metal oxide systems, based on Pb, Co, Ni and many other transition metals, have also been extensively used.

In the recent years, however, the demand generated by newborn electrochemical industries related to green energy, led to increased interest in flexible and easily shapeable electrodes with extensive porosity down to the nanometer level and corresponding high operative surface. Different forms of carbon-based materials

became a new hotspot in the electrode science. The most studied supports included carbon cloth, carbon felt, carbon foams and various pyrolytic carbonaceous coatings. More sophisticated materials and composites based on carbon nanotubes and even diamond have also been investigated. The combination of physical, chemical and process parameters allows these materials to outperform massively over other possible candidates in the majority of modern-day applications.

However, in spite of appealing industrial and economic convenience of carbon-based support materials, their oxidative stability in most cases is much lower compared with the resistance to oxidation of noble metals and even metal oxide systems, which for this reason are still used while dealing with the most challenging oxidants.

Nevertheless, two families of materials belonging to the group of carbon-based supports represent an exception to this general rule – **glassy carbons** and **carbon nitrides**.

The so-called **glassy (or vitreous) carbons**, produced by means of pyrolysis of cheap carbonaceous polymers, possess an exclusive oxidative stability together with high conductivity and chemical inertness. Glassy carbon electrodes perform as a golden standard in research electrochemistry due to combination of stability and absence of own catalytic properties. Their industrial application, however, is limited to the applications where catalytically inactive surfaces are preferred.

The main reason for this lies in the fact that the pyrolysis process, leading to the formation of vitreous carbon, requires noticeably high temperatures (1000 to 3000 ºC). In addition to obviously elevated cost of the material, it results in practical infeasibility of production of catalytically active composites derived therefrom – due to instability demonstrated at elevated temperatures by nearly all catalytic nanoparticles and molecular precursors to catalysts. On the other hand, application of particles or molecular compounds on the surface of preliminary fabricated vitreous carbon support results in unstable coatings due to weak adhesion typical for smooth surface of the material. Its brittleness and difficulty of mechanical processing further complicates the practical use.

Although multiple attempts to limit the pyrolysis temperature, required for glassy carbons formation, have been undertaken, it still remains far above the stability threshold of most nanoparticles, which lies in the range from 200 to 700 ºC.

Another group of material of the carbonaceous family, distinguished for its high oxidative stability, **carbon nitrides**, exhibits the combination of properties making it nearly antipodean to vitreous carbon.

Carbon nitrides are typically produced by means of pyrolysis of melamine, dicyandiamide, urea or some other nitrogen-rich precursors. The pyrolysis temperature,

in contrast with glassy carbon, is rather low, laying in the 400 to 600 ºC range. Resulting material in the classic case is a light yellow powder with imperfect crystalline structure and rough surface, which cannot be directly used as a support matrix material.

As a cornerstone for the present thesis, it was hypothesized the existence of a new member of the carbonaceous materials family, **glassy carbon nitride**, that could be produced by means of pyrolysis of nitrogen-rich polymeric precursors and retain high nitrogen content in the final form. It was also supposed that the material thus obtained would combine the benefits of vitreous carbons and carbon nitride without having their drawbacks. Formation of smooth and mechanically robust surface was identified to be the result of polymer matrix being the precursor for the pyrolytic material, for which reason the new material was expected to form a surface with similar properties. High nitrogen content, on the other hand, was associated with low pyrolysis temperature, which was identified to be characteristic for the new material. As a result, a coating-forming product with the ability to form composites with nanoparticles and complexes with catalytically active transition metals ions, was expected.

The first publication, forming the basis of the present thesis, reports the successful obtainment of this new class of materials by means of pyrolysis of three novel triazinic polymers, also synthesized in this work. All three polymeric precursors belong to insufficiently studied class of linear triazine-based polymers. They demonstrate outstanding solubility in several organic solvents, film-forming properties and a tendency to retain high amounts of nitrogen at pyrolysis. Efficient methods for fabrication of carbon nitride coatings from N,N-dimethylacetamide solutions of the precursor polymers have been elaborated. It was demonstrated that coating materials obtained in this way possesses high mechanical robustness and requires low pyrolysis temperatures, as it have been previously expected. Finally, outstandingly high electrochemical stability of the annealed films in high anodic and cathodic polarizations was shown.

The results were patented and subsequently published in the *Journal of Materials Science*. The main results obtained in the publication form part of Chapter 2 of the present manuscript.

The second research project within the scope of the thesis was devoted to the fabrication of catalytically active coatings on the basis of previously developed polymer precursors. First, it was found that these water-based solutions of the precursors could successfully be produced in alkaline media. Application of water-based polymer solutions on carbon cloth substrate resulted in depositing porous carbon nitride coatings. Using precursor polymer inks containing carbon nanopowder allowed obtaining composite coatings with controlled porosity.

Secondly, coordination of Ni^{2+} in the aqueous media with the precursor polymers was proposed as a method for introduction of catalytically active transition metal centers into the resulting coatings. Ni-loaded coatings on carbon cloth electrodes have been demonstrated to possess excellent activity and prolonged stability as active materials for oxygen evolution reaction.

The results are under consideration in *Angewandte Chemie international edition*.

The last project associated with the topic of the thesis arose from the necessity to measure the electrochemical parameters of the electrodes that have been fabricated in the conditions of intermittent access to research-class potentiostat due to COVID-19 related lockdown. A simple measurement scheme, based on one operational amplifier microchip, was developed and the corresponding device build. Together with programs written in Arduino IDE and Python languages, the system allowed to organize accurate and continuous measurements according to our needs.

The resulting setup can be efficiently used for organizing student practicums with deepen hand-on learning experience and minimum investments.

The corresponding article is under consideration for publication in the *Journal of Chemical Education*.

UNIVERSITAT ROVIRA I VIRGILI
SEMI-AMORPHOUS CARBON NITRIDE FILMS DERIVED FROM SOLUBLE POLYMERIC PRECURSORS: TOWARDS MULTIFUNCTIONAL ELECTROCHEMICAL COATINGS WITH ENHANCED STABILITY
Oleg Dubov

Resumen

En la moderna electroquímica práctica, la estabilidad de las capas superficiales de electrodos activos es uno de los problemas más importantes en diversos procesos industriales. La inevitable degradación de los electrodos es especialmente importante para las transformaciones catalíticas que tienen lugar a altos potenciales de oxidación, como las reacciones de evolución de oxígeno y cloro, la reducción de oxígeno, la electro-oxidación de compuestos orgánicos en medios acuosos, etc. Las implementaciones industriales de procesos, que implican la formación electroquímica o el consumo de oxidantes agresivos, a menudo se basan en el uso de metales nobles como materiales de los electrodos.

Es importante destacar que en muchos casos los metales nobles no se utilizan exclusivamente por su estabilidad contra oxidación, sino que representan un papel clave como catalizadores eficientes en la correspondiente transformación. Por lo tanto, en los electrodos industriales clásicos, a menudo comparten dos funciones, trabajando simultáneamente como catalizadores y matrices de electrodos resistentes a la oxidación. Sin embargo, incluso en las situaciones en las que el uso de metales nobles se considera razonable debido a sus propiedades catalíticas, la cantidad de estas materias escasos y costosos en la mayoría de casos podría reducirse drásticamente. El enfoque más actual para lograr este objetivo se basa en la implementación del correspondiente metal catalítico en forma de nanopartículas.Sin embargo, el sistema catalítico basado en nanopartículas suele requerir un soporte conductor inerte como matriz estable, sobre la cual se depositan las nanopartículas, separando así las funciones del material de la matriz y el componente activo.

La integración de tales sistemas en la práctica industrial, incluidos los casos de elevada importancia para la próxima transición energética, como la industria de las pilas de combustible y la de producción de H_2 por descomposición de agua, está drásticamente limitada por la elección restringida de materiales de matriz conductores adecuados.

Históricamente, los óxidos metálicos conductores depositados sobre metales resistentes a la oxidación debido a sus propias capas de óxido superficiales (por ejemplo, titanio) se han utilizado típicamente para procesos electroquímicos en condiciones muy oxidativos, como la producción de hipoclorito. Estos electrodos suelen ser mecánicamente robustos, pero están limitados en sus posibles formas geométricas y, por lo general, no son porosos o tienen una porosidad mínima, aunque estas limitaciones no son críticas para las industrias clásicas para las que se utilizan. Los metales nobles, en caso de su implementación, se incluyen como óxidos en el sistema de óxidos mixtos, siendo el recubrimiento del ánodo TiO_2 / RuO_2 (ORTA) el ejemplo más clásico. También se han

utilizado ampliamente sistemas de óxidos de metales catalíticos no preciosos, basados en Pb, Co, Ni y muchos otros metales de transición.

En los últimos años, sin embargo, la demanda generada por las industrias electroquímicas recién nacidas relacionadas con la energía renovable ha conducido a un mayor interés en electrodos flexibles y fácilmente moldeables con una porosidad extensa hasta el nivel nanométrico y la correspondiente altamente operativa superficie. Las diferentes formas de materiales a base de carbono se convirtieron en un nuevo punto de atracción para la ciencia de los electrodos. Los soportes más estudiados incluyeron tela de carbono, fieltro de carbono, espumas de carbono y varios recubrimientos pirolíticos carbonosos. También se han investigado materiales y compuestos más sofisticados basados en nanotubos de carbono e incluso diamantes. La combinación de parámetros físicos, químicos y de proceso permite que estos materiales superen enormemente a otros posibles candidatos en la mayoría de las aplicaciones modernas.

Sin embargo, a pesar de la atractiva conveniencia industrial y económica de los materiales de soporte basados en carbono, su estabilidad oxidativa en la mayoría de los casos es mucho menor en comparación con la resistencia a la oxidación de los metales nobles e incluso los materiales basados en óxidos metálicos, que por esta razón todavía se utilizan en procesos que incluyen los oxidantes más agresivos.

De todas formas, dos tipos de materiales pertenecientes al grupo de soportes carbonosos representan una excepción a esta regla general: **los carbonos vítreos** y **los nitruros de carbono**.

Los llamados **carbonos vítreos**, producidos mediante pirólisis de polímeros carbonosos fácilmente disponibles, poseen una estabilidad oxidativa exclusiva junto con una alta conductividad e inactividad química. Los electrodos de carbono vítreo funcionan como un estándar de oro en la investigación de la electroquímica debido a la combinación de estabilidad y ausencia de propiedades catalíticas propias. Sin embargo, su aplicación industrial se limita a las aplicaciones en las que se prefieren superficies catalíticamente inactivas.

La principal razón de esto radica en el hecho de que el proceso de pirólisis, que conduce a la formación de carbono vítreo, requiere temperaturas notablemente altas (1000 a 3000 ºC). Además del costo obviamente elevado del material, resulta una inviabilidad práctica de la producción de compuestos catalíticamente activos derivados del mismo, con motivo de una inestabilidad demostrada a temperaturas elevadas para casi todas las nanopartículas catalíticas y precursores moleculares de los catalizadores. Por otro lado, la aplicación de partículas o compuestos moleculares sobre la superficie del soporte de carbono vítreo fabricado previamente da como resultado recubrimientos inestables

debido a la adhesión débil típica para la superficie lisa del material. Su fragilidad y dificultad de procesamiento mecánico complica aún más el uso práctico.

Asimismo, aunque se han realizado múltiples intentos para limitar la temperatura de pirólisis, necesaria para la formación de carbonos vítreos, todavía se mantiene muy por encima del umbral de estabilidad de la mayoría de las nanopartículas, que se encuentra en el rango de 200 a 700 ºC.

Otro grupo de materiales de la familia carbonácea, que se distingue por su alta estabilidad oxidativa, los **nitruros de carbono**, exhibe la combinación de propiedades que lo sitúan casi en las antípodas del carbono vítreo.

Los nitruros de carbono se producen típicamente mediante pirólisis de melamina, diciandiamida, urea o algunos otros precursores ricos en nitrógeno. La temperatura de pirólisis, en contraste con el carbón vítreo, es bastante baja, situándose en el rango de 400 a 600 ºC. El material resultante en el caso clásico es un polvo amarillo con estructura cristalina imperfecta y superficie rugosa, que no puede usarse directamente como material de matriz de soporte.

Como piedra angular de la presente tesis, se planteó la hipótesis de la existencia de un nuevo miembro de la familia de los materiales carbonosos, el nitruro de carbono vítreo, que podría producirse mediante pirólisis de precursores poliméricos ricos en nitrógeno y retener al mismo tiempo el alto contenido de nitrógeno en su forma final. También se supuso que el material así obtenido combinaría los beneficios del carbono vítreo y el nitruro de carbono sin tener sus inconvenientes. Se identificó que la formación de una superficie lisa y mecánicamente robusta fue el resultado de que la matriz de polímero es el precursor del material pirolítico, por lo que se esperaba que el nuevo material formara dicha superficie. El alto contenido de nitrógeno, por otro lado, se asoció con una temperatura de pirólisis baja, que se identificó como característica del nuevo material. Como resultado, se esperaba un producto generador de recubrimientos con la capacidad de formar compuestos con nanopartículas y complejos con iones de metales de transición catalíticamente activos.

La primera publicación, que forma la base de la presente tesis, informa sobre la obtención exitosa de esta nueva clase de materiales mediante la pirólisis de tres novedosos polímeros triazínicos, también sintetizados durante este proyecto. Estos tres precursores poliméricos pertenecen a una clase insuficientemente estudiada de polímeros lineales basados en triazina y demuestran una excelente solubilidad en varios disolventes orgánicos, propiedades de formación de película y una tendencia a retener grandes cantidades de nitrógeno en su pirólisis. Para ello, se han elaborado métodos eficaces para la fabricación de revestimientos de nitruro de carbono a partir de soluciones de N, N-dimetilacetamida de los polímeros precursores. Se demostró que los

materiales de recubrimiento obtenidos de esta manera poseen una alta robustez mecánica y requieren bajas temperaturas de pirólisis, como se esperaba anteriormente. Finalmente, se demostró una estabilidad electroquímica extraordinariamente grande de las películas recocidas en polarizaciones anódicas y catódicas elevadas.

Los resultados fueron patentados y publicados en el *Journal of Materials Science*. Los principales resultados obtenidos en la publicación forman parte del Capítulo 2 de la presente memoria.

El segundo tema de investigación dentro la estructura de la tesis se dedicó a la preparación de recubrimientos catalíticamente activos a partir de precursores poliméricos previamente desarrollados. En primer lugar, se descubrió que las soluciones acuosas de los precursores podían prepararse con éxito en medios alcalinos. La aplicación de soluciones acuosas de polímero sobre el sustrato de tela de carbono resultó en deposición de recubrimientos porosos de nitruro de carbono. El uso de tintas de polímero precursor que contenían nanopolvo de carbono permitió obtener recubrimientos compuestos de porosidad controlada.

En segundo lugar, se propuso la coordinación de Ni^{2+} en el medio acuoso con los polímeros precursores como un método para la introducción de centros con metales de transición catalíticamente activos en los recubrimientos resultantes. Se ha demostrado que los recubrimientos cargados con Ni sobre electrodos de tela de carbono poseen una excelente actividad y una estabilidad prolongada como materiales activos para la reacción de desprendimiento de oxígeno.

Los resultados están bajo consideración en *Angewandte Chemie edición internacional.*

El último proyecto asociado al tema de la tesis surgió de la necesidad de medir los parámetros electroquímicos de los electrodos que han sido fabricados en las condiciones de acceso intermitente a un potenciostato de calidad de investigación debido al confinamiento relacionado con la pandemia de COVID-19. Se desarrolló un esquema de medición simple, basado en un microchip amplificador operacional, y se construyó el dispositivo correspondiente. Junto con los programas escritos en lenguajes Arduino IDE y Python, el sistema permitió realizar mediciones precisas y continuas. La configuración resultante se puede utilizar también de manera eficiente para organizar prácticas de los estudiantes, con una experiencia de aprendizaje práctica más profunda e inversiones mínimas.

El artículo correspondiente está bajo consideración para su publicación en *Journal of Chemical Education*.

UNIVERSITAT ROVIRA I VIRGILI
SEMI-AMORPHOUS CARBON NITRIDE FILMS DERIVED FROM SOLUBLE POLYMERIC PRECURSORS: TOWARDS MULTIFUNCTIONAL ELECTROCHEMICAL COATINGS WITH ENHANCED STABILITY
Oleg Dubov

LIST OF CONTENTS

Chapter 1. Introduction

Chapter 2. Synthesis of polymeric precursors, fabrication of flexible carbon nitride films and their characterization as electrochemically stable coatings

Chapter 3. Fabrication of nanoporous nickel-coordinated carbon nitride coatings from aqueous solutions of poly(CYA-Cl-AMTAZ) Ni

UNIVERSITAT ROVIRA I VIRGILI
SEMI-AMORPHOUS CARBON NITRIDE FILMS DERIVED FROM SOLUBLE POLYMERIC PRECURSORS: TOWARDS MULTIFUNCTIONAL ELECTROCHEMICAL COATINGS WITH ENHANCED STABILITY
Oleg Dubov

Chapter 1

Introduction

The first chapter of this thesis presents general considerations regarding electrochemical stability of carbonaceous electrodes and describes the spectrum of promising electrode binding materials, comparing their benefits and drawbacks from the point of view of their applicability for fabrication of coatings with high hydrophilicity, high electrical conductivity and high stability in harsh oxidative conditions.

1.1. Carbon-based electrodes: general considerations

The modern-day green energy revolution generates an extensive demand for electrode materials possessing novel or greatly improved characteristics, with fuel cells industry being the leading area where new approaches arise. According to Majlan et al [1], high electrical conductivity, porosity, easy compatibility with contemporary nanoparticle-based catalysts, low critical and costly materials consumption, good mechanical properties is the basic list of prerequisites to an industrially viable electrode support on the example of fuel cells industry. Carbon-based materials attract considerable scientific attention due to good conformance to the majority of these requirements [1]. Recent advancements in electrode research showcase that the cell performance in direct methanol fuel cells is essentially governed by carbon-based support materials as they strongly influence the performance, stability, and efficiency of the electrocatalysts, amalgamated with the support [2]. The group of especial interest for the practical implementation includes soft carbon-based materials: carbon cloth and carbon felt, characterized in addition to the above mentioned general benefits of carbonaceous materials by flexibility, easy processability and availability of numerous applicable post-modification methods [3].

The energy applications of carbon felt-based-electrodes are intensively studied and practically implemented in various fields in addition to classical fuel cells: water-splitting electrolyzers, vanadium redox flow batteries, microbial fuel cells, biofuel cells, capacitors, solar cells and lithium ion batteries. In the field of wastewater treatment, an important process for remediating waters containing biorefractory pollutants is electro-Fenton process, also often relying on soft carbon-based materials as electrode support where the oxidation of organic contaminants is conducted [3].

It is important to emphasize that carbon-based electrodes, including soft carbonaceous materials like carbon felt and carbon cloth, typically do not exhibit any specific catalytic activity, thus being «electrochemically innocent» matrix support materials. A number of various approaches for electrodes modification in order to render them with specific redox properties has been developed.

In fact, however, all these approaches can be split into two main categories [1]:

1. Organizing the interaction of (usually) nanoparticle-based active component and carbon-based electrode material in a mechanical way, by means of physically pressing together the electrode with another surface (usually ion-exchange membrane) with previously applied catalytic ink.

2. Implementing a specific, usually polymeric, binder material in order to attach the particles of catalyst to the electrode surface or create particle-based porous composite.

1.2. Electrode binders: existing solutions and their limitations

Most typically, practically implemented electrodes are represented by polymer-bound composites integrating catalytically active species on the surface or in the bulk of composite electrode materials. As reported by Narayanasamy et al. [4] on the example of microbial fuel cells, nitrogen- and fluorine-containing polymers, such as polyacrylonitrile (PAN), polyaniline (PANI), polytetrafluoroethylene (PTFE), polydopamine (PDA) and polyacrylamide (PAM), have been identified as potential candidates for bulk or surface modification in the presence of redox active species.

However, for electrodes implemented in high polarization anodic regimes and/or in contact with aggressive oxidants like oxygen, peroxides or chloride, one outstandingly important characteristics of the material becomes exceedingly critical: the ability to withstand oxidatively harsh working conditions.

Most non-fluorinated binder polymers undergo oxidation at high anode potentials, resulting in rapid electrode deterioration, as it was demonstrated by Haddadi-Asl et al [5]. Due to this well-known effect, much more stable fluorine-containing polymers, PTFE and PVDF being the simplest examples, are often used as electrode binders and catalyst particles adhesives in the most critical applications, including redox-flow batteries electrodes [6]. Electrically insulating nature of these binders leads to reduced overall conductivity of resulting electrodes, thus limiting the possible concentration of the polymer in the composite mixture. To some extent, this issue can be addressed by means of adding to the composites nano-sized forms of carbon such as nanotubes, which reduces the required concentration of the polymer for the target conductivity and mechanical strength level due to nano-scale mesh formation [6].

A more important contradiction comes out when hydrophilicity and chemical resistance of the binder polymer should be combined. In some cases, fuel cells and metal air batteries cathodes being the classic examples, it is prerequisite for the electrode to retain hydrophobic properties throughout the lifecycle of the device in order to be able to transport gaseous oxygen or air flow through the pores of the material. For such applications, the intrinsically hydrophobic nature of PTFE, PVDF and many other fluorinated polymers is beneficial and intensively used to this end [7, 8]. Albeit, for the majority of other applications where porous electrodes are immersed in aqueous electrolyte, hydrophilicity is required. Surprisingly, only one polymeric binder massively available in the contemporary electrochemical practice is characterized by both by impeccable chemical stability and low contact angles – Nafion ®.

Despite its high cost and poor resistance to heating, Nafion ® has been used for decades as binder for classic porous carbon paste-based electrodes fabrication [9] and, more recently, as stabilizer and adhesive component for cast deposition of nanoparticle-based

inks on carbon-based surfaces [10, 11]. The popularity of the material is not deteriorated even by the proven fact that it partially hinders the surface of many nanoparticles, resulting in decreased catalytic activity of the composite compared to bare nanoparticles suspension [12].

Yet another important limitation, extremely critical for Nafion ® and, to a lesser extent, for other fluorinated and non-fluorinated binder polymers, is pour thermal stability. In the Nafion ® case, the electric conductivity of the material is based on proton transfer in hydrated polymer gel, so the operational temperature limit is set by water boiling point at pressure of the cell, although thermal decomposition only starts above 280º C [13]. For PTFE case, the decomposition starts above 250º C. Only PVDF-based composites are able to continuously withstand temperatures above 400 ºC [15].

It can be concluded that no binder materials that would combine high electrical conductivity, hydrophilicity, thermal and oxidative stability and good compatibility with carbon-based materials and nanoparticles, have been previously reported, while only one product (Nafion ®) combines all these properties with the exception of thermal stability and with conductivity being based exclusively on ionic and not electronic transfer.

This obvious gap in the spectrum of available binders critically limits the development of fuel cells and other electrochemical devices with high (over 300 ºC) operational temperatures, believed to represent an important step forward towards higher power densities in electrochemical power generation and carbon capture [16, 17].

The fundamental issue in the search of new polymer binders can be reflected as following: high chemical and thermal endurance is traditionally achieved in polymer technology by means of chain fluorination, while fluorinated polymers are naturally hydrophobic [18]. Although hydrophilization of fluoro-polymers is possible, it is achieved in difficult to obtain costly structures, combining fluorinated and sulfoacid functionalities (Nafion ®) [19].

This problem can be solved by screening as potential binders other (non-fluorinated) classes of oxidatively stable macromolecules with intrinsic hydrophilicity. Among non-fluorinated structures, the combination of high thermal endurance with resistance against oxidants is often found in aromatic structures with high heteroatoms content: aromatic polyacids, polyamides, nitrogen-rich aromatic heterocycles [20]. Out of these group of materials, three potential candidate materials have been identified: graphene oxide, polyanilines and triazine-based polymers. They have been selected due to the presence of an additional property of intrinsic conductivity or semiconductivity, greatly desirable for an electrode binder. The benefits and drawbacks of these potential candidates are commented below.

1.3. Graphene oxide: high costs and limited overall hydrophilicity

Graphene oxide cannot be considered a polymeric material in the strict sense. However, high molecular weight of graphene oxide particles, excellent film-forming capability and high viscosity of its aqueous solutions due to intensive hydrogen bonding interactions makes it comparable with some classic polymeric binders and promote intensive scientific interest to implement it for obtaining various nanocomposites [21]. Graphene oxide is most typically obtained by means of oxidation of graphite with strong oxidants such as potassium permanganate in massive excess over equivalent quantity in hot highly acidic media [21]. Relatively high cost of permanganate and dangers of manipulating its highly concentrated solutions at high temperatures stimulate the search for milder and cheaper oxidants with nitric acid being intensively studied in the recent years [22]. Another approach consists in finding oxidants that would not require big equivalent excess over graphite to run the process, with ferrate recently shown to drastically reduce oxidative chemicals consumption [23]. Howbeit, existing industrial solutions for graphene oxide synthesis still require huge amounts of aggressive and dangerous chemicals and long processing times, which results in highly elevated costs of graphene oxide [24].

Another important limitation of graphene oxide as binder material is linked with the mechanism of its thermal decomposition. During heating, graphene oxide films loose oxygen and water and undergo transformation into graphene-based carbonaceous material with irregular structure [25]. Due to low oxygen content in the final annealed material, it completely loses the hydrophilic nature of the pristine graphene oxide, resulting from the presence of carboxylic groups, and becomes hydrophobic [26]. Although this issue can be addressed by means of chemical reduction of graphene oxide in thoroughly controlled conditions to achieve only partial loss of oxygen-containing groups [27]; or by means of blending graphene oxide with nanoparticles with high water affinity [28], these approaches cannot be expected to result in highly hydrophilic coatings.

In addition, oxygen-containing carbonaceous materials when applied as cathodes in electrochemical systems are well known to demonstrate tendency to reduce oxygen following the 2-electrone pathway, with corresponding generation of peroxide and hydroxyl radicals [29, 30]. Although in some application beneficial (for instance, for decomposition of recalcitrant organic compounds [28], in many practical cases this behavior results in quick electrode deterioration [30].

With all the discussed issues of graphene oxide as conductive electrode binder taken into account, it can be concluded that, although being extensively studied to this end, it does not fulfill all the prerequisite requirements for effective binder materials.

1.4. Polyanilines: high conductivity with moderate stability

Polyanilines belong to the group of conductive polymers, materials with outstanding and yet only partially discovered industrial potential, although they represent the eldest example of conducting polymers. Polyanilines are highly conductive in their doped form, demonstrate excellent affinity to water, can form composite materials and are synthesized by means of simple methods and from widely available source materials [31]. Although many other conducting polymers have been synthesized, in this topic only polyanilines are discussed due to their improved (over other widely used conductive polymers) oxidation stability and easiness of synthesis.

In the same time, non-solubility in all common solvents is an important drawback of polyanilines. Coatings based on polyanilines are well-known, including composite coatings incorporating nanoparticles, although are typically produced by means of electrooxidation of aniline or its derivatives [32], chemical deposition involving rapid chemicals mixing [33] or in the form of paints by using a complimentary binder [34]. According to the analyzed literature, no method for solution-based coating formation based exclusively on conducting polymers without complimentary adhesive additives has been elaborated.

The main impediment for the efficient use of polyanilines as electrochemical coatings and binders for harsh conditions is related, however, to their insufficient chemical and electrochemical stability in oxidizing media. Stejskal et al [35] have demonstrated that immersion in the hydrogen peroxide mixture with sulfuric acid, a widely used strong oxidant system, resulted in decomposition of 70% polymer mass. Electrochemical anodic degradation of polyanilines has also been investigated by A. Malinauskas [36], who showed a sharp increase in degradation rate process at anode potentials exceeding 0.9 V.

Although it seems very likely that conductive polymers with outstanding electrochemical resistance can be synthesized based on substituted analogs of polyaniline or other conductive polymers, it should be concluded that at the moment the basic conductive polymers structures cannot be considered stable enough to be implemented as stable coatings.

The insolubility of conducting polymers and corresponding difficulty of industrial-scale coatings fabrication further aggravates the problem. Thus, polyanilines cannot be viewed as viable candidates for application in electrode coatings in aggressive anodic regimes.

1.5. Triazines and carbon nitrides: an overlooked alternative?

Surprisingly, according to our knowledge, triazine-based polymers, an important class of oxidatively stable polymeric structures, has never been studied as possible polymeric binders, although they combine all the previously listed properties prerequisite for prosperous electrode surface materials.

Stability to oxidation is a well-known characteristic of nitrogen-containing aromatic heterocycles when compared with benzene ring and derives primarily from delocalization of lone electron pairs of nitrogen, «pumping» the system with excessive electron density [37]. Thus, triazine and heptazine moieties, aromatic structures containing high amount of nitrogen, can be expected to possess high oxidation stability.

This is confirmed by multiple direct experiments for both monomeric and polymeric structures. For instance, Dbira et al. [38] have shown that ring nitrogen atoms of triazine system in nitrogen-based pesticides are not oxidized even in the harsh conditions of photo-Fenton process. Gabriel da Silva et al [39] have demonstrated that in direct oxidation initiated by hydroxyl radical, HO• addition at a carbon ring site proceeds with the largest known barrier for addition to an unsaturated carbon (41 kjoule mol^{-1}). In the same work, easy abstraction of a hydrogen atom in s-triazine by HO•, (barrier of only 13.8 kjoule mol^{-1}), has been shown.

Thus, it can be expected that triazine-based structures without hydrogen substituents (layered or crosslinked linear polymers) should demonstrate high stability to oxidation.

Polymeric systems, completely based on triazine- or heptazine moieties and characterized by low hydrogen content are typically referred to as carbon nitrides. The oxidational stability of carbon nitrides is well-known, the material is intensively used as catalyst support in numerous oxidation reactions, including the processes with highest oxidation potentials: Fenton and photo-Fenton oxidation reactions [40, 41, 42].

Furthermore, carbon nitride is highly hydrophilic due to polar C-N interactions [43] and is effectively used as wettable support for various catalysts in aqueous systems. It possesses semiconductor behavior with a moderate bandgap. Although pure conductive carbon nitride has never been synthesized, phosphorus-doped material demonstrates good conductivity [44].

Surprisingly, no publications describing the application of carbon nitride as electrochemically stable coatings materials have been found in the literature. This topic has been identified as a **research gap** and led to the basis of the present dissertation work.

1.6. Hypotheses

1. Carbon nitride or similar materials, defined as polymeric structures composed mainly by carbon and nitrogen with acceptable presence of some hydrogen, oxygen or chlorine impurities, can be obtained in the form of smooth or porous films with preferably amorphous or semi-amorphous structure, similar to the structure of vitreous carbonaceous materials.

2. Such films can be obtained by means of thermal decomposition of linear nitrogen-rich polymeric precursors, based on triazine imide units as main constituent and, optionally, containing other nitrogen-rich moieties without C-C bonds or with C-C bonds, corresponding with thermally unstable leaving groups such as -COOH. The precursors can contain halogen substituents, -OH groups or other good leaving groups in one of the triazine ring position, permitting thermal crosslinking of the precursor by means of elimination of these leaving groups.

3. Said linear nitrogen-rich precursors can be synthesized by means of condensation reactions in a solvent and some of them, especially those containing halogens as leaving groups, will be soluble at least in aprotic bipolar solvents in the form of salts with bulky organic cations. In the form of salts with ammonium or alkaline metals, solubility in water can be expected. In the same time, free forms of precursor polymers presumably will sparingly dissolve due to strong hydrogen bonding interactions, typical for triazine imides (explaining, for instance, insolubility of classic carbon nitride in all common solvents).

4. Due to projected similarity in decomposition mechanisms, the decomposition temperature of linear nitrogen-rich precursors will not exceed the synthesis temperature, typical for classical carbon nitride synthesis (600-650 ºC), thus allowing combination of materials with various molecular and nano-sized catalytic precursors.

5. Mixing of precursor polymer solutions with transition metals salts will result in formation in N-coordination products, transformed in the course of annealing into carbon nitride-coordinated metal centers, suitable for catalytic applications.

1.7. Objectives:

The main objective of the present thesis work was to develop a synthesis approach to carbon nitride coatings based on the use of soluble polymeric precursors and to characterize the coatings and precursors in order to create a basis for their implementation in future research and industrial practice.

In particular, the objectives to investigate in details basic physical properties of the coatings, important for their practical electrode applications, as well as basic electrochemical properties with the special focus on conductivity and oxidative stability, have been pursued.

One more objective of the proposed work was to investigate the behavior of a transition metal salt (on the example of nickel nitrate) in the aqueous solution of the precursors and demonstrate the catalytic activity of the metal in the annealed film and the oxidative stability of the resulting composite on the example of oxygen evolution reaction.

An additional objective arose from the necessities encountered in the course of electrochemical measurements. It was decided to create a simple potentiostatic electrochemical measurement device based on operational amplifiers and a simple Arduino microcontroller and demonstrate its ability to measure electrochemical parameters in a three-electrode system, including capacitive porous electrode, with practically required level of quality.

1.8. Bibliography for Chapter 1

1. Majlan, E.H., Rohendi, D., Daud, W.R.W., Husaini, T., Haque, M.A., 2018. Electrode for proton exchange membrane fuel cells: A review. Renewable and Sustainable Energy Reviews 89, 117–134.

2. Chatterjee, S., & Sengupta, K. (2020). Carbon-based electrodes for direct methanol fuel cells. Direct Methanol Fuel Cell Technology, Elsevier publishers, 135–176.

3. Thi Xuan Huong Le, Mikhael Bechelany, Marc Cretin. Carbon felt based-electrodes for energy and environmental applications: A review. Carbon, Elsevier, 2017, 122, 564 -591.

4. Narayanasamy, S., Jayaprakash, J., 2020. Application of carbon-polymer based composite electrodes for Microbial fuel cells. Reviews in Environmental Science and Bio/Technology 19, 595–620.

5. Haddadi-Asl, V., 2005. Electrochemical performance of graphite felt/Epr modified carbon-polymer composite electrodes (III) effect of overcharge on electrode deterioration. Amirkabir Journal of Science and Research, 16, 45–58.

6. Liu, Z., Wang, B., Yu, L., 2018. Preparation and surface modification of PVDF-carbon felt composite bipolar plates for vanadium flow battery. Journal of Energy Chemistry 27(5), 1369-1375.

7. Balzarotti, R., Latorrata, S., Mariani, M., Gallo Stampino, P., Dotelli, G., 2020. Optimization of Perfluoropolyether-Based Gas Diffusion Media Preparation for PEM Fuel Cells. Energies 13, 1831.

8. Liu, B., Dai, Y.-K., Li, L., Zhang, H.-D., Zhao, L., Kong, F.-R., Sui, X.-L., Wang, Z.-B., 2020. Effect of polytetrafluoroethylene (PTFE) in current collecting layer on the performance of zinc-air battery. Progress in Natural Science: Materials International 30, 861–867.

9. Boyd, D., Rodríguez, J.R.B., Blanco, P.T., Smyth, M.R., 1994. Application of a Nafion-modified carbon paste electrode for the adsorptive stripping voltammetric determination of fenoterol in pharmaceutical preparations and biological fluids. Journal of Pharmaceutical and Biomedical Analysis 12, 1069–1074.

10. Tsai, Y.-C., Chen, J.-M., Li, S.-C., Marken, F., 2004. Electroanalytical thin film electrodes based on a Nafion™ – multi-walled carbon nanotube composite. Electrochemistry Communications 6, 917–922.

11. Curnick, O.J., Mendes, P.M., Pollet, B.G., 2010. Enhanced durability of a Pt/C electrocatalyst derived from Nafion-stabilised colloidal platinum nanoparticles. Electrochemistry Communications 12, 1017–1020.

12. McGovern, M., Garnett, E., Rice, C., Masel, R., Wieckowski, A., 2003. Effects of Nafion as a binding agent for unsupported nanoparticle catalysts. Journal of Power Sources 115, 35–39.

13. Samms, S.R., Wasmus, S., Savinell, R.F., 1996. Thermal Stability of Nafion® in Simulated Fuel Cell Environments. Journal of The Electrochemical Society 143, 1498–1504.

14. Conesa, J.A., Font, R., 2001. Polytetrafluoroethylene decomposition in air and nitrogen. Polymer Engineering & Science 41, 2137–2147.

15. Ma, J., Haque, R., Larsen, R., 2012. Crystallization and mechanical properties of functionalized single-walled carbon nanotubes/polyvinylidene fluoride composites. Journal of Reinforced Plastics and Composites 31, 1417–1425.

16. Haider, R., Wen, Y., Ma, Z.-F., Wilkinson, D.P., Zhang, L., Yuan, X., Song, S., Zhang, J., 2021. High temperature proton exchange membrane fuel cells: progress in advanced materials and key technologies. Chem. Soc. Rev. 50, 1138–1187.

17. Wang, F., Deng, S., Zhang, H., Wang, J., Zhao, J., Miao, H., Yuan, J., Yan, J., 2020. A comprehensive review on high-temperature fuel cells with carbon capture. Applied Energy 275, 115342.

18. Peng, H., 2019. Synthesis and Application of Fluorine-Containing Polymers with Low Surface Energy. 59, 739–757.

19. Sahu, A.K., Pitchumani, S., Parthasarathi, S., Shukla, A., 2009. Nafion and modified-Nafion membranes for polymer electrolyte fuel cells: An overview. Bulletin of Materials Science 32 (3), 285-294.

20. Ray, S., Cooney, R.P., 2018. Chapter 9 - Thermal Degradation of Polymer and Polymer Composites, in: Kutz, M. (Ed.), Handbook of Environmental Degradation of Materials (Third Edition). William Andrew Publishing, 185–206.

21. Smith, A.T., LaChance, A.M., Zeng, S., Liu, B., Sun, L., 2019. Synthesis, properties, and applications of graphene oxide/reduced graphene oxide and their nanocomposites. Nano Materials Science 1, 31–47.

22. Zaaba, N.I., Foo, K.L., Hashim, U., Tan, S.J., Liu, W.-W., Voon, C.H., 2017. Synthesis of Graphene Oxide using Modified Hummers Method: Solvent Influence. Procedia Engineering 184, 469–477.

23. Yu, H., Zhang, B., Bulin, C., Li, R., Xing, R., 2016. High-efficient Synthesis of Graphene Oxide Based on Improved Hummers Method. Scientific Reports 6, 36143.

24. Lowe, S., Zhong, Y.L., 2016. Challenges of Industrial-Scale Graphene Oxide Production: Fundamentals and Applications. Graphene Oxide: Fundamentals and Applications, 410–431.

25. Jeong, H., Lee, Y., Jin, M., Kim, E., J. J, B., Lee, Y.H., 2009. Thermal stability of graphite oxide. Chemical Physics Letters 470 (4-6), 255-258.

26. Narayanam, P.K., Soni, P., Botcha, V.D., Singh, G., Major, S.S., 2018. Transparent and Hydrophobic "Reduced Graphene Oxide–Titanium Dioxide" Nanocomposites for Nonwetting Device Applications. ACS Appl. Nano Mater. 1, 5691–5701.

27. Liu, W., Speranza, G., 2021. Tuning the Oxygen Content of Reduced Graphene Oxide and Effects on Its Properties. ACS Omega 6, 6195–6205.

28. Shan, D., Deng, S., Jiang, C., Chen, Y., Wang, B., Wang, Y., Huang, J., Yu, G., Wiesner, M.R., 2018. Hydrophilic and strengthened 3D reduced graphene oxide/nano-Fe_3O_4 hybrid hydrogel for enhanced adsorption and catalytic oxidation of typical pharmaceuticals. Environ. Sci.: Nano 5, 1650–1660.

29. Kim, H.W., Ross, M.B., Kornienko, N., Zhang, L., Guo, J., Yang, P., McCloskey, B.D., 2018. Efficient hydrogen peroxide generation using reduced graphene oxide-based oxygen reduction electrocatalysts. Nature Catalysis 1, 282–290.

30. Feng, Y., Li, W., An, J., Zhao, Q., Wang, X., Liu, J., He, W., Li, N., 2021. Graphene family for hydrogen peroxide production in electrochemical system. Science of The Total Environment 769, 144491.

31. Gilhotra, C., Chander, M., Sanjay, 2019. A review: Conducting polyaniline polymer. AIP Conference Proceedings 2142, 150008.

32. Çolak, N., Ozyilmaz, A., 2005. Polyaniline Coating on Iron–Synthesis and Characterization. Polymer-Plastics Technology and Engineering 44, 1547–1558.

33. Venkata Ramana, G., Padya, B., Srikanth, V.V.S.S., Jain, P., 2013. Rapid mixing chemical oxidative polymerization: An easy route to prepare PANI coated small-diameter CNTs/PANI nanofibres composite thin film. Bulletin of Materials Science 37.

34. Samui, A.B., Patankar, A.S., Rangarajan, J., Deb, P.C., 2003. Study of polyaniline containing paint for corrosion prevention. Progress in Organic Coatings 47, 1–7.

35. Stejskal, J., Exnerová, M., Moravkova, Z., Trchová, M., Hromádková, J., Prokes, J., 2012. Oxidative stability of polyaniline. Polymer Degradation and Stability 97, 1026–1033.

36. Malinauskas, A., 2002. Electrochemical stability of polyaniline. European Polymer Journal - EUR POLYM J 38, 1947–1952.

37. Zong, H.-H., Yao, C., Sun, C.Q., Zhang, J.-G., Zhang, L., 2020. Structure and Stability of Aromatic Nitrogen Heterocycles Used in the Field of Energetic Materials. Molecules 25, 3232.

38. Dbira, S., Bedoui, A., Bensalah, N., 2014. Investigations on the Degradation of Triazine Herbicides in Water by Photo-Fenton Process. American Journal of Analytical Chemistry 05, 500–517.

39. Da Silva, G., Bozzelli, J.W., Asatryan, R., 2009. Hydroxyl Radical Initiated Oxidation of s-Triazine: Hydrogen Abstraction Is Faster than Hydroxyl Addition. J. Phys. Chem. A 113, 8596–8606.

40. Zhu, G.X., Lu, T.L., Han, L., Zhan, Y.Z., 2020. Graphitic carbon nitride (g-C3N4) as an efficient metal-free Fenton-like catalyst for degrading organic pollutants: the overlooked non-photocatalytic activity. Water Science and Technology 81, 518–528.

41. Torres-Pinto, A., Sampaio, M.J., Teixo, J., Silva, C.G., Faria, J.L., Silva, A.M.T., 2020. Photo-Fenton degradation assisted by in situ generation of hydrogen peroxide using a carbon nitride photocatalyst. Journal of Water Process Engineering 37, 101467.

42. Oliveira, W.L., Ferreira, M.A., Mourão, H.A.J.L., Pires, M.J.M., Ferreira, V., Gorgulho, H.F., Cipriano, D.F., Freitas, J.C.C., Mastelaro, V.R., Nascimento, O.R., Ferreira, D.E.C., Ramos Fioravante, F., Pereira, M.C., de Mesquita, J.P., 2021. Heterogeneous Fenton-like surface properties of oxygenated graphitic carbon nitride. Journal of Colloid and Interface Science 587, 479–488.

43. Inagaki, M., Tsumura, T., Kinumoto, T., Toyoda, M., 2019. Graphitic carbon nitrides (g-C_3N_4) with comparative discussion to carbon materials. Carbon 141, 580–607.

44. Zhang, Y., Mori, T., Ye, J., Antonietti, M., 2010. Phosphorus-Doped Carbon Nitride Solid: Enhanced Electrical Conductivity and Photocurrent Generation. J. Am. Chem. Soc. 132, 6294–6295.

UNIVERSITAT ROVIRA I VIRGILI
SEMI-AMORPHOUS CARBON NITRIDE FILMS DERIVED FROM SOLUBLE POLYMERIC PRECURSORS: TOWARDS MULTIFUNCTIONAL ELECTROCHEMICAL COATINGS WITH ENHANCED STABILITY
Oleg Dubov

Chapter 2

Synthesis of polymeric precursors, fabrication of flexible carbon nitride films and their characterization as electrochemically stable coatings

Uniform flexible carbon nitride coatings have been synthesized by means of annealing of films, fabricated from soluble triazine-based polymeric precursors. The coatings exhibit fascinating electrochemical stability and drastically increase the capacitance of coated carbon cloth electrodes.

Following the analogue with turbostratic carbons, typically produced by means of polymeric precursors pyrolysis, we demonstrate that annealing of dried nitrogen-rich polymeric films results in coatings, composed by nearly equal atomic quantities of carbon and nitrogen, according to elemental analysis, and exhibiting noticeable mechanical robustness. X-ray diffraction patterns and infrared spectra of the materials allow to characterize them as partially amorphous carbon nitride with presumably heptazinic structure.

Annealed films exhibit extrinsic semiconducting behavior with optical bandgaps in the range from 1.71 to 1.99 eV and fairly good conductivity. The outstanding long-term electrochemical stability of annealed films makes them competitive with pyrolytic carbon, while much lower annealing temperatures allow preparation of nanocomposites with various particles. The precursor polymers were obtained by self-condensation of 2-amino-4,6-dichloro-1,3,5-triazine and condensation of cyanuric chloride with 5-aminotetrazole and 3-amino-1,2,4-triazole-5-carboxylic acid, respectively, in N,N-dimethylacetamide. The polymers contain mainly C-N skeletal bonds and can therefore be viewed as “extension” of typical carbon nitride precursors, like melamine or dicyandiamide, to polymeric structure.

Research paper accepted for publication in the
Journal of Materials Science
«Flexible semi-amorphous carbon nitride films with outstanding electrochemical stability derived from soluble polymeric precursors»
Oleg Dubov, Jaume Giralt Marcé, Agusti Fortuny, Azael Fabregat, Frank Stüber and Jose Font Capafons

Manuscript ID **JMSC-D-21-04914**

2.1. Introduction

Nitrides of carbon represent a family of materials, which includes two layered analogues of graphite with layers consisted of sheets of (poly(tri-s-heptazine imide) and 1,3,5-triazine imide, respectively, as well as different products of incomplete condensation with pending amino groups [1] and, more recently, linear [2] and two-dimensional [3] triazine imides.

Carbon nitrides have become a hotspot in the materials science in the recent years due to a wealth of attractive properties that they possess. Both heptazine-based and 1,3,5-triazine-based structures exhibit fascinating thermal endurance, superior stability against oxidation and hydrolysis, biocompatibility and semiconducting properties with moderate and easily tunable bandgaps, corresponding to excitation with near UV or even blue-violet light, which makes them undoubtedly interesting for photoelectronics and photocatalysis [4].

Bulk heptazine-based graphitic carbon nitride is typically synthesized by simply pyrolyzing (even often without a need for inert atmosphere) of nitrogen-rich precursors - most typically, melamine, dicyandiamide, urea or their mixtures [1]. However, in a great number of implementations, including virtually all the electrochemical applications as well as uses for electronics and photocatalysis, it is prerequisite to deposit the material on a support, forming a film, or fabricate a composite material containing carbon nitride as a binder for nanoparticles possessing structural and catalytic functionality.

Many film deposition techniques, e.g., growing a film from a precursor melt or molten salt with a precursor [5, 6], vacuum sputtering [7], chemical vapor deposition (CVD) [8], electrolysis of soluble precursors using the support as an anode [2], have been successfully used and provided the production of smooth and well-ordered films.

Nonetheless, from the viewpoint of equipment simplicity, industrial feasibility and process cost, solution or suspension-based approaches are always preferred. Suspensions of carbon nitrides are well known. Following the analogue (albeit very imperfect from the structural viewpoint) of graphitic carbon nitride with graphite, chemical or ultrasonic exfoliation are typically used with the objection of obtaining a suspension of graphene-like carbon nitrides nanosheets in a solvent. The suspension is subsequently deposited on the chosen support by one of the standard liquid coating techniques (e.g., dropcasting, spincoating, dipcoating, doctor blade, spraying and still others).

However, no industrially feasible technique for exfoliation of graphitic carbon nitride have been proposed so far. Ultrasonic exfoliation in water and organic solvents typically requires tens of hours of sonication. Furthermore, the concentrations of exfoliated nanosheets are generally very low (in the order of few grams per liter) [9,10].

Another possible approach to liquid coating techniques implies the use of soluble precursors. Although melamine is well known to be very poorly soluble in all common solvents, other popular precursors for carbon nitride, dicyandiamide and urea, can easily be dissolved in both water and organic solvents.

Howbeit, according to our observations and quite expectably, the low molecular weight of these compounds leads to their crystallization during solvent evaporation after the composition is applied and, similarly as with coatings derived from nanoparticles, to formation of carbon nitride particles weakly bound to the support instead of forming a smooth film. Hence, an ideal hypothetical carbon nitride film precursor should be a polymer or supramolecular complex that could form a gel upon evaporation of the solvent.

Intriguingly, the approach to synthesis of carbon nitride materials, starting from reactions of precursors in a solvent is well known, but these condensation reactions typically result in formation of non-soluble, crosslinked products, which are further crosslinked by annealing.

For instance, in the work by Ok-Hee Kim et al. [11], carbon nitride material has been synthesized by the condensation of melamine and cyanuric chloride in N,N-dimethylformamide; Xu et al. [5] used as precursor a supramolecular complex of cyanuric chloride with 2,4-diamino-6-phenyl-1,3,5-tiazine (benzoguanamine). However, to the best of our knowledge no solution-based approaches allowing obtaining mechanically robust carbon nitride coatings have been proposed to date.

On the other hand, this approach does exist and is well developed for carbon-based materials without a substantial nitrogen content. Partially ordered forms of carbon with folded graphitic nano-ribbons, erroneously called «glassy carbon» or, more precisely, pyrolytic carbon, are known from mid-1950s [31, 32]. These materials have emerged into a golden standard in electrochemical measurements, being exceptionally stable in both anodic and cathodic polarization regimes and showing no own catalytic activity.

Pyrolitic carbons are typically synthesized by pyrolysis of crosslinked polymeric precursors, more often phenol-formaldehyde resins. By pyrolyzing crosslinked polymer films deposited on carbon or ceramic substrates, pyrolytic carbon coatings can be obtained.

Pyrolytic materials with some nitrogen content, obtained from polymers, are also well known, although to our knowledge none of them has been reported to have fraction of nitrogen even near to that of graphitic carbon nitride (57.1% at.) and their poor long-term electrochemical stability has recently been reported and related with typically low graphitic nitrogen content in these materials [12].

Although pyrolytic carbons are unique electrochemical materials due to their electrochemical inertness and applicability to fabrication of electrodes with complex

shapes [32], there are three inherent properties of these materials that complicate their use in many practical fields. High elastic modulus and brittleness impede fabrication of thin films and filaments, eminent hydrophobicity results in poor wetting of electrodes in water-based systems, while high fabrication temperature leads to practical unfeasibility of functional composites production that would involve pyrolysis of polymeric precursors of glassy carbon with catalytically active complexes or nanoparticles.

According to our findings, all these issues can be simultaneously addressed by incorporation of high amounts of nitrogen into pyrolytic carbon matrix.

In this work, the synthesis of three soluble polymers is reported. One of the polymers is completely triazine-based and other two represent block polyimides of triazine with nitrogen-rich heterocyclic amines. All the three obtained polymers have never been described before. Moreover, the general family of linear imides composed by triazine moiety and triazole or tetrazole seems to have never been characterized in the literature.

Linear imides of triazine, although previously described [2], have never been synthesized with chloride as side-substituents, presumably important for the solubility of the resulting polymer salt in organic solvents.

Pyrolysis of dried precursor polymer films results in the materials with high nitrogen content, low density and exceptional stability to oxidation and reduction, while their XRD and AFM patterns closely resemble pyrolytic carbons.

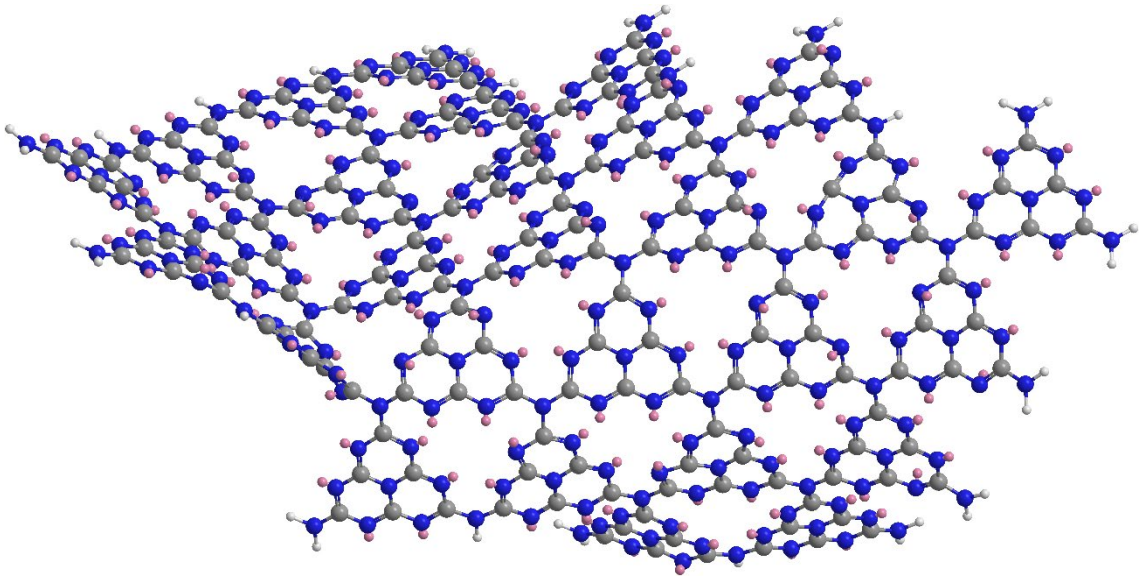

Fig.2.1. Hypothetic twisted monolayer of heptazine-based carbon nitride

2.2. Materials and methods

All chemicals have been purchased from Sigma Aldrich and used without any additional purification. Anhydrous 99.8% pure N,N-dimethylacetamide (DMAc) (Sigma Aldrich), <0.005% water, has been used as a solvent in all polymer syntheses. 3.18 mm thick, carbon cloth (CC) sheets and glassy carbon plates for electrodes fabrication have been purchased from Alfa Aesar.

2-amino-4,6-dichloro-1,3,5-triazine was synthesized according to the published procedure described by Baliani et al in the Supporting Information provided for their publication [13]. Briefly, it was obtained by means of ammonolysis of cyanuric chloride in acetone solution at 0 ºC with 4 equivalents of aqueous ammonia. 5-aminotetrazole was obtained by drying the corresponding monohydrate (purchased from Sigma Aldrich) in air at 105 ºC for 24 hours according to the procedure described in [15], followed by keeping the product two weeks in vacuum desiccator over P_2O_5.

NMR spectra have been recorded using a VARIAN Mercury VX400 spectrometer.

SEC chromatography installation consisted of an Agilent 1260 Isocratic Pump, manual sample injector Rheodyne Model 7125 with 20 mL loop, two PLgel 5 mm Mixed-D 30 x 7.5 mm linear columns (MW 200-400.000) 75970 and 97293 plates/m (1/2 ht)) with an Agilent 1100 series refractive index detector.

JASCO 4700 spectrometer has been used for FTIR spectra recording. Infrared spectra have been processed in free SpectraGryph software.

Thermogravimetric analysis has been carried out with SETARAM SENSYS EVO 3D Tech. For analysis, sample (of around 10 mg) was placed in platinum pan and heated at a constant rate of 4 °C/min.

Elemental analysis of the samples was performed using Perkin Elmer EA2400 serie II elemental analyzer after sample incineration at 930 ºC.

UV-Vis diffuse reflectance spectroscopy measurements were carried out using a Shimadzu UV-3600 equipment with BaSO4-coated integration sphere.

JEOL model 1011 and Thermo Fisher SCIOS 2 with field emitter have been used for transmission and scanning electronic microscopy/EDX, respectively.

STM scanning has been performed on Pico SPM II (Pico+) system.

XRD (X-ray diffraction) measurements were made using a Siemens D5000 diffractometer (Bragg-Brentano parafocusing geometry and vertical θ-θ goniometer) fitted with a curved graphite diffracted-beam monochromator, incident and diffracted beam Soller slits, a 0.06º receiving slit and scintillation counter as a detector.

Contact angles have been measured by the static sessile drop method using Kyowa Interface Science DM211 goniometer for films.

Autolab PGSTAT204 with FRA32M has been used for all electrochemical experiments. Free EIS Spectrum Analyzer software has been used for profile fitting.

2.3. Polymer precursors synthesis and characterization

Three nitrogen-rich triazine-based polymers have been synthesized by self-condensation and condensation reactions, respectively. N,N-dimethylacetamide (DMAc) has been used as a solvent and N,N-diisopropylethylamine (DIPEA) as a non-nucleophilic base in all cases. Sodium and potassium carbonates were also tested and found to be effective acid scavengers for these syntheses, although their utilization derives in prominent increase of reaction suspension viscosity. This high viscosity issue, however, presumably would not be critical for industrial-scale process in a reactor, equipped with a powerful mechanical mixer. Synthesis in the presence of alkali metals carbonates can be an important improvement towards obtaining precursor polymers in their pure imide (acidic) form without the aliphatic organic base (e.g. DIPEA) impurity, important for future development of carbon nitride films with further elevated content of nitrogen.

The first polymer, [azanediyl (2-chloro-1,3,5-triazine-4,6-diyl)], further abbreviated as poly(CYA-Cl-NH), have been synthesized by self-condensation of 2-amino-4,6-dichloro-1,3,5-triazine.

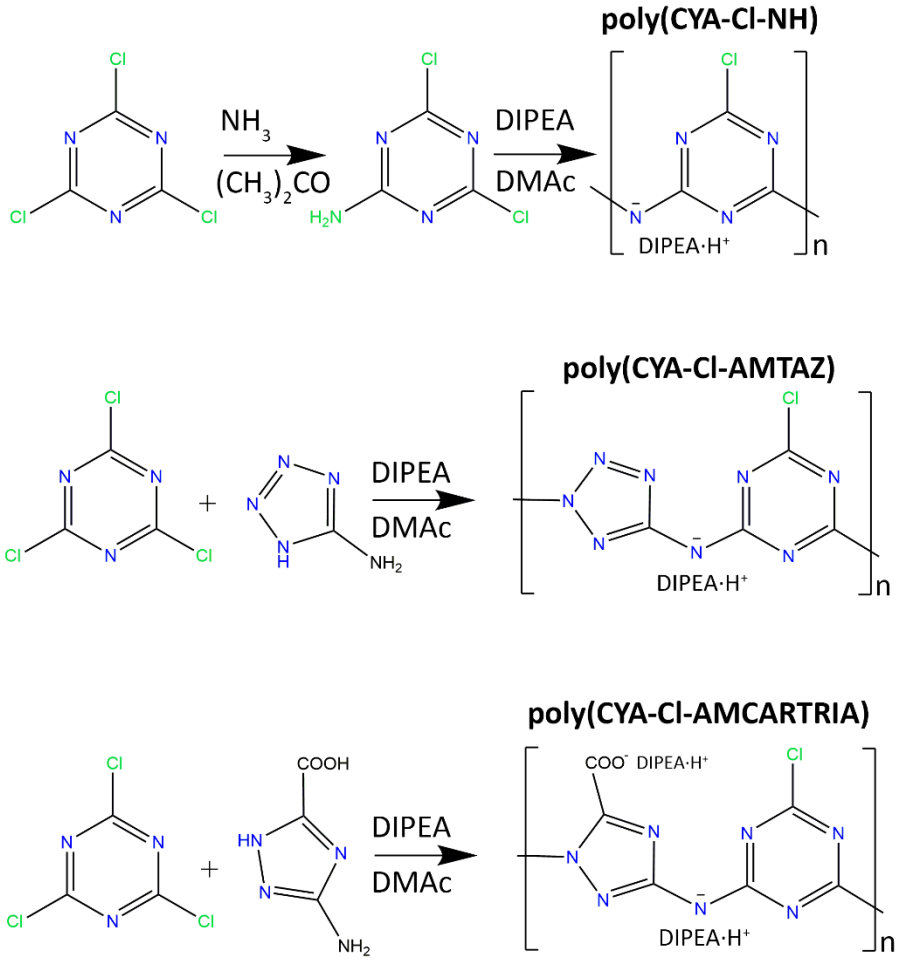

Fig. 2.2. Reaction schemes for the syntheses of precursors

Two other polymers, poly[(2-chloro-1,3,5-triazine-4,6-diyl (5-iminotetrazol-2-yl)], further abbreviated as poly(CYA-Cl-AMTAZ), and poly [(2-chloro- 1,3,5-triazine-4,6-diyl (5-carboxy-3-iminotriazol-1-yl)], further abbreviated as poly(CYA-Cl-AMCARTRIA), were synthesized by condensation of 5-aminotetrazole and 3-amino-1,2,4-triazole-5-carboxylic acid, respectively, with cyanuric chloride.

In all cases, formation of linear polymers with substitution of two of three chlorine groups, present in cyanuric chloride, was expected. For the poly(CYA-Cl-NH) case, this pathway was guaranteed by the presence of two chlorine substituents per each amino group. It two other cases, the 1/1 equivalent ratio between cyanuric chloride (containing three active chlorine groups) and aminotriazole or aminotetrazole, respectively, containing one reactive imine group in the ring and one amino functionality, also provided 3/2 ratio between chlorine and imino/amino groups.

For the poly(CYA-Cl-NH), no isomeric structure within the linear polymer case are possible. For two other polymers, atactic configurations have been expected due to stochastic nature of the polycondensation reaction.

The amount of DIPEA for all polymer syntheses has been chosen so that the base would consume all the HCl, liberated in the course of synthesis, as well as form salts with acidic imide groups (for poly(CYA-Cl-NH) and poly(CYA-Cl-AMTAZ) and imide + carboxyl groups (for poly(CYA-Cl-AMCARTRIA), with no free base remaining.

All the three polymers were originally obtained in the form of 5% wt. solutions of polymeric salts with DIPEA in DMAc, containing also DIPEA·HCl. At higher concentrations, the precipitation of DIPEA*HCl salt from cold solutions takes place.

The syntheses have been operated in accordance with the following protocols:

Synthesis of poly [azanediyl (2-chloro-1,3,5-triazine-4,6-diyl)], further abbreviated as poly(CYA-Cl-NH)

8 mmol (1.32 g) of 2-amino-4,6-dichloro-1,3,5-triazine and 24 mmol (3.10 g) of N,N-diisopropiaylethylamine (DIPEA) were dissolved in 10.3 g of DMAc. The vial was purged with Ar and sealed. The solution was refluxed at room temperature for 20 min, then heated to 110 ºC and left under reflux at this temperature for 72 hours.

No obvious signs of the reaction were mentioned except for slow color change from slightly yellow to brown. Although no systematic study on the optimal reaction conditions have been undertaken, it was mentioned that the samples obtained at lower temperatures and/or with shorter reaction times, upon addition of the DMA solution to acidified water, demonstrated formation of fine colloidal suspensions with poor filterability, probably indicating low molecular weight of condensation products.

Synthesis of poly [(2-chloro-1,3,5-triazine-4,6-diyl (5-iminotetrazol-2-yl)], further abbreviated as poly(CYA-Cl-AMTAZ)

8 mmol (0.68 g) of 5-aminotetrazole and 24 mmol (3.10 g) of N,N-diisopropylethylamine (DIPEA) were dissolved in 20 g of DMAc. The solution was cooled down to -5 ºC. In continuous Ar flow, a solution of 8 mmol of cyanuric chloride (1.48 g) in 6.18 g DMAc was added to the mixture dropwise under cooling in ice + NaCl bath and intensive stirring so that the temperature would not have exceeded 0 ºC. After finishing the addition, the solution was refluxed with gradual heating to room temperature during 20 min, then sealed, heated to 70 ºC and left under reflux at this temperature for 24 hours.

Intensive production of heat and color change to fluorescent-yellow take place immediately after addition of the first portions of cyanuric chloride, indicating that the formation of conjugated condensation products starts instantly even at low temperatures. It is of critical importance to maintain the temperature below 0 ºC during all the process of cyanuric chloride addition. At higher temperatures, an insoluble product is formed, probably as a result of cross-linking due to known noticeable reactivity of the last chlorine atom in cyanuric chloride at elevated temperatures [11].

Synthesis of poly [(2-chloro-1,3,5-triazine-4,6-diyl (5-carboxy-3-iminotetriazol-1-yl)], further abbreviated as poly(CYA-Cl-AMCARTRIA)

8 mmol (1.02 g) of 3-amino-1,2,4-triazole-5-carboxylic acid was suspended in 20 g of DMAc and 40 mmol (5.20 g) of N,N-diisopropylethylamine (DIPEA) were added to the suspension. In continuous Ar flow, a solution of 8 mmol of cyanuric chloride (1.48 g) in 10.62 g DMAc was added to the mixture dropwise at room temperature. In contrast with the CYA-Cl-AMTAZ synthesis, no color change nor heat production have been mentioned during the monomers mixing stage of the reaction towards CYA-Cl-AMCARTRIA, indicating much lower reactivity. For this reason, no cooling of the reaction mixture has been used. After finishing the addition, the solution was sealed, heated to 110 ºC and left under reflux at this temperature for 72 hours.

Reaction solution samples obtained at lower temperatures and/or with shorter reaction time, demonstrated formation of colloidal suspensions upon pouring into acidified water and were probably represented by low molecular weight products.

All three polymers, synthesized according to correct protocols, demonstrate formation of flake-like suspension upon pouring their solutions to the excess of 5% HCl solution. These suspensions can be vacuum-filtered on 0.45 μm cellulose filter within several hours or centrifuged at 5000 RPM within 10 min.

NMR characterization of as-synthesized polymer solutions was performed with ^{1}H spectra of as-synthesized solutions (i.e., in non-deuterated DMAc). Although all polymers can easily be separated by sedimentation in acidified water followed by filtration, the resulting powders after drying demonstrate negligible solubility in DMAc and DMSO even in the presence of DIPEA or triethylamine, thus not allowing to prepare solutions in a deuterated (e.g., for instance DMSO-d6/triethylamine-d15) system.

However, the main objectives of the NMR characterization were to identify the remaining peaks of the reactants/oligomeric products and to measure the concentrations of DIPEA forms in order to characterize the acidity of the polymers. For these purposes, the use of non-deuterated solvents almost did not complicate the analysis.

With the objection to test the hypothesis that partial evaporation of DIPEA in the reaction course could take place, NMR of samples with added carefully metered amount of trifluoroacetic acid was recorded. The results for all polymers clearly demonstrate that DIPEA evaporation during the reaction course was negligible as acid consumption correctly fits the expected DIPEA content.

In order to clearly identify the ratio between free DIPEA and its salts, **direct titration** with 0.1 N HCl of samples of all three reaction mixtures after pouring 1g of reaction mixture to 100 ml of deionized water was accomplished. For poly(CYA-Cl-NH), the pH of 10.7 in the resulting solution was measured and pH-metric titration down to pH 6.0 demonstrated the presence of 38.3% of the added DIPEA in the free form, in good agreement with the NMR data. For poly(CYA-Cl-AMTAZ), the pH of the resulting mixture was 8.1, while the titration demonstrated nearly complete presence of DIPEA in the ionized form. A similar result was obtained for poly(CYA-Cl-AMCARTRIA) with pH equal to 8.6 and 1.8 percent of free DIPEA as given by the titration.

Although the results of titrations cannot be considered precise due to unknown acidity constants and correspondingly unclear equilibrium pH values for solutions with fully ionized DIPEA, the results are in good agreement with data, obtained from the NMR spectra.

The concentration of DIPEA*H^{+} for **poly(CYA-Cl-NH)** solution according to NMR equals to 60% of the total DIPEA content. Taking into account that absorption of HCl, released during the polycondensation, would bind 66.6% of the total DIPEA, the observed value indicates the low acidity of the polymer, mostly existing in the solution in its free form coexisting with free DIPEA.

The presence of impurity peak at 9.05 ppm in the ^{1}H spectrum probably allows to characterize the condensation process as incomplete/leading to low molecular weight polymer.

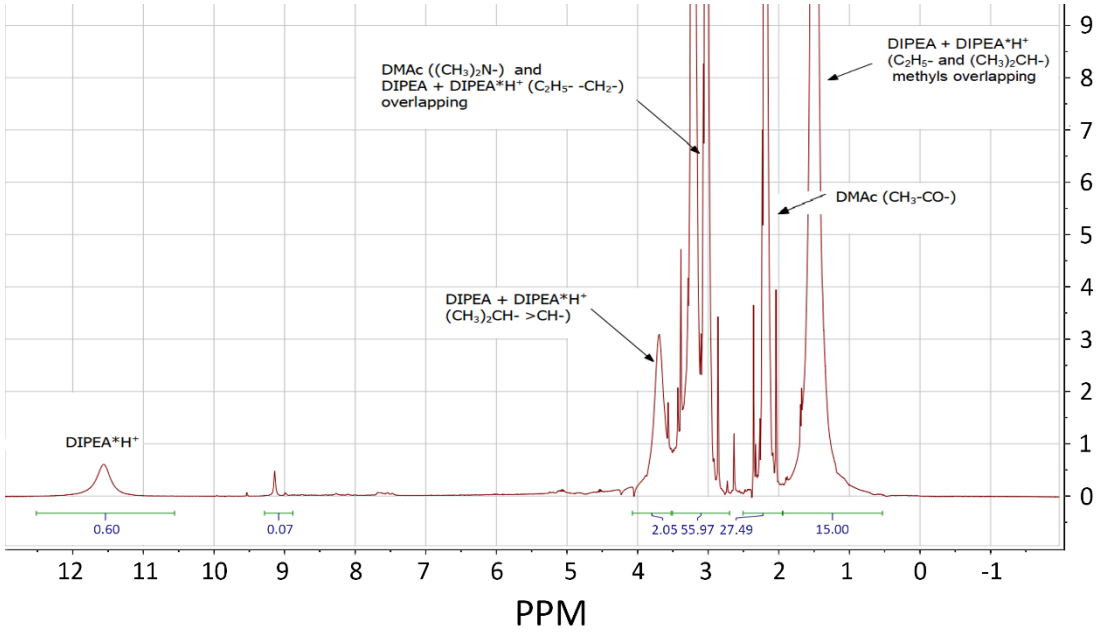

*Fig. 2.3. ^{1}H NMR of poly(CYA-Cl-NH) 5% (as synthesized, contains DIPEA and DIPEA*H^{+}).*

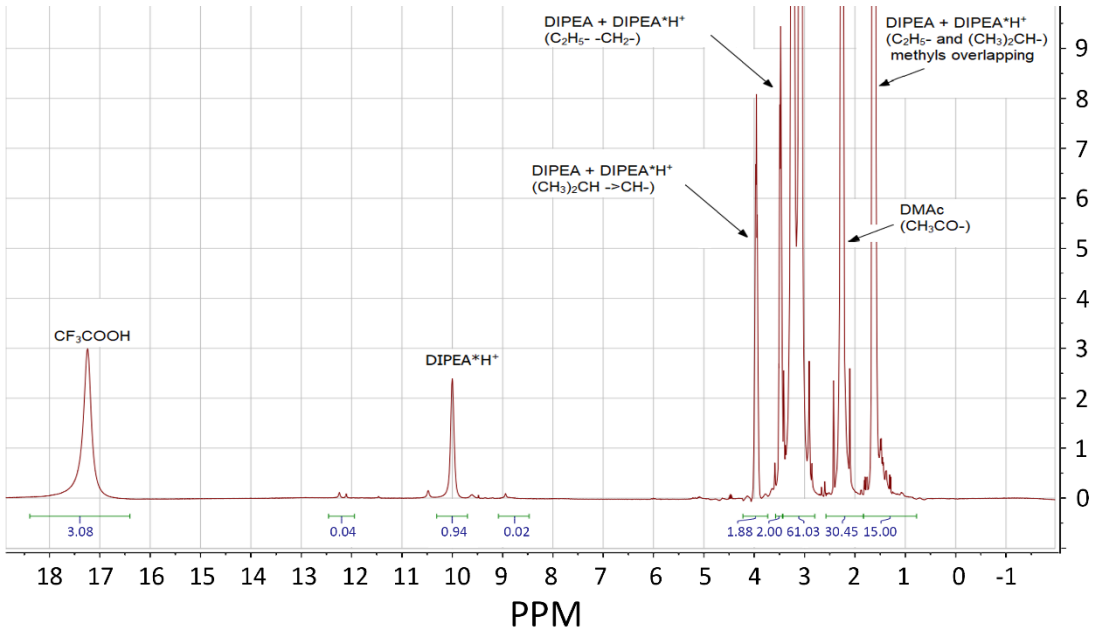

Fig. 2.4. ^{1}H NMR of poly(CYA-Cl-NH) 5% (as synthesized) + CF_3COOH (1.02 mmol/g), corresponds to 4x molar excess over non-reacted DIPEA in the solution.

In the **poly(CYA-Cl-AMTAZ)** case, the intensity of DIPEA*H^{+} peak ideally fits the expected total DIPEA concentration – i.e. the polymer exists as DIPEA salt with all the DIPEA being ionized. Upon addition of CF_3COOH, the intensity of DIPEA*H^{+} peak remains unchanged while all the added acid shows up as free solvated protons, further proving the absence of free DIPEA.

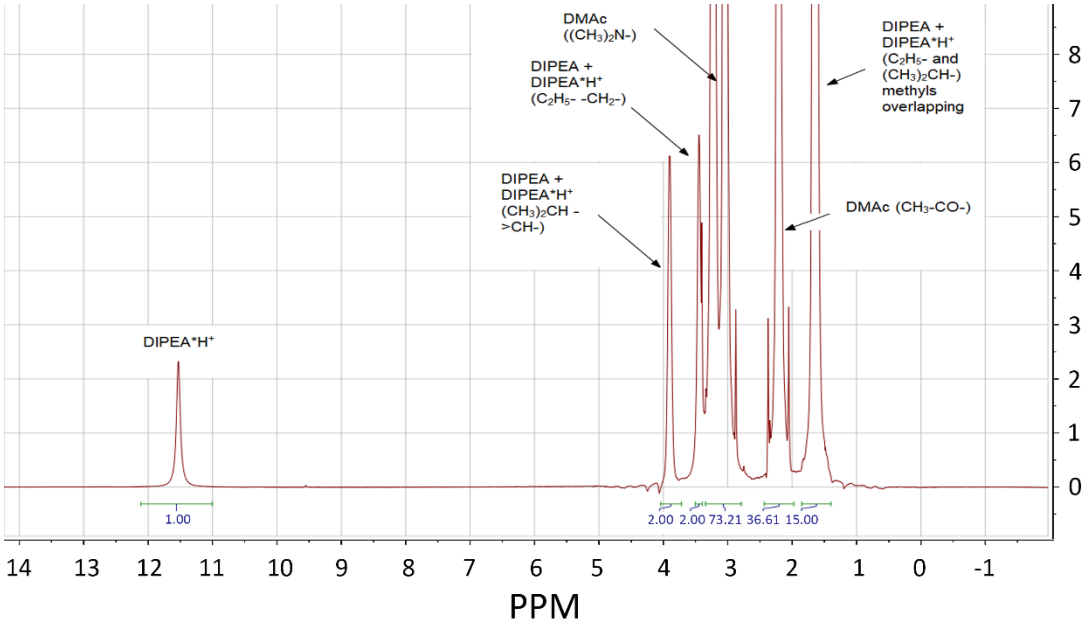

*Fig. 2.5. ^{1}H NMR of CYA-Cl-AMTAZ 5% (as synthesized, contains DIPEA and DIPEA*H^{+}).*

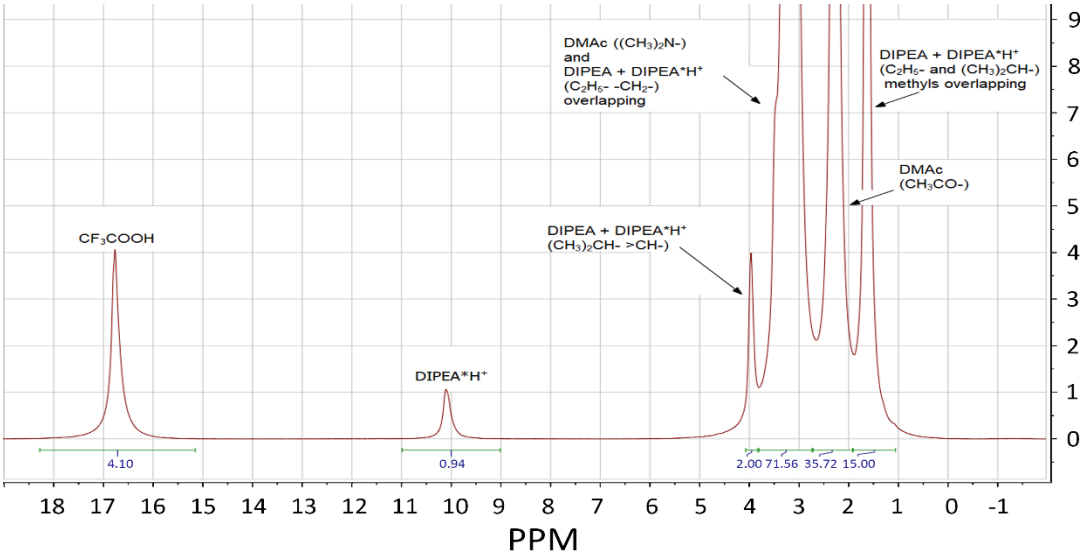

Fig. 2.6. ^{1}H NMR of CYA-Cl-AMTAZ 5% (as synthesized) + CF_3COOH (1.02 mmol/g), corresponds to 4x molar excess over non-reacted DIPEA in the solution.

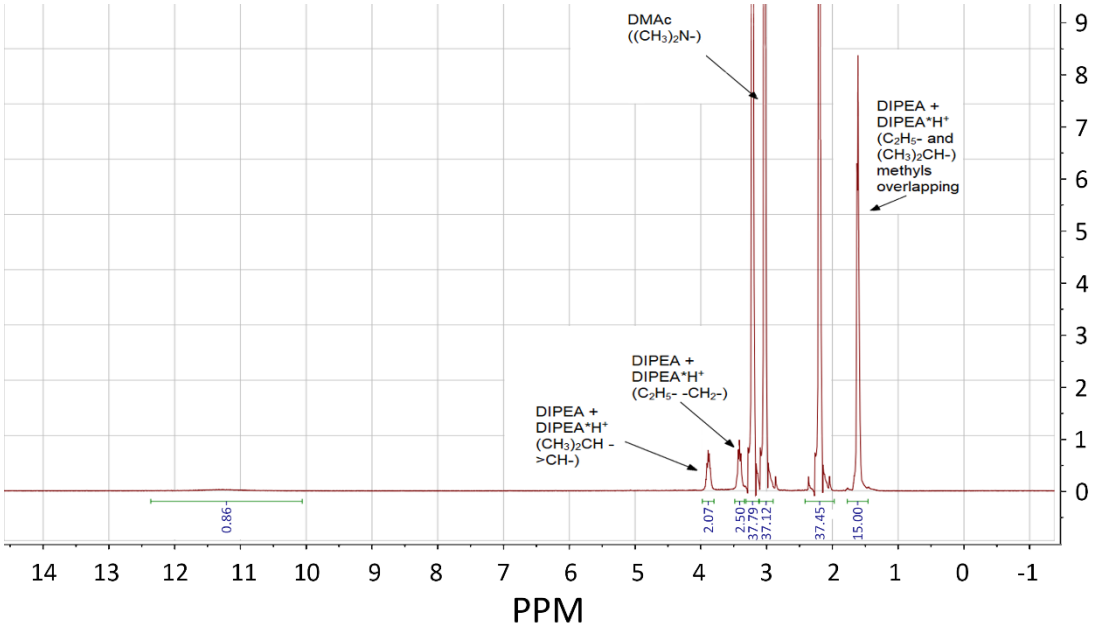

*Fig.2.7. ^{1}H NMR of poly(CYA-Cl-AMCARTRIA) 5% (as synthesized, contains DIPEA and DIPEA*H^{+}).*

The wide signal around 11.2 ppm presumably comes from the exchange between DIPEA*H^{+} and polymer COOH protons.

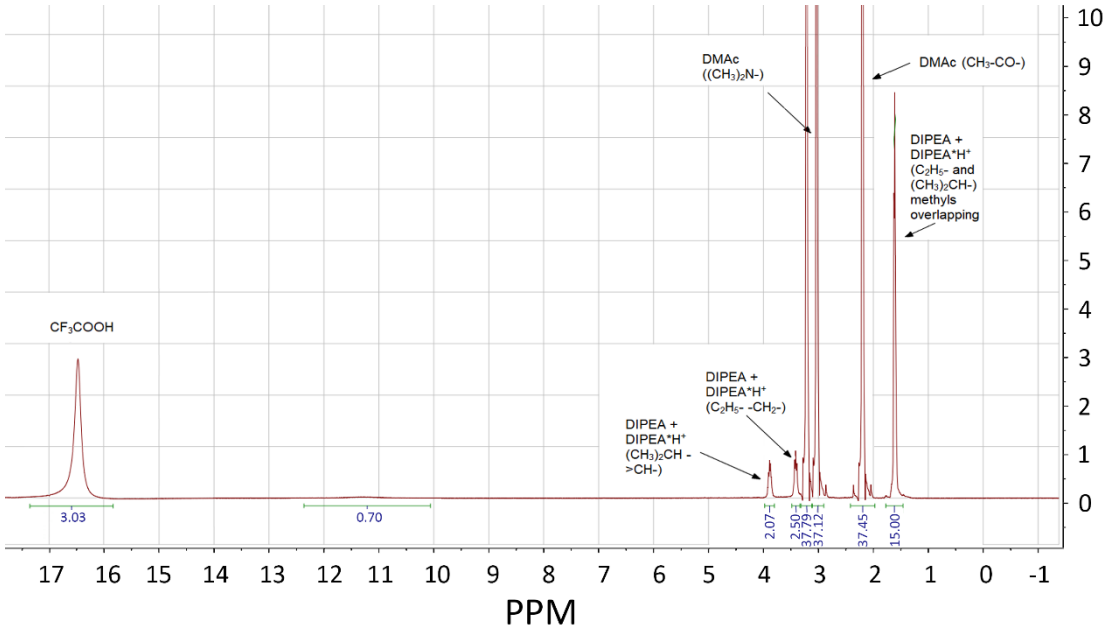

Fig. 2.8. ^{1}H NMR of poly(CYA-Cl-AMCARTRIA) 5% (as synthesized)+ CF_3COOH (1.02 mmol/g), corresponds to 4x molar excess over non-reacted DIPEA in the solution.

CF_3COOH consumption corresponds with the hypothesis of low acidity of the polymer. Surprisingly, even in the acidified solution, the DIPEA*H^{+} peak shows up as a diffused wide signal.

Solvent exclusion chromatography (SEC, GPC) of the polymers was carried out for as-synthesized solutions, diluted by N,N-dimethylformamide (DMF) with LiBr.

The lithium bromide addition was used in order to weaken the H-bonding interactions between imide polymer chains and reduce possible agglomeration and globulation of polymers.

It is important to emphasize that SEC experiments conducted in this study were undoubtedly affected by two inevitable issues: the standard used for calibration (PMMA) was very different from examined polymers in chain mechanics and polarity; the samples were injected "as synthesized", which resulted in impurities peaks way more intensive than polymer peaks.

For this reason, the results of SEC experiments were used exclusively to differentiate between polymeric and oligomeric condensation products and not to characterize the exact values of molecular weights. SEC of the polymers has been carried out with the following recording conditions:

Solvent: DMF, (0.1% w. LiBr), polymethylmethacrylate (PMMA) as calibration standard, toluene as flow rate marker (FRM). Sample preparation: DMF solution (HPLC grade) approx. 100 mkL of synthesis solution in 2.0 mL of DMF. Prepared samples have been filtered through 0.22 μm syringe filter.

The polymer solutions have been diluted by DMF "as synthesized", i.e., the final solutions used for SEC characterization contained DMAc, DIPEA and its hydrochloride.

Although the use of "as synthesized" polymers typically is not recommended for GPC characterization due to intensive peaks of impurities often shading the signals of polymeric components, we found that for our system the signals of polymers were well distinguishable on the chromatograms.

The following abbreviations are used in the molecular weight tables:

Mn = number average molecular weight;
Mw = weight average molecular weight;
Mp = peak maximum molecular weight;
Đ = refractive index.

An intensive peak at around 23.5 minutes as well as two other peaks at 18.0 and 18.8 minutes appear in all chromatography runs even when DMAc/DIPEA/DIPEA*HCl model solution (without a polymer) is injected, so these three peaks have been assigned to solvent and system peaks. Two peaks with high molecular weight appear around 15.5 and 16.7 minutes. Their molecular weight data are provided in the Table 2.1.

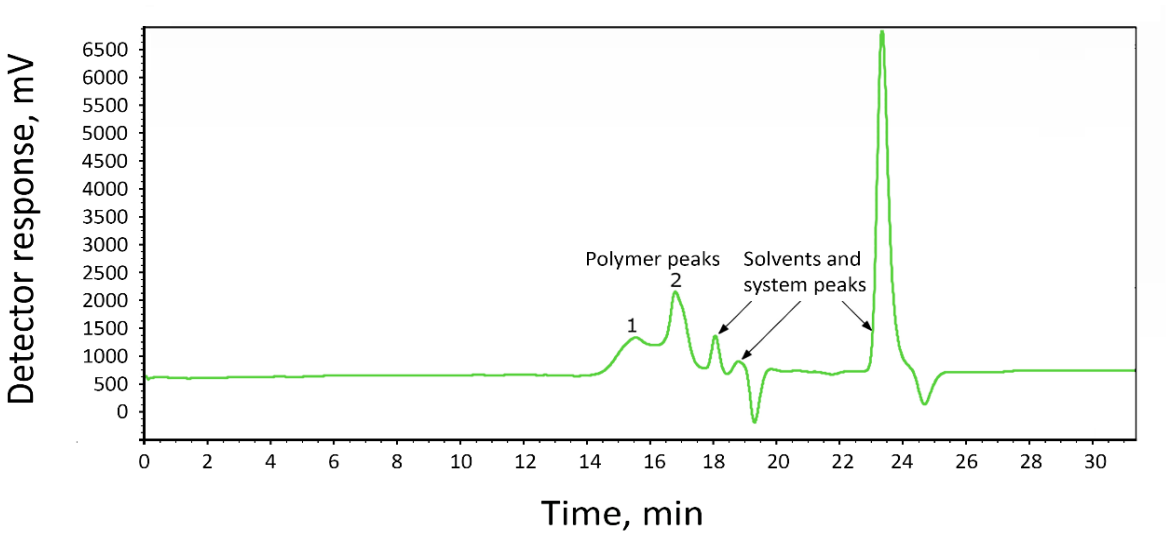

Fig. 2.9. Poly(CYA-Cl-NH) chromatogram general view

Table 2.1. Poly(CYA-Cl-NH) molecular weight data

Polymer	**Mn (Da)**	**Mw (Da)**	**Mp (Da)**	**Đ**
poly(CYA-Cl-NH) (two GPC peaks)	1. 14460 2. 5840	1. 15600 2. 6130	1. 14500 2. 6120	1. 1.079 2. 1.048

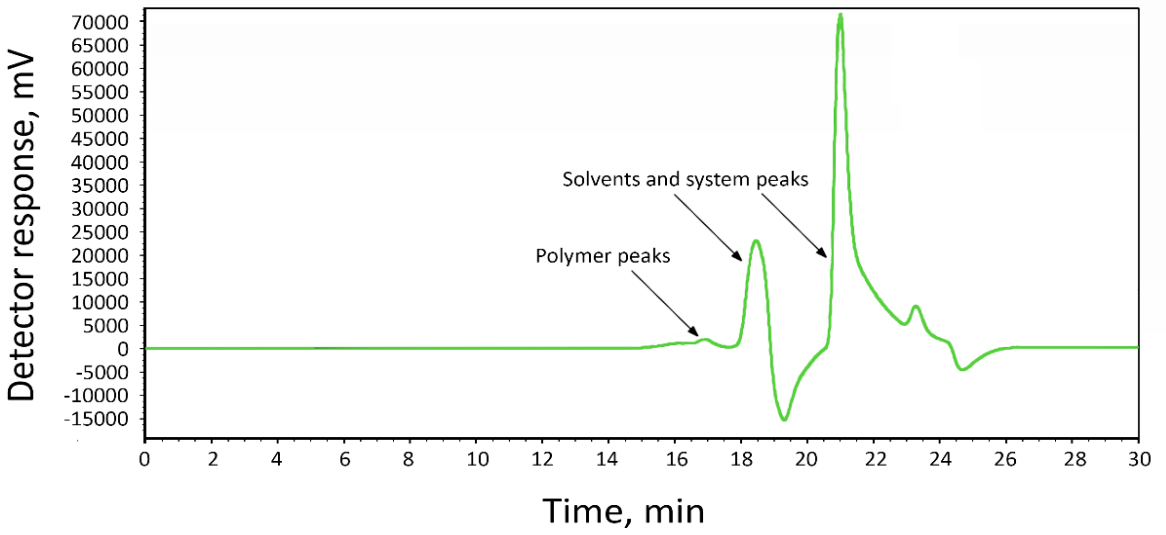

Fig. 2.10. Poly(CYA-Cl-AMTAZ) chromatogram general view

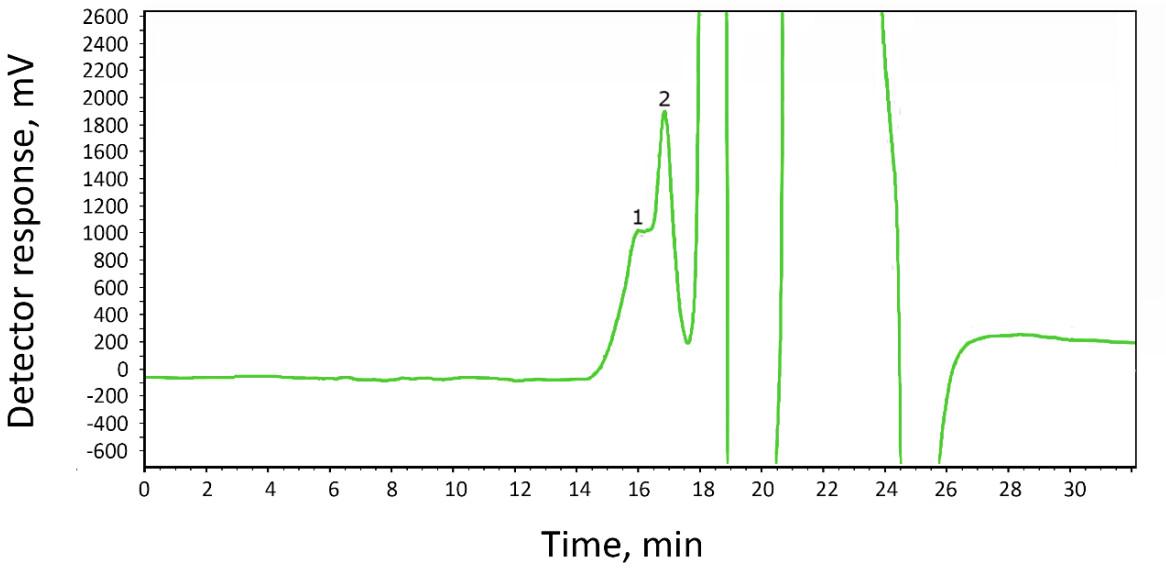

Fig. 2.11. Poly(CYA-Cl-AMTAZ) chromatogram scaled to show polymer peaks

Fig. 2.10 and Fig. 2.11 represent the general view and the scaled product peak signal for poly(CYA-Cl-AMTAZ). Intensive peaks after 17.5 min retention are system and solvent peaks, while the polymer appears as weak signal at around 17 min. The molecular weight data for the peaks is provided in the Table 2.2.

Table 2.2. Poly(CYA-Cl-AMTAZ) molecular weight data.

Polymer	**Mn (Da)**	**Mw (Da)**	**Mp (Da)**	**Đ**
poly(CYA-Cl-AMTAZ)	1+2. 78697	1+2. 91041	1. 84706 2. 64875	1.157

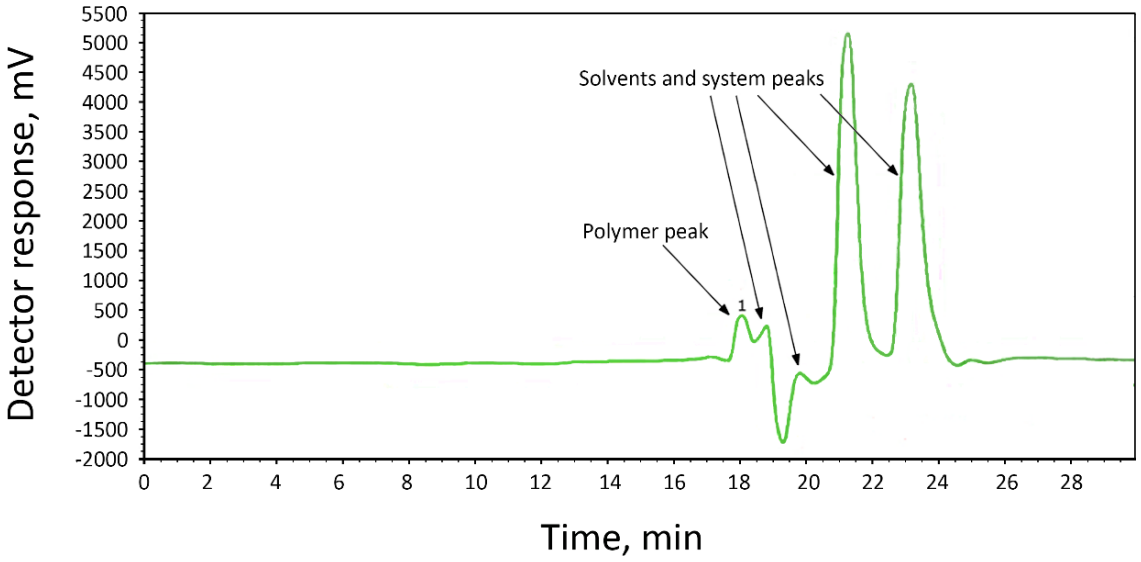

Fig. 2.12. Poly(CYA-Cl-AMCARTRIA) chromatogram.

Fig. 2.12 represents the chromatogram obtained for poly(CYA-Cl-AMCARTRIA) sample. Data are provided in the Table 2.3.

Table 2.3. Poly(CYA-Cl-AMCARTRIA) molecular weight data.

Polymer	**Mn (Da)**	**Mw (Da)**	**Mp (Da)**	**Đ**
poly(CYA-Cl-AMCARTRIA)	552	566	592	1.025

Table 2.4 summarizes the results with molecular masses, corresponding with all peaks believed to be linked with products. Indexes in bold go along with numbers of peaks, provided in the SI.

Table 2.4. Molecular masses, determined by SEC

Polymer	**Mn (Da)**	**Mw (Da)**	**Mp (Da)**	**Đ**
poly(CYA-Cl-NH) (two peaks)	1. 14460 2. 5840	1. 15600 2. 6130	1. 14500 2. 6120	1. 1.079 2. 1.048
poly(CYA-Cl-AMTAZ) (two nearly merging peaks)	1+2. 78697	1+2. 91041	1. 84706 2. 64875	1+2. 1.157
poly(CYA-Cl-AMCARTRIA)	552	566	592	1.025

2.4. Preparation of polymer precursor coatings from DMAc solutions and FTIR characterization of their annealing at different temperatures

Application of as-synthesized solutions of all three polymers on any thermally stable support (glassy carbon, carbon cloth, Al_2O_3 ceramics plate or Ti foil have been used in our experiments) with subsequent drying at 110 ºC for 24 hours allows evaporating the solvent as well as DIPEA and its hydrochloride (ascertained by drastically reduced intensity of sharp peaks with maximums at 2920 and 2960 cm^{-1} in FTIR spectrum, corresponding with the absorption of DMAc and DIPEA species, as discussed below in this chapter) and obtaining smooth, well-adhered films. In order to examine the process of thermal transformation of the precursors, the films applied on glassy carbon plates were subjected to pyrolysis in Ar atmosphere. The temperature range that is practically used for pyrolytic synthesis of carbon nitride materials is well established and relatively narrow, according to all the cited literature sources [1, 3, 4, 5, 6, 8, 10, 11, 19, 21]. When using melamine or dicyandiamide as starting materials, condensation to melem (2,5,8-triamino-heptazine) and similar oligomeric intermediates is typically believed to start at about 350 ºC [1, 18]. Temperatures above 700 ºC are commonly reported to cause decomposition of most carbon nitride materials. In our experiments, in agreement with the latter, pyrolysis at temperatures exceeding 650 ºC always resulted in disappearance of coating.

In all experimental runs, the standard pyrolysis procedure started from annealing the sample at 200 ºC for 1 hour, followed by ramping the temperature at 1 ºC per minute to the desired temperature – 300, 350, 400, 450, 500 or 550 ºC. Non-annealed films spectra were recorded after standard drying (110 ºC for 24 hours in air). The spectra recorded for all three precursor polymers as well as for the annealed materials derived therefrom show peculiar similarity in the position of peaks, albeit the intensity of absorption steadily decreases with increase of pyrolysis temperature.

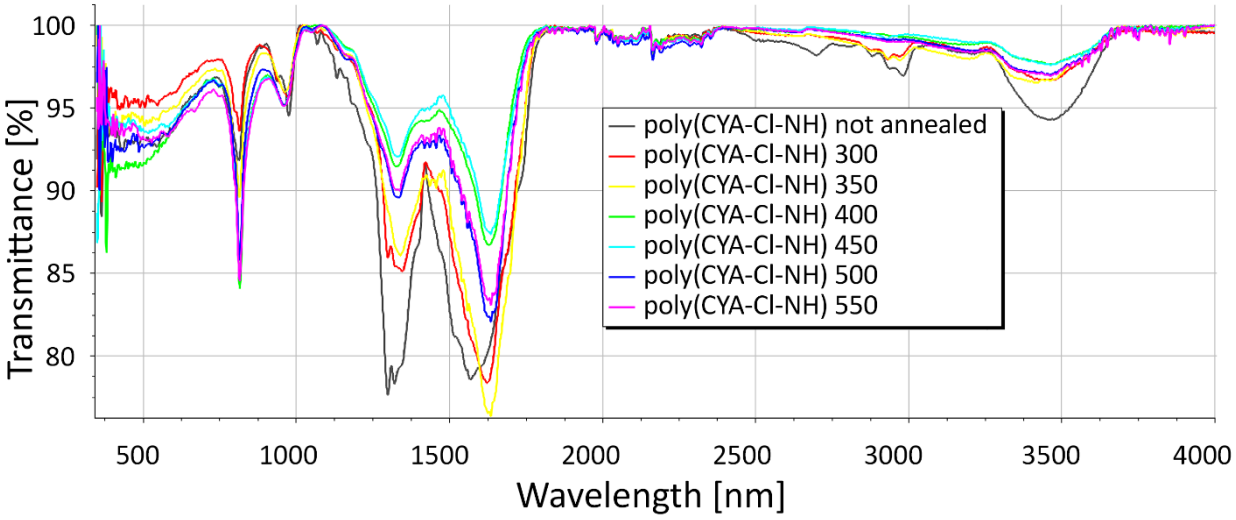

Fig. 2.13. Infrared spectra of poly(CYA-Cl-NH) films on vitreous carbon support, annealed at different temperatures

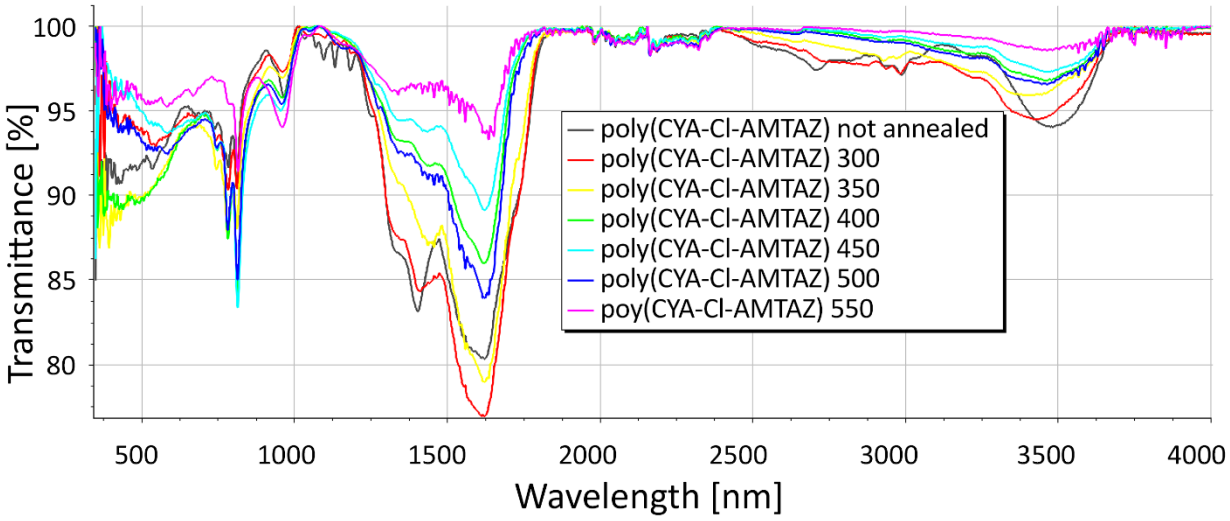

Fig. 2.14. Infrared spectra of poly(CYA-Cl-AMTAZ) films on vitreous carbon support, annealed at different temperatures

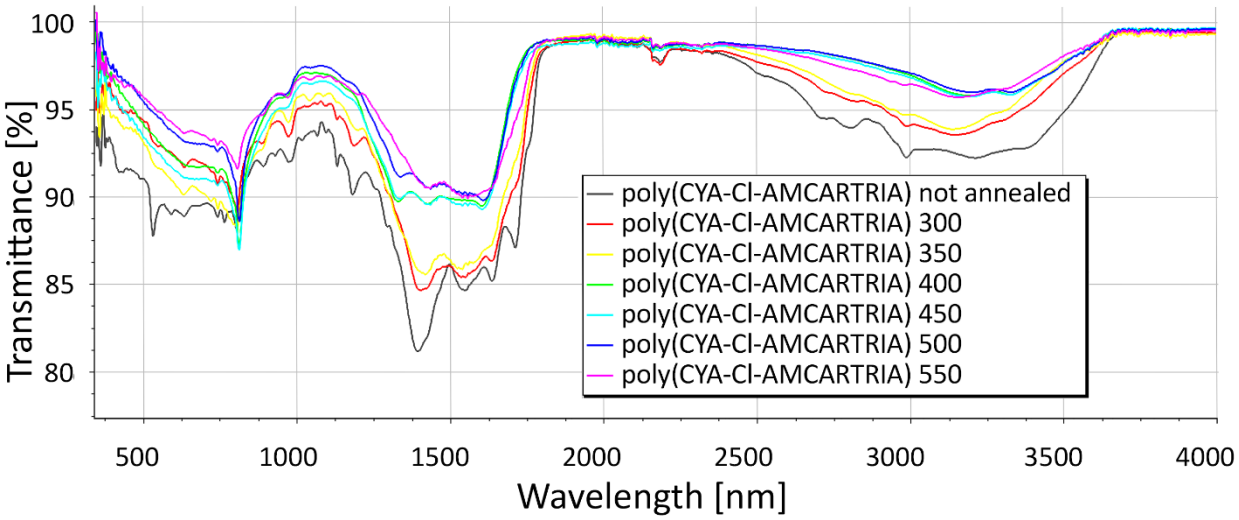

Fig. 2.15. Infrared spectra of poly(CYA-Cl-AMCARTRIA) films on vitreous carbon support, annealed at different temperatures

As can be seen from the spectra provided (Fig. 2.13 – 2.15), all the precursor polymers as well as films obtained by their annealing, show wide high-intensity band composed by overlapping peaks in between 1450—1800 cm^{-1}, diffuse absorption region placed between 2600 and 3700 cm^{-1} and sharp peak around 816 cm^{-1}. Two small sharp peaks at 2920 and 2960 cm^{-1}, disappearing after annealing at 400 ºC or above, were assigned to the remaining DMAc and DIPEA species, respectively, decomposing at high temperatures.

The DMAc and DIPEA salt characteristic peaks were acquired by preliminary recording the corresponding spectra of pure DMAc and DIPEA*HCl samples. These

absorption maximums with much higher intensities appear in the spectra of films, dried at lower temperatures or lesser time.

2.5. Thermogravimetric characterization of polymers annealing

For the purpose of TGA characterization, DMAc as-synthesized solutions of all three precursor polymers were placed in Petri dishes with liquid layer thickness of about 1 mm and dried in air at 110 ºC for 20 days in order to provide a maximum possible efficiency of DMAc and DIPEA species removal. It was previously found out in our experiments that DMAc/DIPEA/DIPEA·HCl solution with the ratio of components similar to that found in as-synthesized polymer solutions, completely evaporates at this temperature and in the same layer within 12 hours.

Taking into account previously mentioned disappearance of all polymeric films at annealing temperatures exceeding 650 ºC, we have recorded TGA in the temperature range from 70 ºC to 700 ºC (Fig. 2.16).

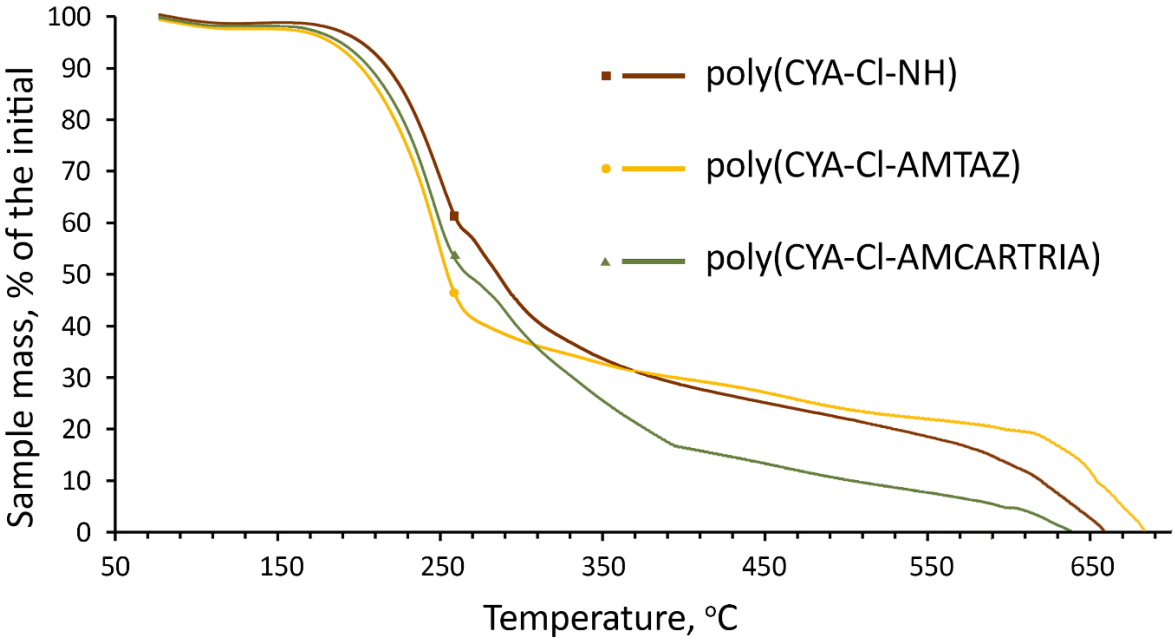

Fig. 2.16. TGA curves for the three precursor polymers

For all curves, at temperatures below 160 ºC, only minor depletion of mass has been observed, presumably linked to evaporation of traces of DMAc and DIPEA/DIPEA·HCl.

Albeit additional research is needed to explore the pathway of decomposition, it can be assumed that the pattern of mass loss in the interval from 180 to 260 ºC, nearly identical for all the three materials, is related to the decomposition of the polymer-bound DIPEA, i.e. DIPEA serving as counter-cation for the polymer and hence not sublimed in the DIPEA-HCl form during preliminary drying.

At higher temperatures, the actual transformation of polymer chains supposedly starts. Increased mass loss dynamics demonstrated by poly(CYA-Cl-AMCARTRIA) above 300 ºC can be related to decarboxylation of the precursor.

Although it would have been logical to expect the poly(CYA-Cl-AMTAZ) precursor to exhibit comparatively quicker decomposition or/and lower onset temperature due to presence of unstable tetrazole ring, its actual mass loss curve have not demonstrated any significant differences from other polymers. It goes in line with the observation already made in the FTIR spectra analysis, supporting the assumption that tetrazole cycle stability in triazineimide-linked polymers is fairly high in comparison with monomeric tetrazole compounds.

All preliminary transformations terminate above 400 ºC for all the three polymers, with subsequent process likely corresponding to steady decomposition of already formed carbon nitride product, which goes in line with minor FTIR spectra changes above this point. This process accelerates above 600 ºC, resulting in complete disappearance of all materials in the temperature range from 640 to 690 ºC.

2.6. Elemental analysis

Elemental analysis was performed on samples, prepared according to the same procedure as used for TGA. The results for mass % contents of C, N and H are provided in the Table 2.5.

Table 2.5. Elemental analysis results for the synthesized polymers

Precursor polymer	**C (wt%)**	**N (wt%)**	**H (wt%)**	**Others (wt%)**	**Formula**
poly(CYA-Cl-NH)	51.40	47.31	0.71	0.58	$CN_{0.79}H_{0.17}$
poly(CYA-Cl- AMTAZ)	48.35	49.26	0.48	1.91	$CN_{0.87}H_{0.12}$
poly(CYA-Cl-AMCARTRIA)	54.22	42.12	2.08	1.58	$CN_{0.67}H_{0.46}$

It was expected that the remaining mass of samples to be represented mainly by chlorine and oxygen. Although the elemental analysis procedure did not allow us to determine these elements, we attempted to estimate their content using FSEM-integrated EDX spectrometry. EDX spectrometry can only be viewed as a rough semi-quantitative technique for light elements such as C, N and O, while typically providing more reliable results for Cl. Although the figures were fluctuating boldly between samples, for all the measured instances of films the atomic % contents of carbon and nitrogen, calculated in the assumption of zero hydrogen content due to inability of EDX to detect hydrogen, were in ranges 45-52 at% and 31-45 at%, respectively, thus being well in agreement with elemental analysis data. For chlorine (also in

the assumption of zero hydrogen content) the values were measured to be in the range 0.2-0.4 at% for poly(CYA-Cl-NH) samples and 0.5-0.9 at% for poly(CYA-Cl-AMTAZ) and poly(CYA-Cl-AMCARTRIA). Oxygen content for all the samples fluctuated in the 0.3-0.6 at% range regardless the precursor, but increasing noticeably for samples kept in air before measurement.

Thus, it can be concluded that values, obtained in the course of EDX measurements, although lack accuracy, allow stating that all the remaining mass of the samples can be explained by presence of relatively small amounts of chlorine and oxygen. The oxygen (and hence hydrogen) contents are at least partially related to the presence of absorbed water, so measurement procedure with complete moisture protection is to be implemented for precise determination of oxygen and hydrogen. Higher apparent content of hydrogen in poly(CYA-Cl-AMCARTRIA)-derived films is probably related to increased water absorption rate of this film.

2.7. UV-Visible diffuse reflectance spectroscopy and optical bandgap determination

Films, annealed in Ar atmosphere, derived from all three precursors on Ti foil support without secondary treatment were taken for characterization. The represented spectra are baseline-corrected, $BaSO_4$-coated white standard plug used for recording the baseline. Pure Ti foil DRS has been determined and have shown more efficient reflection than the standard $BaSO_4$ plug which resulted in values exceeding 100% for Ti reflection.

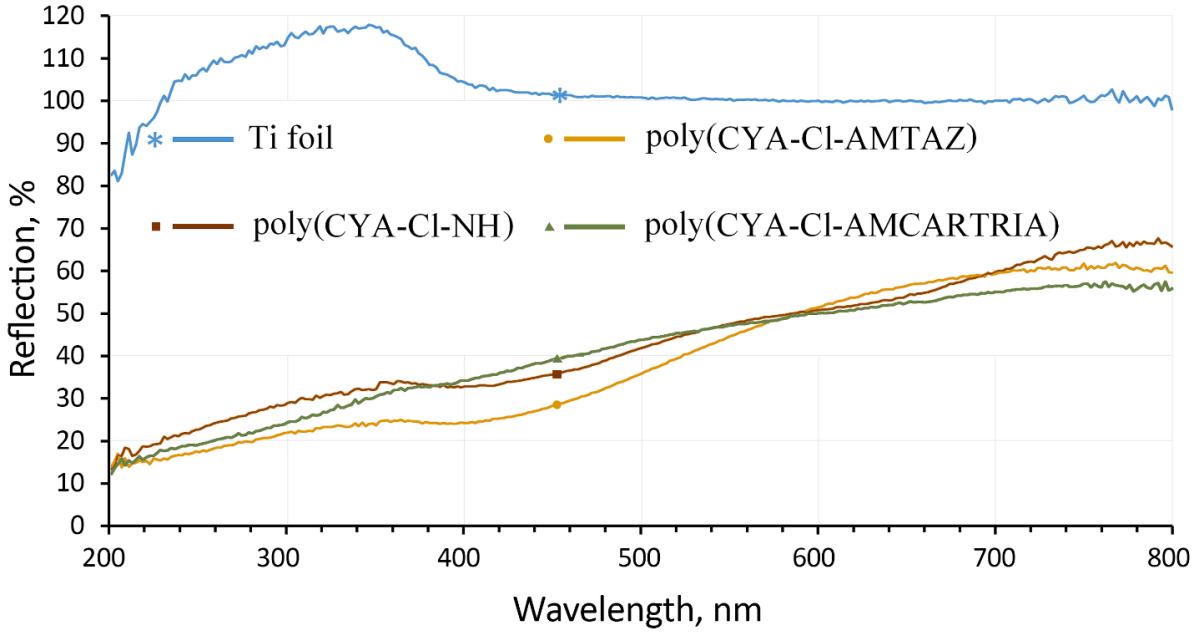

Fig. 2.17. UV-VIS DRS for annealed coatings on Ti support

As can be observed in the Fig. 2.17, all polymers demonstrate very similar UV reflection behavior. Optical bandgaps for three polymer-derived materials were determined by outlining the corresponding Tauc plots.

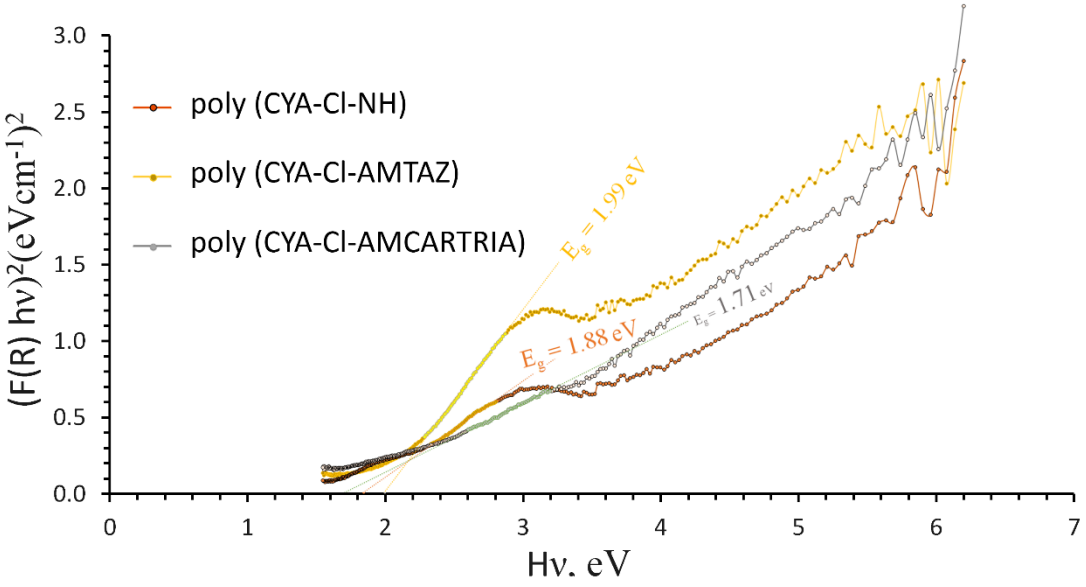

Fig 2.18. Tauc plot, used for optical bandgap calculations, and the corresponding values

The optical bandgaps were calculated to be 1.88, 1.99 and 1.71 eV for poly(CYA-Cl-NH), poly(CYA-Cl-AMTAZ) and poly(CYA- Cl-AMCARTRIA), respectively. These values are way below the bandgap of graphitic and polymeric carbon nitride, typically reported to be 2.8-2.9 eV [4,5], and correspond with visible light excitation (623 to 725 nm). Hence, all the materials can be regarded as low-bandgap semiconductors.

We suppose that the reduced bandgap values are related to carbon doping of the films. It can easily be noted that the bandgap correlates with the content of nitrogen in the annealed sample, with poly(CYA-Cl-AMTAZ)-based sample 49.26% N wt. demonstrating the highest bandgap (1.99 eV), followed by samples based on poly(CYA-Cl-NH) with 47.31 % N wt. and 1.88 eV and, finally, on poly(CYA-Cl-AMCARTRIA) containing 42.12% N wt% and showing the lowest bandgap of 1.71 eV. For such a low bandgap range, noticeable dark conductivity can be expected.

2.8. SEM, TEM and STM characterization

SEM of all annealed films demonstrate non-informative, extremely smooth surfaces. For this reason, SEM images are not provided.

TEM of films, mechanically scratched out of Ti support, reveals their hazy structure with small nebulous clumps. No obvious distinction between films, derived from different precursors, has been mentioned.

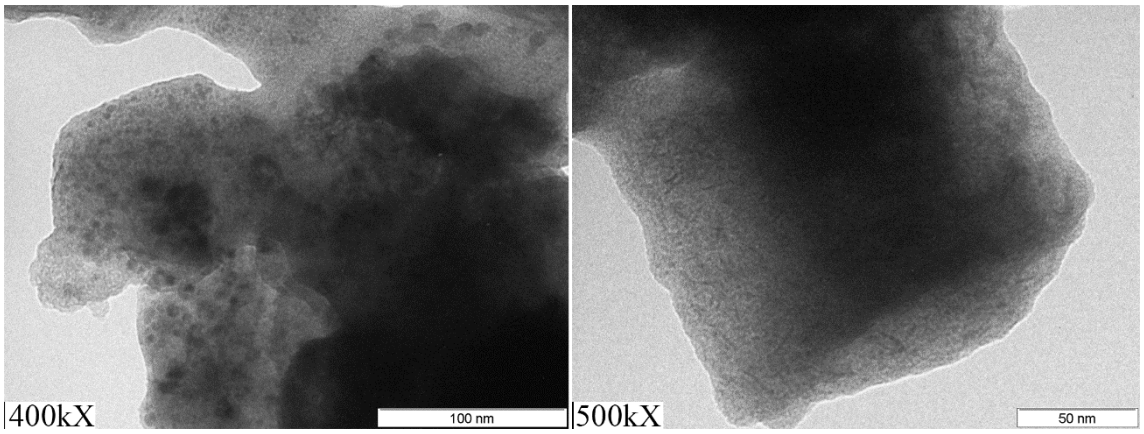

Fig. 2.19. Poly(CYA-Cl-AMTAZ)-based films, annealed at 550 °C, TEM at 400 kX and 500 kX magnifications (kX stands for thousand times).

High-resolution STM microscopy (Fig. 2.20), carried out in non-contact mode in ambient conditions, supports the conviction that surface of all the films is smooth down to the level of hundreds nanometers. At higher magnification the FM mode scans show wave-like protrusions on the surface sized in the range of dozens of nanometers and small (2-5 nm) ripple, which can be related to chaotically packed protuberances of melon-like nanoribbons. STM images of glassy carbons, existing in the literature [24, 25], support this point of view, demonstrating similar granular, fiber-like or groove-like nanostructures on their surface, although typically of marginally larger size.

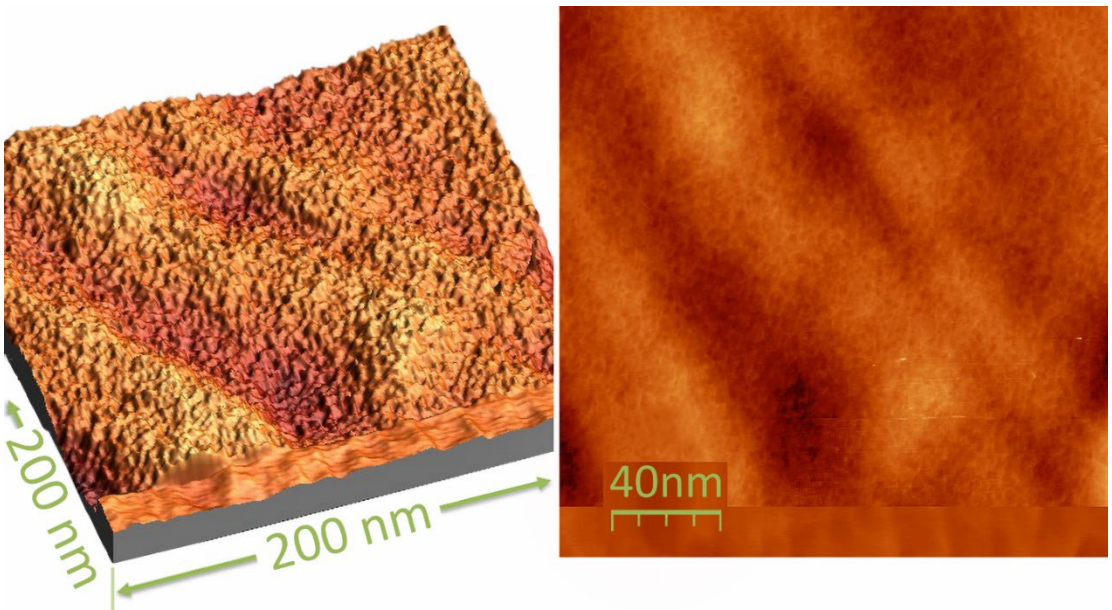

Fig. 2.20. High resolution STM images of poly(CYA-Cl-AMTAZ) film on Ti substrate, annealed at 550 °C

2.9. XRD of annealed films and glassy carbon powder reference

As it was previously shown in TGA experiments, drying and subsequent pyrolysis of polymeric precursors in thick layers (more than 200 µm after solvent drying) implies incomplete evaporation of DMAc and DIPEA species, typically leading to altered structure and mechanical properties.

For this reason, samples for XRD characterization were prepared by means of spreading as-synthesized solutions of polymers on 100 µm Ti foil with subsequent drying for 24 hours at 110 ºC and annealing in Ar with starting temperature of 200 ºC, final temperature of 550 ºC and 1 ºC/min ramp. The resulting coating thickness was in the range from 30 to 55 µm according to microscopic measurement. The annealed foils with carbon nitride coatings were then dissolved in 5% hydrofluoric acid at room temperature, the exfoliated carbon nitride flakes washed with deionized water to neutral pH and dried on paper filter at 110 ºC in air for 24 hours. They were grinded before XRD characterization, although due to extreme mechanical resilience of films, the shape of the resulting particles remained lamellar with 10-15 µm average diameter. Glassy carbon powder (grinded from glassy carbon rod, Alfa Aesar) was used as reference material with confirmed turbostratic structure.

The references, cited in this chapter (2.8) and related to XRD characterization, are provided separately at the end of the chapter.

2.9.1. Measurement conditions

The angular 2θ diffraction range was between 5 and 70º. The data were collected with an angular step of 0.05º at 3 s per step and sample rotation. A low background Si(510) wafer was used as sample holder. Cuk α radiation was obtained from a copper X-ray tube operated at 40 kV and 30 mA.

2.9.2. Profile fitting

Profile fitting was performed with the TOPAS v6 software (Bruker AXS GmbH, 2017) (Coelho, 2018). The background was fitted with a 2nd order Chebyschev polynomial. The instrumental contribution to the diffraction profile was calculated with the Fundamental Parameters Approach (Cheary, Coelho, & Cline, 2004). The peak width of each phase was modelled with the Double-Voigt Approach (Balzar, 1999) by considering only the Lorentzian contribution of the crystallite size effect and discarding any contribution of the microstrain to the peak width. The averaged integral breadth was obtained from the resulting fitted Voigt function to the whole diffractogram. The Scherrer equation (Stokes & Wilson, 1942) was then applied to obtain the apparent crystallite size.

2.9.3. Measurements results and their interpretation

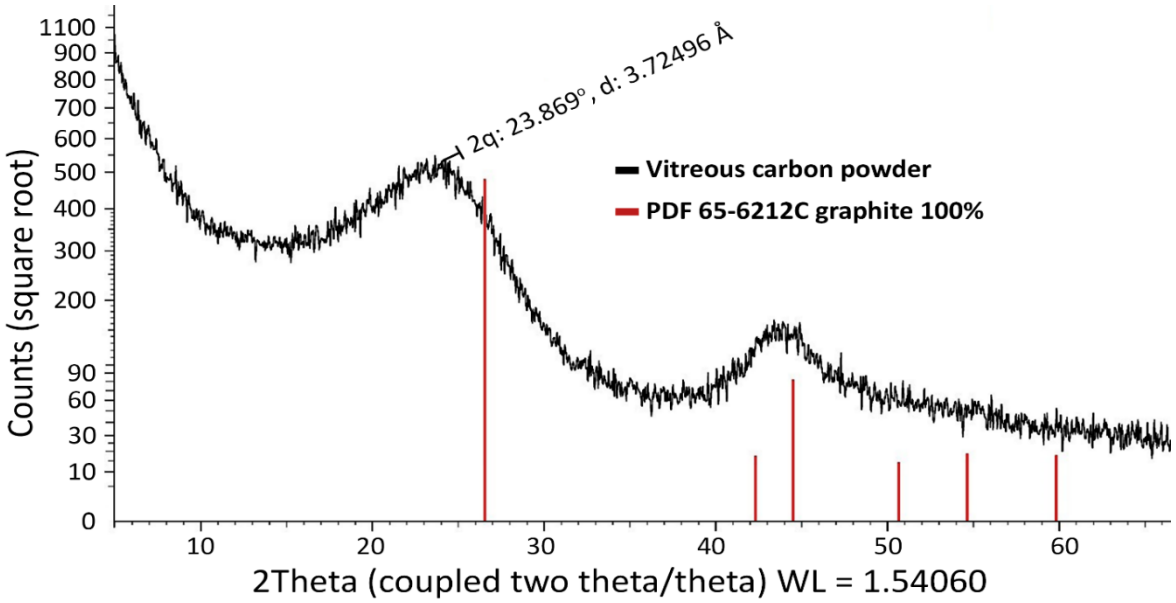

Fig. 2.21. XRD spectra of HF-detached films, annealed at 550 °C

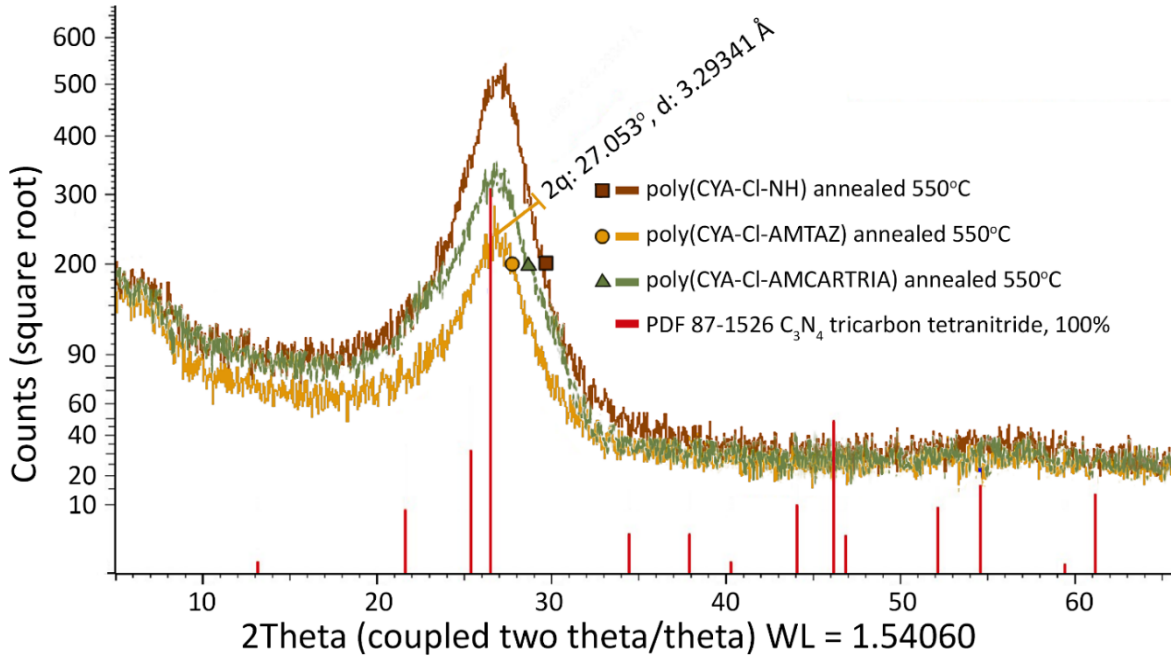

Fig. 2.22. XRD spectra of glassy carbon powder

The X-ray diffraction patterns of all the three annealed films, given in the Fig. 2.21, demonstrate evident similarity, with one diffuse peak centered at 27.05º and well-corresponding with characteristic (002) plane reflection of theoretically considered fully polymerized hexagonal carbon nitride, typically ascribed as arising from interlayer reflection. The absence of other relatively weak reflections, described for graphitic carbon nitride, e.g., from planes (100), (600) or (004) [20], has been related to flat shape of

particles that resulted in anisotropicity of the sample.The glassy carbon powder diffraction pattern, provided in the Fig. 2.22, corresponds well with previously reported results. The main peak at 23.87º and lower intensity maximum at 44.14º are typically found in similar positions in glassy carbon difractograms and are usually ascribed as (002) and (100) indices of graphite lattice, respectively [26].

The main (002) reflections have similar shapes in both polymer-derived carbon nitride and glassy carbon samples and are cardinally widened when compared to corresponding reflexes of graphitic carbon nitride [27] and graphite powder, respectively. In the glassy carbon case, this widening is explained by most authors in terms of semi-cristalline or so called turbostratic structure of the latter: the material arrangement can be represented as ribbons or globules of ordered graphene-based phase immersed in amorphous carbon matrix.

If the same model is applicable to our novel polymer-derived carbon nitrides, the average size of ordered units in their structure can be calculated by fitting Voigt function and finally using Scherrer equation to obtain the sizes of crystallites (calculation details in the SI). From this approach, the following values of apparent crystallite sizes were obtained: 1.89 nm for poly(CYA-Cl-NH)-derived film, 1.44 nm for poly(CYA- Cl-AMTAZ)-derived film, 1.47 nm for poly(CYA-Cl-AMCARTRIA)-derived films, 0.89 nm for reference glassy carbon powder. Hence, although more precise experiments are required in order to elucidate the explicit structure of newly synthesized polymer-derived carbon nitride films, their X-ray diffraction patterns allow identifying them as semi-amorphous materials with crystallite sites of the same order of magnitude as in glassy carbons.

2.10. Contact angle measurements

Water wettability of coatings is of immense importance for all applications where films are brought in contact with water-based liquid. Contact angles have been measured by the static sessile drop method for films on Ti foil support, annealed in standard regime with 550 ºC final temperature in Ar and air atmosphere.

Table 2.6. Measured contact angles

Precursor polymer	**Annealed in Ar, degrees**	**Annealed in air, degrees**
Poly(CYA-Cl-NH)	76	31
poly(CYA-Cl-AMTAZ)	48	<20
poly(CYA-Cl-AMCARTRIA)	51	<20

Table 2.6 shows that air-annealed samples demonstrated much lower contact angles, presumably due to oxidative elimination of surface pollution by trace hydrophobic contaminants. In all measurement where contact angles below 20 degrees were recorded, drops have been slowly spreading on the film during the procedure, so the exact value has not been determined.

2.11. Characterization of electrochemical properties of annealed films

UV-VIS DRS measurements concede to characterize all films, annealed at 550 ºC, as low bandgap semiconductors (1.71-1.99eV). The massive difference between these observed values with the bandgap value reported for graphitic carbon nitride, allows considering the newly synthesized coatings to be extrinsic semiconductors with bandgap reduced presumably by carbon doping.

In order to investigate electrochemical parameters of films in a way reflecting their potential practical application, all three solutions of precursor polymers were applied on carbon cloth (CC) electrodes, produced from Alfa Aesar 3.18 mm thick carbon cloth sheets. 3.18x3.18x50 mm electrodes were cut out of the cloth and half-dipped in a vial with as-synthesized solution of precursor polymers. The vial with electrode vas sonicated for 1-2 min to ensure complete wetting of the dipped part, then electrode fixed with coated end downwards in a vacuum chamber and dried in 0.3 Pa vacuum for 12 hours, then in air at 110 ºC for 24 hours. The treated electrodes were annealed at 550 ºC in Ar flow according to the standard heating regime. A control uncoated CC electrode of the same dimensions was annealed in the same conditions.

Electric impedance measurements were carried out by means of EIS spectroscopy. 0.01N $Fe(CN)_6^{3-}$/ 0.01N $Fe(CN)_6^{4-}$/0.1N KCl solution was chosen as redox-buffered electrolyte. Annealed bare CC and film-coated CC electrodes were immersed into solution by 5 mm, forming solid-liquid geometric interface surface of approximately 0.7 cm^2 and immersed electrode volume of about 0.05cm^3, 6 cm^2 Pt mesh has been used as a counter-electrode in all electrochemical experiments. The following EIS experiment parameters were chosen: frequency range from 0.1 Hz to 100000 Hz, 10 points/decade, sinus amplitude 10 mV, direct current (DC) potential 0 mV versus Ag/AgCl/saturated KCl .

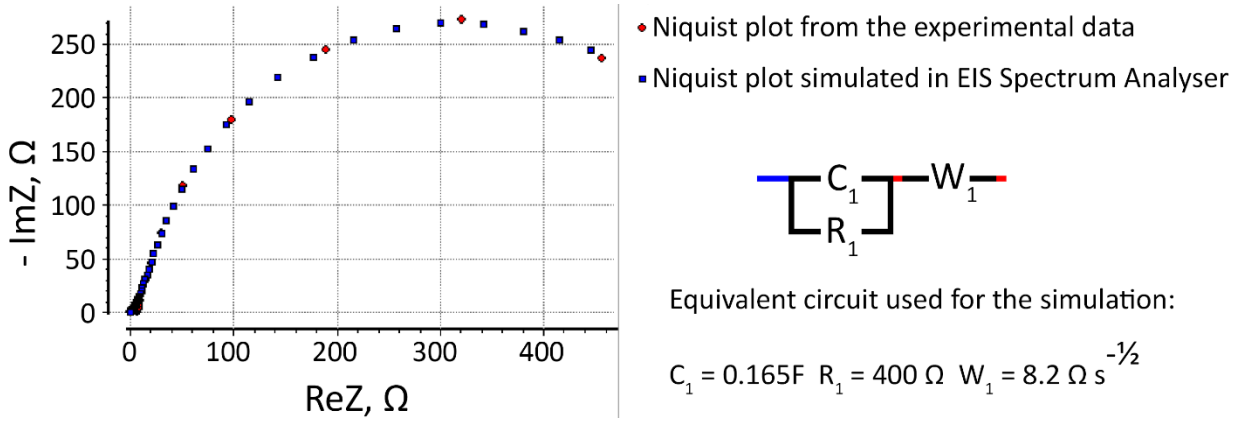

Fig. 2.23. Fitted Niquist plot for poly(CYA-Cl-AMTAZ)-derived coating

As can be seen from Fig. 2.23, almost perfect fitting of the experimental data with the corresponding simple equivalent circuit was achieved. The best-fitting circuit is represented by a capacitor and a resistor connected in parallel together with a serially connected Warburg element.

A control EIS experiment carried out with an uncoated electrode afforded a spectra that was ideally fitted by the same equivalent circuit, with capacitance and resistance of 0.008 F and 13 kΩ, respectively, and Warburg impedance of 270 Ω $s^{-1/2}$. The aerial capacitance of untreated carbon cloth is reported by Yi-Jie Gu et al. [28] and Dong Ye et al. [29] to be 0.96 mF cm^{-2} and 0.8-0.9 mF cm^{-2}, respectively. Both works report treated CC (calcined in air and electrochemically oxidized/reduced, respectively) to have largely higher aerial capacitances with respective maximum values 1136.7 and 505.5 mF cm^{-2}.

The measured aerial capacitance of annealed carbon cloth (0.008 F per 0.7 cm^2 of projected area), or 11.4 mF cm^{-2} can hence be classified as rather low, being only one order of magnitude larger than untreated CC aerial capacitance reported. At the same time, the aerial capacitance of coated electrodes (236 mF cm^{-2}) is comparable with the reported CC-based modified electrodes proposed for super capacitor applications.

The resistance measured for both coated and uncoated CC electrodes, corresponding to the semicircle diameter on the Niquist plots, coincides with the interfacial resistance, while the internal resistance of both cells, given by the high-frequency Z′ value, was in the range of several Ohms. The impedance-frequency behavior of both cells allows assuming their impedance as classically faradaic, with double layer capacitance and redox process-mediated resistance standing for C_1 and R_1 values, respectively, and Warburg impedance probably originating from diffusion kinetics. The effective resistivity on the solid-electrolyte junction of the coated electrodes can be calculated in the assumption of uniform 50 μm coating to be 56 kOhm cm according to EIS, allowing to classify the coatings as conductive rather than semi conductive. Moreover, the intrinsic resistivity of films is most likely fairly lower, as the faradaic resistivity is affected by reaction transfer kinetics.

In order to further elucidate the efficiency of electron transfer through electrode-electrolyte interphase, cyclic voltammetry (CV) curves of annealed bare CC/annealed poly(CYA-Cl-AMTAZ)-coated CC electrodes were recorded in the same Fe^{3+}/Fe^{2+} electrolyte and in the same conditions. To reduce capacitive currents, all scans were operated at low scanning speed of 10 mV/s. For the coated electrode at scanning speed of 50 mV/s the capacitive currents were in the range of dozens mA/cm^2 and resulted in unstable measurement, making the experiment unreliable and further supporting high capacitance of coated electrodes. The results are provided in the Fig. 2.24.

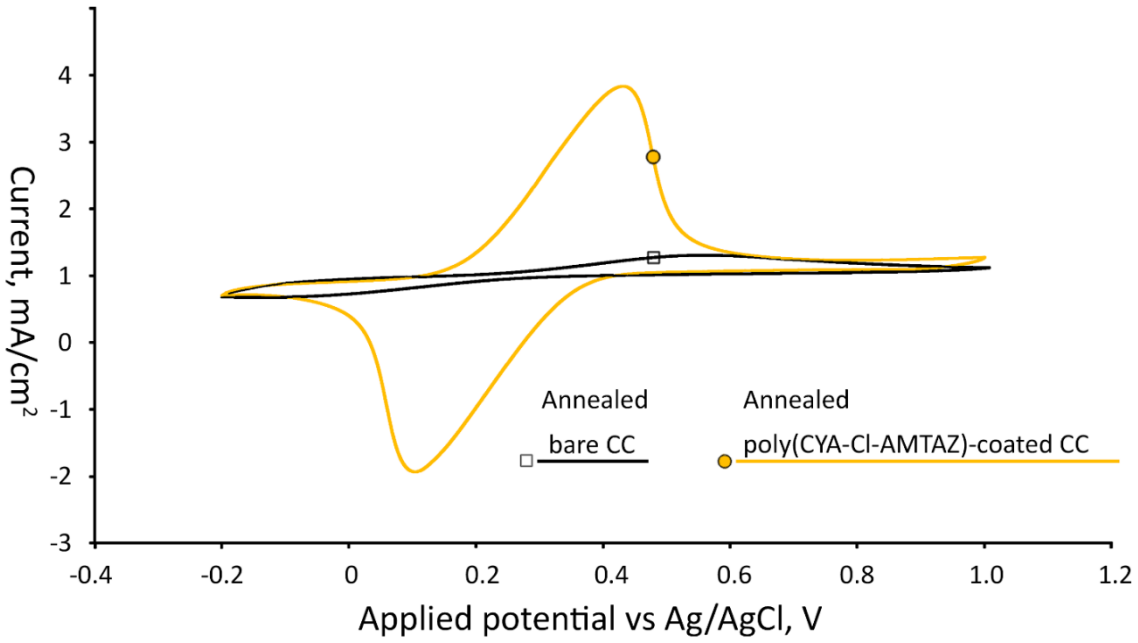

Fig. 2.24. CV scans of bare and coated CC in 0.01N $Fe(CN)_6^{3-}$/ 0.01 N $Fe(CN)_6^{4-}$/0.1 N KCl solution

Surprisingly, although in agreement with high faradaic resistances measured by EIS, annealed bare CC electrodes provided very low specific currents in both oxidation and reduction half-waves. In contrast, all coated CC electrodes developed pronounced half-waves with maximum currents, exceeding 6-7 times the corresponding currents for both oxidation and reduction peaks on untreated CC electrodes.

In order to investigate the electrochemical activity and stability of coatings at high overpotentials in acidic aqueous media, 100 CV scans in 1 N sulphuric acid in the potential range from -1 V to +1.5 V versus Ag/AgCl at 10 mV/s were undertaken. Prior to scanning, the electrodes were conditioned for 10 min at +1. 5V versus Ag/AgCl to eliminate possible surface contamination.

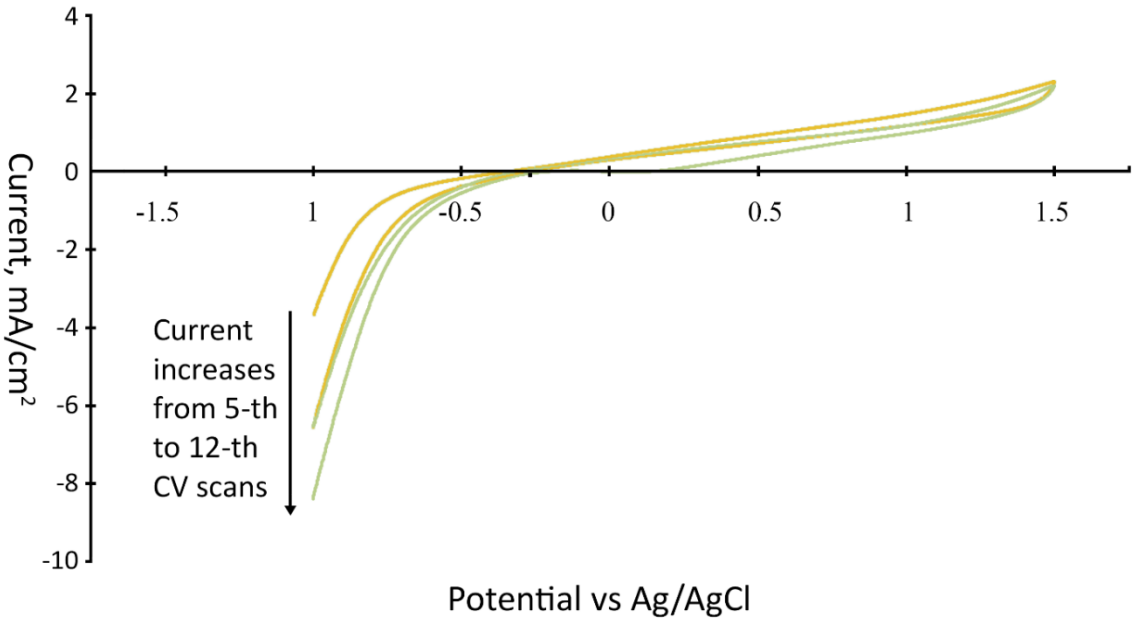

Fig. 2.25. Voltammetric scans for CYA-Cl-AMTAZ-coated electrodes in 1N H_2SO_4

As can be seen from the Fig. 2.25, coated electrodes, after first several scans, demonstrate extremely stable electrochemical behavior. In the negative branch of the CV, currents increase progressively from 1st to 12th scans and stabilize during all the following CV passes with only negligible differences between 12th and 100th scans. Positive currents expose noticeable reproducibility with no apparent changes after first 3 scans. Surprisingly, voltamperograms in sulphuric acid demonstrate low capacitive currents, corresponding to only dozens of μF-level capacitances. Supposedly, it can be related to ion-exchange behavior of carbon nitride coatings, driving considerable elteration of electric double layer structure in dependance on the pH and ionic composition of the electrolyte.

The most intriguing, however, is the presence of noticeable and reproducible anodic current, appearing above -0.25 V vs Ag/AgCl and almost linearly increasing with potential.

Chronoamperometric characterization (Fig. 2.26) of electrodes provides furthermore support for the hypothesis of reversible oxidation and reduction of the surface, demonstrating quick current deterioration with time at applied static potential in both oxidation and reduction modes.

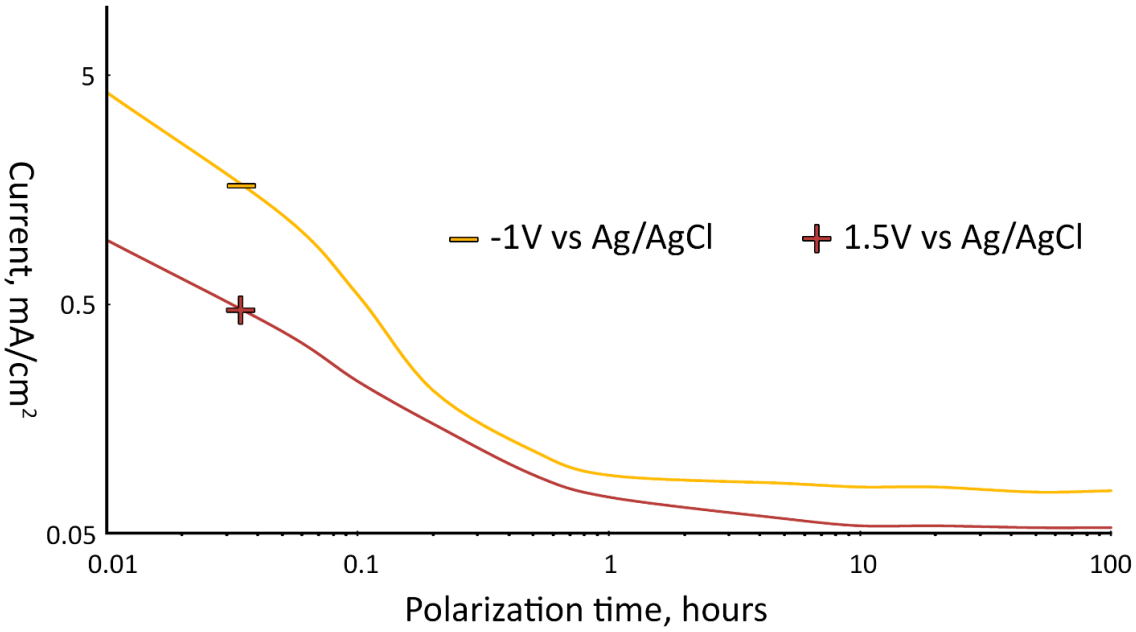

Fig. 2.26. Chronoamerometric curves for poly(CYA-Cl-AMTAZ)/CC annealed at 550 °C at cathodic and anodic polarizations (current modules shown)

2.12. Results and discussion

In this paper, we demonstrate a way to fabricate carbon nitride analogues of glassy carbons by means of pyrolysis of ultra-nitrogen-rich polymeric precursors. The logics behind the selection of possible precursors has been based on an observation that nearly all the compounds, used as precursors for carbon nitride, do not contain C-C bonds, being instead based on C-N or N-N sequences. It seemed reasonable to assume that this could be a critical factor affecting pyrolysis pathway and determining the kinetic selection mechanism for azagraphene/azine based structure instead of graphene-derived structural motifs, represented in «classical» pyrolytic carbons.

Likewise, we wanted the precursor to be a polymer in order to render amorphous or semi-amorphous structure of the annealed material. In the seek for «C-C free» polymers, we synthesized by means of classical polycondensation a linear imide of chlorotriazine (poly(CYA-Cl-NH) and two block-polymers based on triazine/tetrazole poly(CYA-Cl-AMTAZ) or carboxytriazole (poly(CYA-Cl-AMCARTRIA), respectively. The latter, although containing a C-C bond linking the carboxylic group, can be viewed a C-N polymer due to decarboxylation, presumably taking place before main pyrolysis steps.

All these polymers exhibit excellent solubility in aprotic solvents in the form of DIPEA salts, directly obtainable from syntheses. According to the ^{1}H NMR spectra and titration results, poly(CYA-Cl-AMTAZ) and poly(CYA-Cl-AMCARTRIA) are strongly acidic and appear to exist in DMAc solution in the form of corresponding DIPEA salts with

imide protons fully dissociated and showing up in the ^{1}H spectrum as DIPEA·H^{+} signals, while poly(CYA-Cl-NH) possesses less acidity, coexisting with free DIPEA in the solution. The alternative explanation of free DIPEA existence in the poly(CYA-Cl-NH) case could be incomplete condensation reaction with oligomeric products, although this point of view is not supported by SEC results and by the absence of signs of amino-signals of the monomer or oligomers in the ^{1}H spectrum.

From the SEC chromatography data it can be concluded that poly(CYA-Cl-NH) and poly(CYA-Cl-AMTAZ) are high molecular weight polymers with two maximums in the molecular mass distribution. The poly(CYA-Cl-AMCARTRIA), according to SEC results, should be considered as oligomer containing on average 2 triazine-NH-carboxytriazole units. This presumption, however, goes in contradiction with the previously mentioned (similarly to the CYA-Cl-NH case) absence of any noticeable signals in the ^{1}H NMR spectra that could be related to the presence of amino or imino hydrogens of free triazine monomer or oligomers.

IR spectra of all the synthesized polymers reveal their structural similarity with "classical" carbon nitride materials as well as annealed films obtained therefrom, albeit with several specific absorption maximums. The spectrum of poly(CYA-Cl-AMTAZ) demonstrates a noticeable adsorption at 783 cm^{-1}, which gradually fades upon annealing of the polymer and does not show up in the spectra of poly(CYA-Cl-NH) and poly(CYA-Cl-AMCARTRIA) or annealed films obtained from these polymers. According to the IR spectra of substituted 1,2,3,4-tetrazoles, published in the literature, this signal can be viewed as characteristic for tetrazole systems. For instance, it appears at 790.47 cm^{-1} for 5-phenyl-1H-tetrazole, at 791.77 cm^{-1} for 5-(4-hydroxyphenyl)-1H-tetrazole, at 778.32 cm^{-1} for 1-(3-bromophenyl -1H-tetrazole [14].

Accordingly, almost complete disappearance of this peak at 550 ºC for poly(CYA-Cl-AMTAZ) can be attributed to full decomposition of tetrazole precursor at this temperature – a surprisingly high thermal stability for tetrazoles, especially in comparison with the monomeric 5-aminoterazole [15].

The intensive asymmetric shoulder placed between 1270 and 1400 cm^{-1} for poly(CYA-Cl-NH) and 1200-1500 cm^{-1} for other two polymers is essential for understanding the spectra.

In the family of films derived from poly(CYA-Cl-NH), two maximums of this peak are originally observed at 1295 cm^{-1} and 1320 cm^{-1} and, upon heating, decrease and move towards steadily to produce one bell-shaped maximum at 1330 cm^{-1} for the film, annealed at 550 ºC. In the case of poly(CYA-Cl-AMTAZ), this band shows up at 1402 cm^{-1} for the source polymer and, upon annealing, quickly decreases in intensity and moves to higher wavenumbers to finally disappear at 550 ºC.

Spectra of poly(CYA-Cl-AMCARTRIA) films exhibit widened peaks with few characteristic features. Expectably, non-annealed film demonstrates C=O vibration at 1707 cm^{-1}, disappearing already when pyrolized at 350 ºC . A small peak at 2985 cm^{-1}, corresponding presumably to -OH vibrations of -COOH groups, fades at pyrolysis above 350 ºC. Thus, FTIR data for poly(CYA-Cl-AMCARTRIA) support the presumption that this polymer easily decarboxylates in relatively mild heating conditions.

With the goal to assign the spectral features appearing in the spectra of carbon nitride (CNx) films, we compared the spectra of films, measured in this work, with published FTIR data on monomeric triamino s-triazine (melamine) and triamino tri-s-heptazine (melem) along with spectra of other materials of carbon nitride family, believed to consist of triazine, heptazine or mixed structural motifs.

The work on vibrational-mode assignment for IR spectra of crystalline and gas phase melamine performed by Yuan et al. [16] reasserts the assignments reported by other authors, for instance referring the vibrations at 1424 cm^{-1} and 1577 cm^{-1} with the HCN and NH_2 bending coupled with ring deformation and CN stretching or CN stretching and NH_2 bending, respectively.

This finding supports the hypothesis that the shoulder showing up between 1270 and 1400 cm^{-1} and gradually disappearing when annealing temperature increases, can be related to free -NH_2 and other H-containing functionalities, depleting with heating.

Comparison of melamine spectrum with IR spectra of monomeric alkylamides of heptazine, published by Zambon et al. [17], along with IR characterization of melem, performed by Jürgens et al. [18], allows to outline the same pattern in all studied spectra of monomeric compounds: appearance of two intensive absorption maximums in the proximity of 1430 cm^{-1} and 1530-1600 cm^{-1}, respectively, with a pronounced low absorption region between them.

Notably, four polymeric CN_x materials synthesized by means of solution-based reactions of cyanuric chloride with nitrogen sources, reported in the literature ([5,12,19,20]), demonstrate the same tendency to possess an absorption gap between two intensive peaks in the area. On the other hand, the spectrum of G-C_3N_4 presented by Li et al. [21], along with spectra of melon [4] and other CNx polymers reported to be based at least partially on heptazinic structural units ([19,22]), exhibit multiple peaks or continuously filled absorption band in the range from 1430 cm^{-1} to 1530- 1600 cm^{-1}.

It should be noted that previous studies on interpretation of IR spectra of amorphous CNx films, performed by Ferrari et al. [23], led them to conclude that the entire region between 1000 and 2000 cm^{-1} should only be assigned to skeletal vibrations due to insensitivity of local maximums in this region to deuteration of film.

However, considering intensive absorption in this range demonstrated for monomeric triazines and heptazines, it remains contentious if these conclusions are applicable to

azine-based polymers. Nevertheless, taking into account the fact that monomeric heptazines do not show any characteristic absorption nearby 1430 cm^{-1} but all heptazine-containing polymers exhibit characteristic absorption in this area, we suppose that this maximum is related to vibrations of π-delocalized polymeric system based on heptazinic framework – purely skeletal or combined with bending of substituting groups.

Another curious observation relates to the notable sharp peak always appearing in FTIR spectra of both triazine and heptazine-based materials at around 800 cm^{-1}, assigned by Yuan et al. [16] to ring out-of-plane deformation (808 cm^{-1}). According to our examination, in all spectra of triazine-based materials, hitherto reviewed as presenting an absorption gap in between 1430 and 1530 cm^{-1} and described in their research as triazine-based, this sharp peak appears in the range from 808 to 820 cm^{-1}. In the materials believed to be based on heptzinic framework, this peak shows up in the 780-802 cm^{-1} region.

Hence, although the difference in the position of this vibration is small, it might be helpful in distinguishing between triazine- and heptazine-based structures. Interestingly, all reported amorphous carbon nitride films, obtained by means of reactive sputtering, do not demonstrate this signal in their IR spectra. This may be an additional indication in favor of the viewpoint that these materials do not contain imide bringing nitrogen and rather represent graphite-like structures with partial substitution of carbon by nitrogen.

DMAc solutions of all three polymers can easily be applied on different solid supports by most of conventional coating methods and make well-adhered films upon evaporation of the solvent. Presumably, DIPEA plays a critical role, rendering solubility of all the synthesized precursors by forming their salts, as it was demonstrated by NMR spectroscopy. Simultaneously, difficulties with DIPEA removal during films drying prior to their pyrolysis, confirmed by FTIR, results in inevitable doping of the resulting coatings with carbon, arising greatly reduced optical bandgaps (according to Tauc plot analysis) and relatively high conductivity.

The hypothesis of significant doping by carbon of the resulting coatings was further supported by the elemental analysis data. Although the content of nitrogen in the annealed films is extremely high for the scale of nitrogen-rich carbons, it is significantly lower than the content of nitrogen in “classical” nitrides of carbon. XRD and microscopic characterization data both allow to consider the annealed films as semi-amorphous materials, smooth down to the level of dozens of nanometers. Although some signs of existence of nanometer-sized structural units have been observed, the evidences collected during the present study does not allow to characterize this structure.

Measured electrochemical characteristics of the annealed films undoubtedly make them engaging coatings for applications, involving the requirements of low electrical resistance, high electrochemical stability and high capacitance. Although the elucidation of supercapacitive properties of the coated carbons was not in the focus of the current

study, the obtained capacitance value of 236 mF cm^{-2} allows proposing the newly synthesized coatings for further capacitors-related research.

The most remarkable finding, however, is the combination of outstanding long-term electrochemical stability with high and reproducible anodic currents.

For graphitic carbon, the phenomenon of relatively high currents at positive polarizations well below the OER onset potentials is well described in the literature. For instance, Yi et al. [30] relates this observation to electrochemically active surface groups assuming formation of surface oxides in the course of surface oxidation with oxidation/reduction peak maximums at 0.6 V and 0.5 V versus RHE, respectively. This and other previous works even describe peeling off the formed oxidized carbon layer in the form of nanoflakes or soluble polycyclic compounds, resulting in yellow-brown color change of electrolyte easily observable with polarization time. In contrast, no changes of electrolyte color during long-term polarization of carbon-nitride-coated electrodes was observed even after tens of hours of polarization at potentials exceeding 1.5 V versus Ag/AgCl.

Our explanation of these observations includes reversible formation of carbon nitride oxide on the surface of the electrodes. Although further research is required to elucidate the precise surface chemistry of new electrode materials, it seems reasonable to assume that oxidized surface layers, in contrast with surface oxides formed on glassy carbon, are not detached from electrodes surface into electrolyte and undergo further reduction at negative scanning potentials. Thus, the negative current appearing below -0.3 V may at least partially correspond to surface groups reduction and not HER.

In this light, it worth mentioning that visible hydrogen evolution on coated electrodes does not happen during the first minutes even at high negative polarizations, corresponding to cathodic currents as large as 8 mA/cm^2. This observation further supports this hypothesis of pre-oxidized coating reduction. After some period of time at high negative polarization, bubbles of hydrogen can be observed, supposedly signaling the end of reduction process.

On the other hand, oxygen evolution at high anodic polarizations takes place easily, thus showing that material oxidation probably easily kinetically competes with the O_2 evolution reaction.

The observed voltamperograms shapes without any conspicuous peaks can be explained in terms of high diversity of surface groups energy states and/or their kinetic availability, corresponding to a continuum of apparent redox potentials.

2.13. Conclusions

Three novel linear 1,3,5-triazineimides have been synthesized by self-condensation of 2-amino-4,6-dichloro-1,3,5-triazine and condensation of cyanuric chloride with 5-aminoterazole or 3-amino-5-carboxytriazole, respectively.

All polymers exhibit excellent solubility in bipolar solvents in the form of the corresponding salts with N, N-diisopropylethylamine. Polymer solutions allow formation of well-adhered thin films on metallic, ceramic and carbonaceous surfaces by spin-coating, dip-coating, spraying or other conventional coating techniques, followed by evaporation of the solvent. Annealing of polymer films on different substrates at 350-550 ºC leads to their transformation to smooth partially ordered hydrophilic carbon nitride coatings with approximately 31 to 45 at.% of nitrogen and noticeable oxygen and chlorine content.
Combined FTIR, XRD, elemental analysis and EDX data have allowed us to conclude that annealed films represent the new member of the family of carbon nitrides, based on heptazine structural motifs, although with noticeable carbon and oxygen doping and semi-amorphous structure. The surface of annealed films is smooth down to the level of tens of nanometers, as demonstrated by STM. UV-VIS diffuse reflectance spectroscopy has allowed classifying the materials as low-bandgap semiconductors with bandgap presumably lowered due to carbon doping and negatively correlating with carbon content. The properties of annealed films have exhibited only tiny dependence on the type of precursor polymer used, being to a greater extent associated with annealing conditions. Electrochemical impedance spectroscopy of coatings reveals their effective resistivity in the range of tens kOhm cm, although the intrinsic resistivity value can be much lower. It allows classifying coatings as conductive rather than semiconductive and supports the hypothesis of carbon doping.

Our preliminary assessment of electrochemical stability of coatings, in strongly acidic environment, has demonstrated outstanding endurance even at high anodic and cathodic polarizations, combined with clear evidence of redox non-innocence of materials. We hypothesize formation of surface carbon nitride oxides at high positive potentials and their reversible reduction below -0.3 V Ag/AgCl.

In general, the newly synthesized coating materials exhibit the overall properties and electrochemical behavior allowing to characterize them as heptazine-based analogues of turbostratic carbons, although more research is required to elucidate their specific structural patterns. In contrast with glassy carbon, its novel heptazine-based analogs can easily be obtained as coatings and require notably modest annealing temperatures. This opens up the opportunity to create electrochemically active composites with catalytic complexes and nanoparticles with moderate thermal sensitivity. In addition, low contact angles of coatings result in hydrophilic surfaces, potentially giving way for wettable coatings with properties, attractive for fuel cell, sensors, supercapacitors, MEMS devices and membrane applications.

2.14. Chapter 2 references

1. Schwarzer A, Saplinova T, Kroke E. (2013). Tri-s-triazines (s-heptazines) — From a «mystery molecule» to industrially relevant carbon nitride materials. Coordination Chemistry Reviews 257(13-14), 2032–2062.

2. Heymann L, Schiller B, Noei H, Stierle A, Klinke C. (2018). A New Synthesis Approach for Carbon Nitrides: Poly(triazine imide) and Its Photocatalytic Properties. ACS Omega 3(4), 3892–3900.

3. Algara-Siller G, Severin N, Chong SY, Björkman T, Palgrave RG, Laybourn A, et al. (2014). Triazine-Based Graphitic Carbon Nitride: a Two-Dimensional Semiconductor. Angewandte Chemie International Edition 53(29), 7450–7455.

4. Dong G, Zhang Y, Pan Q, Qiu J. (2014). A fantastic graphitic carbon nitride (g-C_3N_4) material: Electronic structure, photocatalytic and photoelectronic properties. Journal of Photochemistry and Photobiology C: Photochemistry Reviews 20, 33–50.

5. Xu J, Brenner TJK, Chabanne L, Neher D, Antonietti M, Shalom M. (2014). Liquid-Based Growth of Polymeric Carbon Nitride Layers and Their Use in a Mesostructured Polymer Solar Cell with Voc Exceeding 1 V. Journal of the American Chemical Society 136, 39, 13486–13489

6. Zhao J, Ma L, Wang H, Zhao Y, Zhang J, Hu S. (2015). Novel band gap-tunable K-Na co-doped graphitic carbon nitride prepared by molten salt method. Applied Surface Science 332, 625–630.

7. Zhou ZB, Cui RQ, Pang QJ, Hadi GM, Ding ZM, Li WY. (2002). Schottky solar cells with amorphous carbon nitride thin films prepared by ion beam sputtering technique. Solar Energy Materials and Solar Cells 70, 487–493.

8. Urakami N, Kosaka M, Hashimoto Y. (2019). Thermal chemical vapor deposition and luminescence property of graphitic carbon nitride film for carbon-based semiconductor systems. Japanese Journal of Applied Physics,58(1), 010907–010907.

9. She X, Xu H, Xu Y, Yan J, Xia J, Xu L, et al. (2014). Exfoliated graphene- like carbon nitride in organic solvents: enhanced photocatalytic activity and highly selective and sensitive sensor for the detection of trace amounts of Cu^{2+}. J Mater Chem A. 2, 2563–2570.

10. Yang S, Gong Y, Zhang J, Zhan L, Ma L, Fang Z, et al. (2013). Exfoliated Graphitic Carbon Nitride Nanosheets as Efficient Catalysts for Hydrogen Evolution under Visible Light. Advanced Materials 25(17), 2452– 2456.

11. Kim OH, Cho YH, Chung DY, Kim MJ, Yoo JM, Park JE, et al. (2015). Facile and Gram-scale Synthesis of Metal-free Catalysts: Toward Realistic Applications for Fuel Cells. Scientific Reports 5, 8376–8376.

12. Cong K, Radtke M, Stumpf S, Schröter B, McMillan DGG, Rettenmayr M, et al. (2015). Electrochemical stability of the polymer-derived nitrogen-doped carbon: an elusive goal? Materials for Renewable and Sustainable Energy. 4(2), 5.

13. Baliani A, Peal V, Gros L, Brun R, Kaiser M, Barrett MP, et al. (2009). Novel functionalized melamine-based nitroheterocycles: synthesis and activity against trypanosomatid parasites. Organic & Biomolecular Chemistry 7(6), 1154–1154.

14. Zamani L, Mirjalili BBF, Zomorodian K, Zomorodian S. (2015). Synthesis and characterization of 5-substituted 1H-tetrazoles in the presence of nano-$TiCl_4.SiO_2$. South African Journal of Chemistry 68, 133–137.

15. Paletsky AA, Budachev NV, Korobeinichev OP. (2009). Mechanism and kinetics of the thermal decomposition of 5-aminotetrazole. Kinetics and Catalysis 50(5), 627–635.

16. Yuan X. (2016). Combinatorial Vibration-Mode Assignment for the FTIR Spectrum of Crystalline Melamine: A Strategic Approach toward Theoretical IR Vibrational Calculations of Triazine-Based Compounds. J Phys Chem A. 120, 7427–7433.

17. Zambon A. (2016). s-Heptazine oligomers: promising structural models for graphitic carbon nitride. Chem Sci. 7, 945–950.

18. Jürgens B. (2003). 8-Triamino-tri-s-triazine, an Important Intermediate during Condensation of Melamine Rings to Graphitic Carbon Nitride: Synthesis, Structure Determination by X-ray Powder Diffractometry, Solid-State NMR, and Theoretical Studies. J Am Chem Soc. 5(2), 10288– 10300.

19. Gu, Q., Jia, Q., Zhang, S., Gao, Z., Yang, P. (2019). In-situ growth of triazine-heptazine based carbon nitride film for efficient (photo)electrochemical performance. Catal. Sci. Technol. 9, 425-435.

20. Chaudhary, M., Nayak, A., Muhammad, R., Pradhan, D. & Mohanty, P. (2018). Nitrogen-Enriched Nanoporous Polytriazine for High-Performance Supercapacitor Application. ACS Sustainable Chem. Eng. 6, 5, 5895–5902.

21. Li, X., Zhang, J., Shen, L. et al. (2009). Preparation and characterization of graphitic carbon nitride through pyrolysis of melamine. Appl. Phys. A 94, 387–392.

22. Lin, Z., Lin, L. & Wang, X. (2015). Thermal nitridation of triazine motifs to heptazine-based carbon nitride frameworks for use in visible light photocatalysis. Chinese Journal of Catalysis 36(12), 2089-2094.

23. Ferrari AC, Rodil SE, Robertson J. (2003). Interpretation of infrared and Raman spectra of amorphous carbon nitrides. Physical Review B. 67(15), 155306–155306.

24. Shi, K., Shiu, K.-K. (2002). Scanning Tunneling Microscopic and Voltammetric Studies of the Surface Structures of an Electrochemically Activated Glassy Carbon Electrode. Anal. Chem. 74, 879–885.

25. McDermott, M.T., McDermott, C.Allred., McCreery, R.L. (1993). Scanning tunneling microscopy of carbon surfaces: relationships between electrode kinetics, capacitance, and morphology for glassy carbon electrodes. Anal. Chem. 6, 937–944.

26. Bukalov SS, Zubavichus YV, Leites L, Sorokin AI, Kotosonov AS. (2014). Structural changes in industrial glassy carbon as a function of heat treatment temperature according to Raman spectroscopy and X-Ray diffraction data. Nanosyst Phys Chem Math. 5, 186–191.

27. Fina F, Callear SK, Carins GM, Irvine JTS. (2015). Structural Investigation of Graphitic Carbon Nitride via XRD and Neutron Diffraction. Chemistry of Materials. 27(7), 2612–2618.

28. Gu YJ, Wen W, Wu JM. (2018). Simple air calcination affords commercial carbon cloth with high areal specific capacitance for symmetrical supercapacitors. J Mater Chem A 6, 21078–21086.

29. Ye D, Tang J, Wu Y. (2016). Electrochemical activation of Carbon Cloth in Aqueous Inorganic Salts Solution for superior capacitive performance. Nanoscale 8, 10406-10414.

30. Yi Y. (2017). Electrochemical corrosion of a glassy carbon electrode. Catalysis Today 295, 32–40.

31. V. D. Chekanova and A. S. Fialkov (1971). Vitreous Carbon (Preparation, Properties, and Applications). Russ. Chem. Rev., 40, 413

32. Sharma, S. (2018). Glassy Carbon: A Promising Material for Micro- and Nanomanufacturing. Materials 11(10), 1857.

XRD-related references

33. Balzar, D. (1999). Voigt-function model in diffraction line-broadening analysis. In R. L. Snyder, J. Fiala, & H. J. Bunge (Eds.), Defect and Microstructure Analysis by Diffraction (International Union of Crystallography Monographs on Crystal) (pp. 94–124). Oxford: Oxford University Press.

34. Bruker AXS GmbH. (2017). TOPAS 6 Technical Reference.

35. Cheary, R. W., Coelho, A. A., & Cline, J. P. (2004). Fundamental parameters line profile fitting in laboratory diffractometers. Journal of Research of the National Institute of Standards and Technology, 109 (1).

36. Stokes, A. R., & Wilson, A. J. C. (1942). A method of calculating the integral breadths of Debye-Scherrer lines. Mathematical Proceedings of the Cambridge Philosophical Society, 38 (3), 313-322.

Chapter 3

Fabrication of nanoporous nickel-coordinated carbon nitride coatings from aqueous solutions of Ni complexes of ultra-nitrogen-rich polymeric precursors and their characterization as outstanding oxygen evolution electrocatalytic coating on carbon felt substrate.

Nanoporous carbon nitride coatings, containing atomically dispersed N-coordinated nickel, have been obtained on carbon felt and vitreous carbon supports by solution deposition of aqueous Ni complex of a triazine-based ultra-nitrogen-rich polymer precursor, followed by drying and mild pyrolysis. Coated carbon felt electrodes demonstrate outstanding activity in oxygen evolution reaction (OER) in alkaline media, with no noticeable decrease of activity after 1000 hours of continuous operation. Dip-coating, spin-coating or other solution processing methods can be used for precursor layer formation. This technique provides a general approach to fabricating carbon nitride layers with tailored catalytic properties on different support materials, using transition metal complexes of water-soluble triazine polymers, capable to decompose with nitrogen elimination on moderate heating. The globular polymeric nature of the precursors together with supposed nitrogen coordination interaction with metal promote formation of coatings with highly variable porous structure and catalytic properties.

Research paper planned for submission to ***Angewandte Chemie international edition***

«Single-atom Ni catalysis on carbon nitride coatings, derived from water-soluble polymeric precursors – towards efficient oxygen evolution without noble metals»

Oleg Dubov, Jaume Giralt Marcé, Agustí Fortuny, Azael Fabregat, Frank Stüber and Josep Font Capafons

3.1. Introduction

Oxygen evolution reaction (OER) is a limiting step for the efficiency of water splitting and hence is a process of tremendous importance for the emerging sustainable energetics, together with its counterpart – oxygen reduction reaction (ORR) [1, 2]. Sluggish O_2 evolution kinetics typically calls for the use of expensive and scarce precious metals or their oxides, most habitually Ru, Ir, Pt, to design efficient anodes [2, 3], with RuO_2 being the most active oxide for OER due to small electronegativity difference between oxygen and metal that results in the absence of a band gap [3].

In the search for precious-metal-free catalytic systems, nitrogen-enriched carbon materials, especially derived from templated pyrolysis of polymers, have recently attracted considerable research interest for OER and ORR ([4, 5]). Amorphous or semi-amorphous structure is an important practical benefit of polymer-derived materials, permitting easy formation of diverse coatings and composites with porosity, easily controllable by template use. While different nitrogen functionalities have been shown to possess catalytic activity on alkaline OER and ORR, the presence of graphitic N atoms has been linked to most active and stable catalysts [6]. Moreover, it was demonstrated that a significant content or pyrrolic and pyridinic nitrogen functionalities inevitably results in reduced long-term electrochemical stability [5]. Thus, easily fabricable nitrogen-rich materials containing nitrogen in predominantly graphitic form are a coveted target for efficient precious-metal-free OER electrodes development. Although various modifications of electrochemically stable pyrolytic carbons have been developed, the content of nitrogen in all these materials is typically low in comparison with carbon content due to massive loss of nitrogen in the carbonization process [5].

The so-called polymeric carbon nitride (PCN) possesses a molecular structure with heptazine-based 1D chains and 2D ribbons, conjugated via hydrogen bonding and partially stacked with interlayer van der Waals interactions between planar heptazine units [7]. PCN with idealized formula C_3N_4 is the most stable and easy-to-obtain form of graphitic nitrogen, belonging hence to appreciably promising electrocatalytic materials [6, 8, 9]. In addition to demonstrating inherent ability to catalyse OER, it also promotes preferably 4-e way to oxygen reduction (ORR) [8]. The «classic» PCN is easily obtained in bulk by pyrolysis of melamine, dicyandiamide or some other nitrogen-rich precursors [10]. On the other hand, complete insolubility of PCN in all common solvents results in the need for complicated and costly methods for fabricating porous coatings of this material, required for catalytic electrodes preparation. Template-based methods are often used [6, 8, 11]. On the contrary, amorphous forms of carbon nitride are also well investigated. In the same time, known amorphous films and coatings are non-porous and

are typically produced by even more sophisticated techniques such as sputtering and plasma deposition [12-14].

A revolutionary approach to the synthesis of amorphous porous carbon nitride composite with carbon nanotubes (acting as conductive and structural filler), was demonstrated by Kim et al [15]. They obtained the material by means of pre-condensation of melamine with cyanuric chloride in a solvent, followed by mixing the triazine-based preliminary condensation product with carbon nanotubes and annealing the mixture in order to achieve complete condensation. The resulting porous conductive PCN composite demonstrated outstanding ORR performance in alkaline media. The preliminary condensation product in their work, however, was insoluble, which would significantly complicate the applicability of this approach to fabrication of thin active coatings. We addressed this issue in our previous work [16], where we synthesized novel soluble triazine-based polymers with ultra-high nitrogen content and obtained stable polymer layers on metallic, ceramic and carbonaceous surfaces. Annealing of these layers resulted in well-adhered flexible semi-amorphous carbon nitride coatings on all these surfaces. For coated carbon felt electrodes, outstanding long-term electrochemical stability in both cathodic and anodic polarizations was shown.

Semi-amorphous PCN coatings thus obtained demonstrate noticeable structural and functional similarity to so called glassy or vitreous carbon, produced by means of pyrolysis of polymeric precursors at temperatures well exceeding 1000 ºC and finding extensive use as electrochemically stable material for electrodes and sensors production [17]. However, new semi-amorphous carbon nitrides require for their production much lower pyrolysis temperatures (300 to 600 ºC). This makes feasible the combination of a polymer precursor with transition-metal-based molecular precursors and nanoparticles with subsequent mild pyrolysis at temperatures noticeably below the threshold of decomposition for typical catalytic species (e.g., transition metals nitrides, oxides, phosphides) or melting degradation of nanoparticles.

The objective of the present work was to explore this opportunity and synthesize OER-active coatings, based on the combination of triazinic precursor polymer with transition metal salt and subsequent annealing. The choice of Ni as catalytic enhancer was based on the previously reported activity of Ni-N active sites in nickel nitride [18], Ni-embedded nitrogen-rich carbon [19], carbon nitride doped with nickel oxide nanocristals [20], N-doped carbon nanofibers containing $FeNi/NiFe_2O_4$ [21] and nickel nitride grown on Ni foam [22] in various electrochemical processed, including hydrogen and oxygen evolution reactions (HER/OER) and oxygen reduction reaction (ORR), its low cost and low toxicity. The logics behind the selection of triazole and tetrazole-based amines for the synthesis of efficient polymeric precursors for semi-

amorphous carbon nitride was described in details in our previous publication [16], where two polymers of this type and one completely triazine-based soluble imide precursor for semi-amorphous carbon nitride were originally synthesised.

The polymer obtained by condensation of cyanuric chloride with 5-aminotetrazole was abbreviated as poly(CYA-Cl-AMTAZ) [16]. In that first publication [16], we directly used N,N-dimethylacetamide (DMAc) solutions of polymeric precursors for elaboration of smooth non-porous films with outstanding stability against anode oxidation. In the current work, we discovered that evaporation of water-based alkaline solutions of precursors results in nanoporous films with enhanced activity. Poly(CYA-Cl-AMTAZ) demonstrated the best solubility in aqueous systems, low viscosity and good stability of aqueous solutions in pure form as well as acceptable gelation time after complexation with Ni, for which reasons it was chosen for the present work. The original synthesis of the polymer, however, was carried out in DMAc with subsequent solvent change.

3.2. Results and discussion

3.2.1. Materials and methods

All chemicals were purchased from Sigma Aldrich and used without any additional purification. Anhydrous 99.8% pure N,N-dimethylacetamide (DMAc) (Sigma Aldrich), <0.005% water, has been used as a solvent during the polymer synthesis.arbon felt (CF) sheets (3.18 mm thick) for electrode fabrication were purchased from Alfa Aesar. Carbon nanopowder with <100 nm particle size was used as structural filler.

5-aminotetrazole was obtained by drying the corresponding monohydrate (purchased from Sigma Aldrich) in air at 105 ºC for 24 h, followed by keeping the product two weeks in vacuum desiccator over P_2O_5.

Lovibond XD 7000 spectrophotometer was used for recording optical spectra of solutions.

NMR spectra were recorded using a VARIAN Mercury VX400 spectrometer.

Thermo Fisher SCIOS 2 with field emitter has been used for scanning electronic microscopy and EDX mapping.

Autolab PGSTAT204 has been used for all electrochemical experiments.

JASCO 4700 spectrometer was used for FTIR spectra recording. Infrared spectra were processed in free SpectraGryph 1.2 software.

STM scanning was performed on Pico SPM II (Pico+) system.

XPS spectra were recorded using a PHOIBOS 150 EP hemispherical energy analyzer with MCD-9 detector and Mg anode.

3.2.2. Precursor polymer synthesis, coordination with Ni^{2+} and characterization of pure and complexed polymers

The precursor polymer poly [(2-chloro-1,3,5-triazine-4,6-diyl (5-iminotetrazol-2-yl)], further abbreviated as poly(CYA-Cl-AMTAZ), was synthesized by condensation of 5-aminotetrazole with cyanuric chloride in the presence of N,N-diisopropylethylamine (DIPEA) as a non-nucleophilic base. The polymer was originally obtained in the form of 5% wt. solutions in DMAc, containing also DIPEA and DIPEA·HCl.

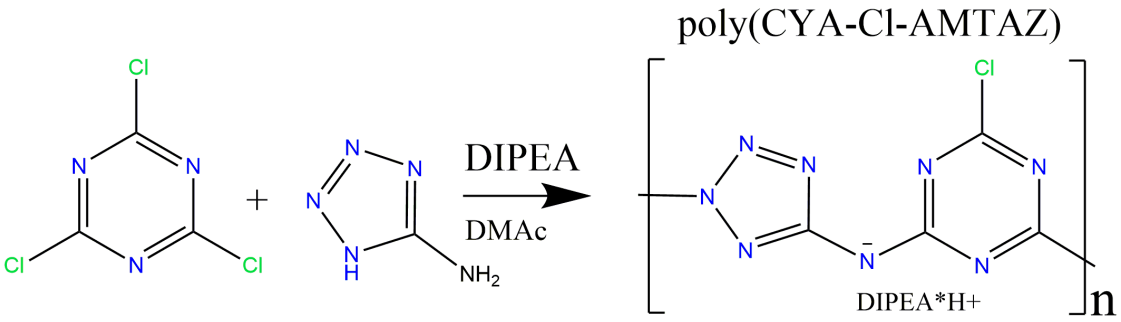

Fig. 1. Poly(CYA-Cl-AMTAZ) precursor synthesis scheme

The following synthesis protocol was used:

8 mmol (0.686 g) of 5-aminotetrazole and 24 mmol (3.102 g) of N,N-diisopropylethylamine (DIPEA) were dissolved in 20 g of DMAc. The solution was cooled down to -5 °C. In continuous Ar flow, a solution of 8 mmol of cyanuric chloride (1.475 g) in 6.18 g DMAc was added to the mixture dropwise under cooling in ice + NaCl bath and intensive stirring so that the temperature would not exceed 0 °C. After finishing the addition, the solution was refluxed at room temperature for 20 min, then sealed, heated to 70 °C, left under reflux at this temperature for 24 h and finally cooled to room temperature.

The solution, obtained according to this procedure, was poured to 1000 ml of intensively stirred 5% HCl solution. Suspension of deeply orange fine flakes was thus obtained.

The product was filtered on 0.45µm cellulose membrane filter, washed on the filter with 1000 ml 5% HCl, finally washed with water and dried in air at 80 °C for 24 h to obtain 1.34 g of fluorescent yellow powder (theoretic formula weight 196.55 g/mol, 85.2% of the theoretic yield, 6.82 mmol).The powder was dissolved with magnetic stirring in 65.7 g of a 3% aqueous ammonia solution to give 2% aqueous mother solution of the polymer. For NMR characterization, the same powder dissolution step was performed in the 3% solution of ND_3 in 99.9% D_2O (also to give 2% by weight polymer solution).

For **FTIR** characterization, a drop of polymer solution was dried in air at 80 ºC during 24h. Nickel complex of the polymer (complex preparation is described further in this section) was dried in the same conditions. FTIR spectra of pure and Ni-loaded polymers are provided in Fig. 2.

As can be seen from the spectra, the precursor polymer in pure form shows wide high-intensity shoulder composed of two peaks centered at 1310 cm^{-1} and 1485 cm^{-1} and a diffuse absorption region placed between 1850 and 3650 cm^{-1}.

In addition, small sharp peaks at 783 cm^{-1} and 808 cm^{-1} can easily be noticed.

Non-appearance of two small sharp peaks at 2920 and 2960 cm^{-1} that were assigned to the remaining DMAc and DIPEA species, respectively, in our previous work [16], demonstrates effective elimination of these compounds from the polymer.

The intensive shoulder with two maximums in the 1300-1600 cm^{-1} range is exhibited by all solid materials, synthesized by means of solution-based reactions of cyanuric chloride with nitrogen sources, reported in the literature [5, 26, 27) and can supposedly be viewed as characteristic for conjugated triazine system.

The signal at 783 cm^{-1} can be denoted as characteristic for tetrazole system according to published IR spectra of substituted 1,2,3,4-tetrazoles. For instance, it appears at 790.47 cm^{-1} for 5-phenyl-1H-tetrazole, at 791.77 cm^{-1} for 5-(4-hydroxyphenyl)-1H-tetrazole, or at 778.32 cm^{-1} for 1-(3-bromophenyl-1H-tetrazole [24].

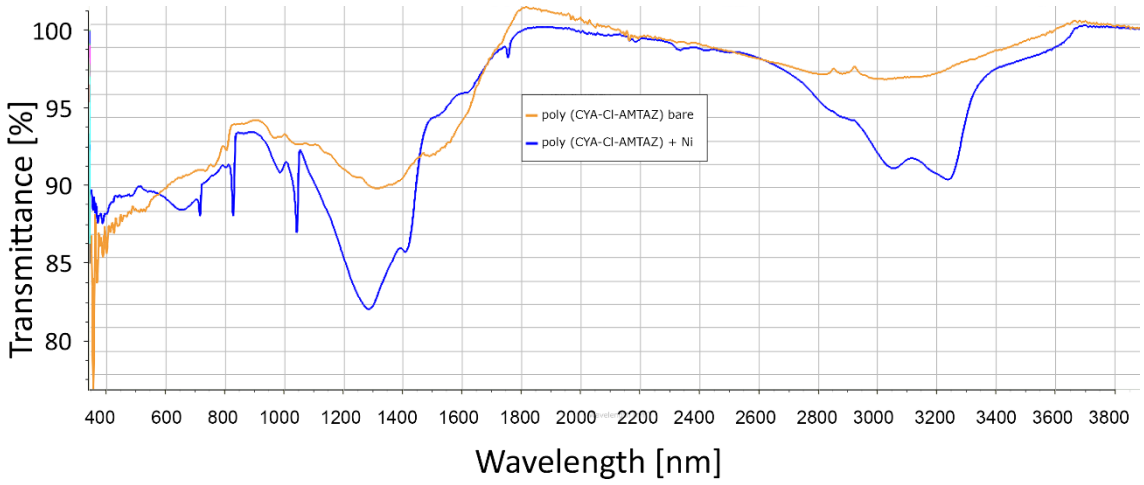

Fig.2 FTIR spectra of pristine and Ni-loaded PCN

The spectrum of Ni-coordinated polymer contains multiple sharp signals (at 714, 826 and 1041 cm^{-1}), that can partially be related to absorption of $Ni(NH_3)_6^{2+}$ and NO_3^- species. Well-noticeable shift of this peak in the Ni-coordinated polymer spectrum can thus be

related to coordination of tetrazole system with nickel. However, the peak at 826 cm^{-1} can be viewed as shifted due to coordination with Ni^{2+} signal, appearing at 783 cm^{-1} in the original polymer. Such shift, for instance, has been demonstrated by Frija et al. [24], for the tetrazolo-sacharinate complex of Ni (II), for which this sharp peak appears at 799.47 cm^{-1}.

3.2.3. Fabrication of electrodes and samples for SEM/EDX and XPS

1% polymer working solution was prepared by dilution of 2% solution with equal mass of water. **1% polymer working solution with Ni** was obtained by mixing 10 g of the 2% polymer solution with the same weight of aqueous solution of 148 mg $Ni(NO_3)_2 \cdot 6H_2O$ (29.9 mg/g Ni), followed by intensive stirring during 30 min. Typically, 2/1 atomic ratio between polymer repeating units and Ni was maintained.

1% polymer working solution with Ni and carbon nanoparticles was obtained by mixing 10 g of the 2% polymer solution with the same weight of aqueous solution of 148 mg $Ni(NO_3)_2 \cdot 6H_2O$ (29.9 mg/g Ni), containing also 200 mg of 100 μm carbon nanoparticles (Sigma Aldrich, TEM 7440-44-0), followed by intensive stirring during 30 min. The suspension was then sonicated for 2 h until stable black ink was obtained.

Carbon felt (CF) strips with approximate dimensions of 3.18x3.18x40mm were immersed into working solutions with 15 mm of the strip length being covered and sonicated for 5 min to guaranty full impregnation. Then, the strips were taken out and dried in air at 80 ºC for 24 h.

In addition to electrodes, samples for XPS characterization were prepared by placing 0.3 μL drops of 1% polymer working solution and 1% polymer working solution with Ni on the surface of preliminary polished glassy carbon plates and drying the drops in air at 80 ºC for 24 h.

Finally, the electrodes as well as samples, prepared for characterization, were annealed in air under the following regime: at 200 ºC for 1 h, followed by ramping the temperature at 1 ºC per minute until reaching 550 ºC and kept 30 min at this temperature. Ni-loaded and Ni + C (nano) + PCN coatings were abbreviated as Ni-PCN and Ni-C-PCN, respectively.

3.2.4. Scanning electronic microscopy (SEM)

SEM imaging was performed on individual fibers of coated carbon felt. EDX elemental mapping for Ni and N were conducted in order to further elucidate the uniformity of nickel and nitrogen distribution within coatings. Microscopic appearances of pristine PCN and Ni-PCN coatings were very similar, for which reason only microphotographs of Ni-PCN are presented.

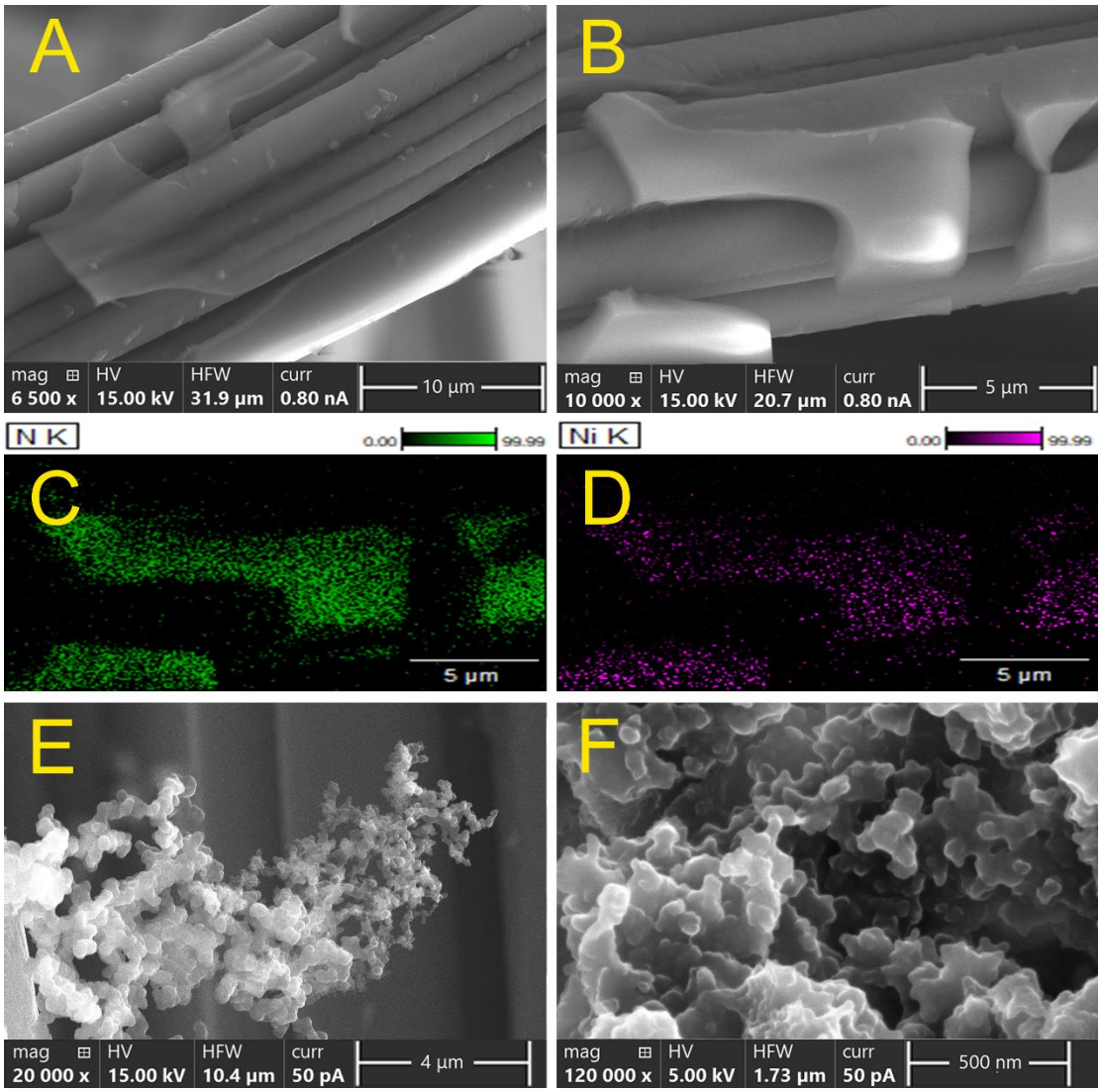

Fig. 3. Scanning microscopy and EDX mapping of Ni-PCN and Ni-C-PCN coatings

A, B :*Ni-PCN coating on the surface of a carbon cloth fiber.*

C, D :*EDX density maps of N and Ni, respectively, corresponding to the top images*

E, F :*Porous structure of Ni-C-PCN coating containing C nanoparticles (on carbon cloth fiber)*

3.2.5. XPS characterization

XPS characterization of samples was performed ex-situ in an ultra-high vacuum (10^{-8} Pa). XPS spectra were obtained using 1253.6 eV radiation from a Mg anode x-ray source. In the survey spectrum of virgin PCN coatings, intensive peaks of carbon, nitrogen and oxygen were detected, as well as trace peaks of chlorine. The spectrum of Ni-loaded coatings was nearly identical in these main constituent peaks, although also contained Ni 2p and Ni LMM (Auger) signals. Carbon 1s, nitrogen 1s, oxygen 1s and nickel 2p XPS spectra are provided on the Fig.4.

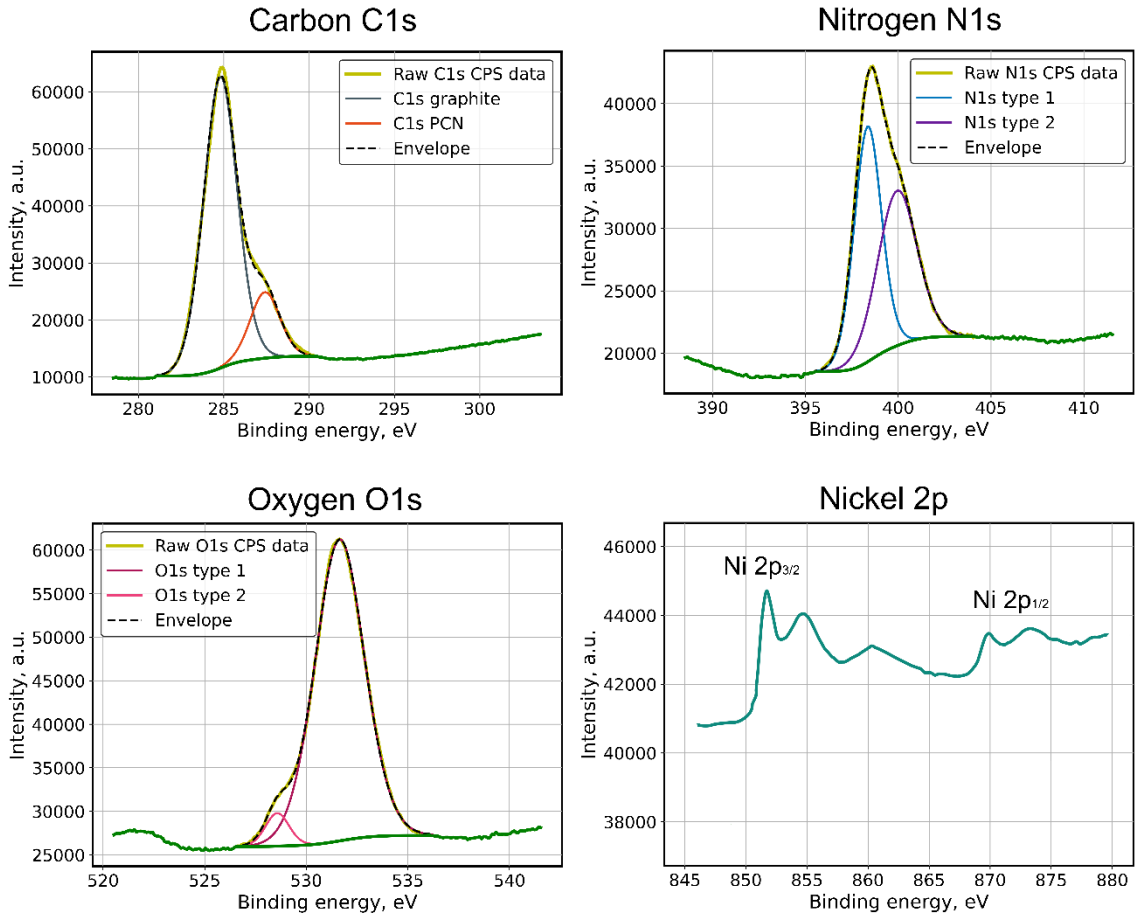

Fig. 4. XPS spectra of Ni-loaded PCN

Carbon is represented by two peaks with maximums at 284.8 and 287.42 eV and 0.833/0.167 relative intensity, respectively. The first intensive peak was undoubtedly related to the absorption of vitreous carbon support plate and, possibly, adventitious carbon (graphitic or hydrogenated carbonaceous impurities) on the surface of PCN film. The second peak, consequently, is the only type of carbon clearly belonging to the PCN structure itself. Interestingly, the position of this signal does not correspond with typically observed for «classic» pyrolytic carbon nitride materials and related to sp^2-bonded carbon (N–C=N) range of 288.2-288.4 eV [28]. On the other hand, carbon peaks with similar energy are often found in amorphous PCN films, obtained by means of reactive sputtering [29] and containing lowered nitrogen content.

Nitrogen signal was deconvoluted to give two peaks with binding energies of 398.35 eV (N type 1) and 399.94 eV (N type 2) and nearly equal relative intensities (0.513/0.487, respectively). The first signal type is usually ascribed to graphitic nitrogen [28-30], while the second is often related to tertiary nitrogen $N–(C)_3$, i.e., the central nitrogen of the heptazine ring or, according to other interpretation, to NH nitrogen [28].

References with model compounds, provided by Gammon et al. [30], are of special interest due to obvious structural non-ideality of the amorphous PCN material with

massive substitution of nitrogen for carbon (in the assumption of C_3N_4 idealized formula), demonstrated in our previous work [16]. According to these reference values, binding energy of 398.4 eV is found in 2,2-biquinoline, thus permitting to refer N type 1 signal to various types of graphitic nitrogen, including nitrogen, belonging to partially C-substituted conjugated heptazine or triazine systems. N type 2 finds the nearest prototype in triphenylamine, characterized by N 1s binding energy of 399.9 eV [30].

In general, positions of carbon and nitrogen peaks support the identification of the amorphous PCN material as mainly heptazinic carbon nitride material, although with significant number of nitrogen atoms exchanged for carbon preferentially in heptazine core. This characterization explains the shift of sp^2-bonded carbon binding in (N–C=N) moieties to the range, characteristic for less nitrogen-rich compounds; triphenylamine-like peaks positions of type 2 nitrogen find their explanation in the same way.

Oxygen is represented by two signal types with hugely different intensities (O1s type 1 with 531.64 eV and type 2 with 528.57 eV, having 0.950/0.050 relative area, correspondingly). In the virgin PCN film case, the type 2 does not appear. Type 1, according to existing literature data [31], was ascribed to surface oxide, resulting from oxidation of vitreous carbon or, probably, partial surface oxidation of the PCN material. Type 2 corresponds well with Ni(II) oxide [32] and presumably comes from minor presence of oxygen-coordinated Ni, indicating low representation of nickel surface oxides in the surface structure of the material.

Chlorine 2p shows low intensity signal with maximum at 198.94 eV, well-corresponding with position of organo-linked chloride (on the example of polyvinylchloride [23]).

Nickel 2p spectrum was in good agreement with previously reported spectra of nickel (II) compounds [32, 33]. Although reported data on nickel nitride XPS spectrum [22] seem to demonstrate no difference with O-coordinated nickel, the presence of Ni in non-oxide form can be suggested based on almost complete absence of corresponding oxide.

Table 1 summarizes the XPS data and provides information on calculated atomic concentrations of all measured elements in the superficial layer of Ni-PCN sample. Adventitious carbon signal is excluded from calculations.

No difference in deconvoluted signal positions for carbon, nitrogen, oxygen or chlorine has been registered between PCN and Ni-PCN samples with the exception of low-intensity O1s type 2 at 528.57 eV, which was absent in the pristine PCN case.

The atomic composition of pristine PCN sample was consistent with the formula $C_{0.402}N_{0.398}O_{0.198}Cl_{0.002}$. In turn, for Ni-PCN, the corresponding formula is $C_{0.283}N_{0.304}O_{0.155}Cl_{0.006}Ni_{0.252}$, demonstrating very similar basic elemental composition regardless the presence of Ni in high concentration.

Table 1. XPS data summary

Overall at. concentration by element	*Binding energy, eV*	*Content (at.) by type*	*Assumed identification in the composite structure*
C, 0.283	284.8	Excluded	Adventitious
	287.4	0.283	Heptazine-like
N, 0.304	398.3	0.156	Pyridinic
	399.9	0.148	Tertiary
O, 0.155	528.6	0.148	Oxidized carbon
	531.6	0.007	NiO
Cl, 0.006	198.9	0.006	Organic
Ni, 0.252	850-877	0.252	N-coordinated

3.2.6. Electrochemical characterization of pristine and Ni-containing electrode coatings

Three types of electrodes have been implemented for electrochemical performance comparison: bare carbon cloth, carbon cloth coated with pristine PCN and carbon cloth with Ni-PCN coatings. Corresponding carbon felt electrode strips, prepared as described in 3.2.3 section, were immersed in intensively stirred 1N KOH solution to keep approximately 8 mm of electrode length covered by liquid (corresponding to approximately 1.1 cm^2 geometric surface), while 6 cm^2 platinum wire was used as counter-electrode. Ag/AgCl/3M KCl double junction reference electrode was used to prevent solution contamination with chlorides. Oxygen evolution was studied in Linear Sweep Voltammetry (LSV) mode by increasing potential from 1.4 V to 1.75 V vs Reversible Hydrogen Electrode (RHE) at 10 mV/sec. **Bare carbon felt** demonstrated negligible oxygen evolution rate until 1.75 V vs RHE. Maximum current reached at this potential did not exceed 0.2 mA/cm^2, Tafel coefficient of 129 mV/deg and starting overpotential of 0.32V vs RHE were measured. **Carbon felt with PCN** coating demonstrated at 1.75V much higher performance with current over 1.2 mA/cm^2, 94.6 mv/deg Tafel coefficient and starting overpotential shifted to 0.3 V vs RHE. Coating CF electrodes with **Ni-PCN** allowed to achieve 100-fold current increase to 24 mA/cm^2 at the same potential and intensive visible oxygen bubbles formation. The Tafel coefficient and overpotential achieved (61.8 mV/deg and 0.26 V vs RHE, respectively) make this system among the most efficient electrodes for OER reaction ever reported.

Ni-PCN coating also demonstrated impressive stability in prolonged operation with 12% increase of maximum current within first 4 hours of operation, followed by 4% efficiency loss within the course of 1000 hours of operation at 1.75 V vs RHE. As can be seen en Fig. 5, it is worth mentioning that Tafel plots of both PCN-coated and NI-PCN-coated samples exhibited almost perfectly linear behavior in the studied potential range, indicating unvaried reaction mechanism within the whole potential range.

Implementing Ni-PCN coating with carbon nanopowder filler (Ni-C-PCN) exhibited further increased maximum current (46 mA/cm^2 at 1.75 V vs RHE), although addition of nano-carbon did not affect neither Tafel coefficient nor starting overpotential of the reaction, indicating that the effect of carbon nanoparticles can be completely explained in terms of geometric surface enhancement.

It is interesting to point out, however, that the PCN material served as efficient binder for carbon nanoparticles, forming uniformly porous structure with pore size corresponding with the dimensions of the carbon nanoparticles filler.

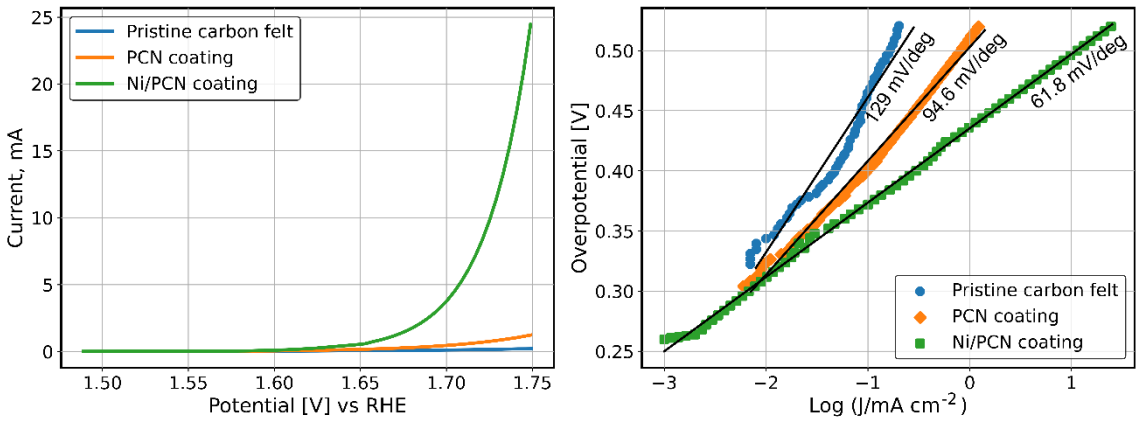

Fig. 5. OER LSV curves and corresponding Tafel plots for bare CF, PCN-coated CF and Ni-PCN coated CF electrodes

3.3. Conclusions

In this work, we demonstrate the formation of porous carbon nitride films by means of annealing of ultra-nitrogen-rich triazine-based polymeric precursor (poly [(2-chloro-1,3,5-triazine-4,6-diyl (5-iminotetrazol-2-yl)]) and its Ni complex. Both pristine polymer and the Ni-coordinated compound exhibit good solubility in aqueous ammonia in the form of corresponding ammonium salts. Solutions can efficiently be used for production of coatings on carbon felt and vitreous carbon by liquid coating methods with subsequent drying.

NMR spectroscopy confirms the proposed linear structure and high purity of the polymer. FTIR spectrum of the polymer allows to distinguish vibrations of triazine moieties and tetrazole system and confirm the presence of imide bonds.

Upon annealing, the polymer undergoes transformation to well-adhered porous polymeric carbon nitride with C/N ratio close to 1 and high oxygen content, according to XPS spectroscopy. Intriguingly, pristine and Ni-loaded PCN samples demonstrate nearly identical positions and relative intensities of C, N, O and Cl peaks with only Ni signals allowing to distinguish between two types of samples. This behavior can be explained in a most logical fashion in the assumption that Ni existence in atomically distributed state with almost exclusive coordination to nitrogen of heptazine tectonic units (or heptazine-like azo- polycyclic moieties with reduced nitrogen content). EDX mapping of nickel and nitrogen support this point of view, demonstrating perfectly uniform distribution of these elements within Ni-PCN coatings.

Electrochemical activity of Ni-PCN coatings in alkaline media (Tafel plot of 61.8 mV/deg starting overpotential of 0.26 V vs RHE, respectively), combined with outstanding long-term stability, makes this system among the most efficient OER electrodes ever reported.

In general, this work demonstrates exceptional importance of soluble ultra-nitrogen-rich triazine-based polymers as precursors to carbon nitride, enabling tailored design of metal-coordinated PCN coatings and composites with controlled catalytic activity and porosity.

Addition of carbon nanoparticles to the precursor solution has been demonstrated to result in secondary porosity in hundred nanometers range, further increasing active surface and performance of catalytic coatings.

Further studies are required to elucidate the mechanism of thermal decomposition of novel polymeric precursors to carbon nitride and exact coordination surrounding of metal dopant, as well as the full range of catalytic processes, accessible with this new class of carbon-nitride-based composite electrode materials.

3.4. Chapter 3 references

1. Seh ZW, Kibsgaard J, Dickens CF, Chorkendorff I, Nørskov JK, Jaramillo TF (2017). Combining theory and experiment in electrocatalysis: Insights into materials design. Science, Jan 2017, 13, 355(6321).

2. Katsounaros, I., Cherevko, S., Zeradjanin, A.R., Mayrhofer, K.J.J., 2014. Oxygen Electrochemistry as a Cornerstone for Sustainable Energy Conversion. Angewandte Chemie International Edition 53, 102–121.

3. Zeradjanin, A.R., Masa, J., Spanos, I., Schlögl, R., 2021. Activity and Stability of Oxides During Oxygen Evolution Reaction---From Mechanistic Controversies Toward Relevant Electrocatalytic Descriptors. Frontiers in Energy Research 8, 613092.

3. Wahab, Md.A., Joseph, J., Atanda, L., Sultana, U.K., Beltramini, J.N., Ostrikov, K., Will, G., O'Mullane, A.P., Abdala, A., 2020. Nanoconfined Synthesis of Nitrogen-Rich Metal-Free Mesoporous Carbon Nitride Electrocatalyst for the Oxygen Evolution Reaction. ACS Appl. Energy Mater. 3, 1439–1447.

4. Lv, Q., Si, W., He, J., Sun, L., Zhang, C., Wang, N., Yang, Z., Li, X., Wang, X., Deng, W., Long, Y., Huang, C., Li, Y., 2018. Selectively nitrogen-doped carbon materials as superior metal-free catalysts for oxygen reduction. Nature Communications 9, 3376.

5. Cong K, Radtke M, Stumpf S, Schröter B, McMillan DGG, Rettenmayr M, et al. (2015). Electrochemical stability of the polymer-derived nitrogen-doped carbon: an elusive goal? Materials for Renewable and Sustainable Energy, 4(2), 5.

6. Merzougui, B., Bukola, S., Zaffou, R., 2016. Further Understanding of Nitrogen-Doped Carbon Catalytic Property towards Oxygen Reduction Reaction (ORR). Materials Today: Proceedings 3, 691–695.

7. Li, Y., Wang, Y., Dong, C.-L., Huang, Y.-C., Chen, J., Zhang, Z., Meng, F., Zhang, Q., Huangfu, Y., Zhao, D., Gu, L., Shen, S., 2021. Single-atom nickel terminating sp^2 and sp^3 nitride in polymeric carbon nitride for visible-light photocatalytic overall water splitting. Chem. Sci. 12, 3633–3643.

8. Tahir, M., Mahmood, N., Zhu, J., Mahmood, A., Butt, F.K., Rizwan, S., Aslam, I., Tanveer, M., Idrees, F., Shakir, I., Cao, C., Hou, Y., 2015. One Dimensional Graphitic Carbon Nitrides as Effective Metal-Free Oxygen Reduction Catalysts. Scientific Reports 5, 12389.

9. Zheng, Y., Jiao, Y., Chen, J., Liu, J., Liang, J., Du, A., Zhang, W., Zhu, Z., Smith, S.C., Jaroniec, M., Lu, G.Q. (Max), Qiao, S.Z., 2011. Nanoporous Graphitic-

C_3N_4@Carbon Metal-Free Electrocatalysts for Highly Efficient Oxygen Reduction. J. Am. Chem. Soc. 133, 20116–20119.

10. Schwarzer A, Saplinova T, Kroke E. (2013). Tri-s-triazines (s-heptazines) — From a «mystery molecule» to industrially relevant carbon nitride materials. Coordination Chemistry Reviews. 257(13-14), 2032–2062.

11. Yang, Z., Zhang, Y., Schnepp, Z., 2015. Soft and hard templating of graphitic carbon nitride. J. Mater. Chem. A 3, 14081–14092.

12. Kang, Y., Yang, Y., Yin, L.-C., Kang, X., Liu, G., Cheng, H.-M., 2015. An Amorphous Carbon Nitride Photocatalyst with Greatly Extended Visible-Light-Responsive Range for Photocatalytic Hydrogen Generation. Advanced Materials 27, 4572–4577.

13. Zhou ZB, Cui RQ, Pang QJ, Hadi GM, Ding ZM, Li WY. (2002). Schottky solar cells with amorphous carbon nitride thin films prepared by ion beam sputtering technique. Solar Energy Materials and Solar Cells, 70, 487–493.

14. Ech-chamikh, E., Essafti, A., Ijdiyaou, Y., Azizan, M., 2006. XPS study of amorphous carbon nitride (a-C:N) thin films deposited by reactive RF sputtering. Solar Energy Materials and Solar Cells 90, 1420–1423.

15. Kim OH, Cho YH, Chung DY, Kim MJ, Yoo JM, Park JE, et al. (2015). Facile and Gram-scale Synthesis of Metal-free Catalysts: Toward Realistic Applications for Fuel Cells. Scientific Reports 5, 8376–8376.

16. Dubov, O., Marcé, J.G., Fortuny, A., Fabregat, A., Stüber F. and Font J. Flexible semi-amorphous carbon nitride films with outstanding electrochemical stability derived from soluble polymeric precursors. J Mater Sci (2022).

17. Carbon Materials for Advanced Technologies, ed. by Burchell T.D, 1999. Pergamon, Amsterdam, 535 p.

18. Kreider, M.E., Gallo, A., Back, S., Liu, Y., Siahrostami, S., Nordlund, D., Sinclair, R., Nørskov, J.K., King, L.A., Jaramillo, T.F., 2019. Precious Metal-Free Nickel Nitride Catalyst for the Oxygen Reduction Reaction. ACS Appl. Mater. Interfaces 11, 26863–26871.

19. Chen T, Guo S, Yang J, Xu Y, Sun J, Wei D, Chen Z, Zhao B, Ding W. Nitrogen-Doped Carbon Activated in Situ by Embedded Nickel through the Mott-Schottky Effect for the Oxygen Reduction Reaction. Chemphyschem. 2017 Dec 6, 18(23), 3454-3461.

20. Liao, C., Yang, B., Zhang, N., Liu, M., Chen, Guoxin, Jiang, X., Chen, Gen, Yang, J., Liu, X., Chan, T.-S., Lu, Y.-J., Ma, R., Zhou, W., 2019. Constructing Conductive

Interfaces between Nickel Oxide Nanocrystals and Polymer Carbon Nitride for Efficient Electrocatalytic Oxygen Evolution Reaction. Advanced Functional Materials 29, 1904020

21. Aziz, I., Lee, J., Duran, H., Kirchhoff, K., Baker, R.T., Irvine, J.T.S., Arshad, S.N., 2019. Nanostructured carbons containing FeNi/$NiFe_2O_4$ supported over N-doped carbon nanofibers for oxygen reduction and evolution reactions.

22. Shalom, M., Ressnig, D., Yang, X., Clavel, G., Fellinger, T.P., Antonietti, M., 2015. Nickel nitride as an efficient electrocatalyst for water splitting. J. Mater. Chem. A 3, 8171–8177.

23. Guo, J., Lin, Z.-Y., Chang, C.-J., Lu, H., Chen, J.-K., 2018. Protein Valves Prepared by Click Reaction Grafting of Poly(N-isopropylacrylamide) to Electrospun Poly(vinyl chloride) Fibrous Membranes. Applied Surface Science 439, 312–322.

24. Zamani L, Mirjalili BBF, Zomorodian K, Zomorodian S. (2015). Synthesis and characterization of 5-substituted 1H-tetrazoles in the presence of nano-$TiCl_4.SiO_2$. South African Journal of Chemistry 68, 133–137.

25. Frija, L.M.T., Rocha, B.G.M., Kuznetsov, M.L., Cabral, L.I.L., Cristiano, M.L.S., Pombeiro, A.J.L., 2020. Well-defined nickel(II) tetrazole-saccharinate complex as homogeneous catalyst on the reduction of aldehydes: scope and reaction mechanism. Pure and Applied Chemistry 92, 151–166.

26. Gu, Q., Jia, Q., Zhang, S., Gao, Z., Yang, P. (2019). In-situ growth of triazine-heptazine based carbon nitride film for efficient (photo)electrochemical performance. Catal. Sci. Technol. 9, 425–435.

27. Chaudhary, M., Nayak, A., Muhammad, R., Pradhan, D. & Mohanty, P. (2018). Nitrogen-Enriched Nanoporous Polytriazine for High-Performance Supercapacitor Application. ACS Sustainable Chem. Eng. 6, 5, 5895–5902.

28. Alwin, E., Nowicki, W., Wojcieszak, R., Zieliński, M., Pietrowski, M., 2020. Elucidating the structure of the graphitic carbon nitride nanomaterials via X-ray photoelectron spectroscopy and X-ray powder diffraction techniques. Dalton Trans. 49, 12805–12813.

29. Titantah, J.T., Lamoen, D., 2007. Carbon and nitrogen 1s energy levels in amorphous carbon nitride systems: XPS interpretation using first-principles. Diamond and Related Materials 16, 581–588.

30. Gammon, W.J., Kraft, O., Reilly, A.C., Holloway, B.C., 2003. Experimental comparison of N(1s) X-ray photoelectron spectroscopy binding energies of hard and

elastic amorphous carbon nitride films with reference organic compounds. Carbon 41, 1917–1923.

31. Lee, W.H., Lee, J.G., Reucroft, P.J., 2001. XPS study of carbon fiber surfaces treated by thermal oxidation in a gas mixture of O2/(O2+N2). Applied Surface Science 171, 136–142.

32. Al-Kuhaili, M., Ahmad, S., Durrani, S., Faiz, M., Ul-Hamid, A., 2015. Application of nickel oxide thin films in NiO/Ag multilayer energy-efficient coatings. Materials Science in Semiconductor Processing 39, 84-89.

33. Salunkhe, P., Ali A.V, M., Kekuda, D., 2020. Investigation on tailoring physical properties of Nickel Oxide thin films grown by dc magnetron sputtering. Materials Research Express 7, 016427.

UNIVERSITAT ROVIRA I VIRGILI
SEMI-AMORPHOUS CARBON NITRIDE FILMS DERIVED FROM SOLUBLE POLYMERIC PRECURSORS: TOWARDS MULTIFUNCTIONAL ELECTROCHEMICAL COATINGS WITH ENHANCED STABILITY
Oleg Dubov

Chapter 4

A potentiostat from scratch: building an extremely simple yet precise Arduino-based platform for voltammetry, chronoamperometry and capacitance measurements

This piece is a satellite development arisen from the unavailability research-class equipment during the COVID-19 lockdown and the need for continuing the research project under very stringent conditions.

A three-electrode potentiostat, based exclusively on non-expensive breadboard-compatible electronic components, is reported. We have optimized the design with the objection to make feasible the assembly of the device directly by students in a non-specialized practicum.

In spite of its simplicity, the device allows to perform a broad array of experimental techniques, including capacitance measurement, previously not reported for simple do-it-yourself devices. In addition to the instrument design and the microcontroller program required for its basic functioning, we offer an open-source Python-based PC application including presets for Linear Sweep Voltammetry, Cyclic Voltammetry and Chronoamperometry experiments, as well as Capacitance measurements.

We also describe a simple and convenient method for DIY preparation of reference Ag/AgCl/KCl electrodes required for electrochemical experiments.

Research paper submitted to ***Journal of Chemical Education***

«Building potentiostat from scratch: simple yet precise Arduino-based platform for voltammetry, chronoamperometry and capacitance measurements»

Oleg Dubov, Josep Font and Alexey Shavel

Manuscript ID **ID ed-2022-00107w**

UNIVERSITAT ROVIRA I VIRGILI
SEMI-AMORPHOUS CARBON NITRIDE FILMS DERIVED FROM SOLUBLE POLYMERIC PRECURSORS: TOWARDS MULTIFUNCTIONAL ELECTROCHEMICAL COATINGS WITH ENHANCED STABILITY
Oleg Dubov

4.1. Introduction

Deep understanding of laboratory equipment operation principles is a skill of immense importance that should unquestionably be in focus throughout the educational process. However, modern-day experimental devices typically grant the user with a simple-to-operate interface, often hiding behind the scene physical processes taking place during measurements. Fortunately, the situation is well balanced with do-it-yourself culture quickly invading educational labs and allowing students building surprisingly sophisticated and efficient setups, not only suitable for education but also often serving demonstrational and even some basic research needs [1,2].

Although multiple potentiostat designs, based on Arduino Atmega or other microcontrollers, have already been proposed, none of them, to our knowledge, has been intentionally optimized for quick assembly by students without a noticeable background in electronics. Moreover, for most of the proposed systems, no convenient measurement software for PC is provided. Au contraire, our goal was to present a device that could easily be mustered in a chemical laboratory with a minimum set of prerequisite materials and skills. The schematic being presented is possibly the simplest three-electrode potentiostat design ever published – mainly due to limiting the utilization of operational amplifiers to only four, the maximum number available in a single-chip assembly, which allowed to reduce drastically the complexity of connections and simplify markedly the design.

We also present not only an Arduino IDE program enabling the device with the basic functionality, but furthermore a Python-based PC software designed to communicate with the Arduino to perform automated measurement routines.

The closest antecedent for the proposed design is the device, created by G.N. Melony [5]. We further simplified the schematic to avoid bipolar feed of the operational amplifiers and limited their number to just four, which allowed us to implement the single-chip 4-channel precision operational amplifier LMC6484. It is one of the very few op-amps with femtoampere-level input current, which is available in Plastic Dual In-Line Package (PDIP), letting on quick breadboard prototyping.

A Digital to Analog Converter (DAC), creating the offset potential, is of critical importance for potentiostat functioning. In previously proposed designs, required potential offsets have been generated by charging capacitors with Arduino pulse width modulation (PWM) signal [3,5] or even by using a PWM-controlled op-amp integrator [4]. The first approach works quite well; although lacks the precision in the potential control even for basic experiments, since the PWM of most Arduino's has resolution of only 8 bit. The second method solves this problem, albeit leading to complicated operation logics, making device design less clear from the educational viewpoint.

We implemented a more precise and straightforward solution, using a 12-bit MCP4725 DAC pre-assembled module, specially designed for use with Arduino by Sparkfun Electronics. The application of the breadboard-based variant of the system for voltammetry, chronoamperometry and capacitance measurements is demonstrated. Measurement quality is shown to fully fit the precision requirements, typical for a student practicum, with noise being significantly reduced by software averaging.

On the other hand, the noise level in the measured data can be noticeably reduced by soldering all the connections. Soldering is recommended when using the proposed schematic as stationary educational setup and is prerequisite for any research applications. The difference in quality given by soldered and breadboard-based versions, respectively, is demonstrated in Experimental part section.

4.2. Operation principles and design

The basic principle of potentiostat operation is appealingly simple. In a typical three-electrode cell, a desired potential is applied between working (WE) and reference (RE) electrodes. To drain (and measure) the current, counter electrode (CE) is used.

The potential of the working electrode is controlled by digital to analog converted (DAC), which transforms digital commands, arriving from the microcontroller, into analog signal. On operational amplifier (OA), this signal is summed with the reference electrode potential and the resulting potential is applied to the working electrode. Additionally, a reference voltage supply and some resistors and capacitors are required.

One of the key issues in design of classical potentiostats is the necessity to manage bipolar currents. Although operational amplifiers work natively in the bipolar mode, the Arduino is not designed for measurement of signals with alternating polarity. In addition, the classical (bipolar) potentiostat design requires voltage regulators and often reference sources for both polarities, which complicates drastically the schematic.

Fortunately, in most basic electrochemical experiments, especially in aqueous media, the practically required potential window for typical measurements is quite narrow, usually lying between -2 to +2 V versus Ag/AgCl reference electrode. This allows simplifying the design by choosing a positive voltage, corresponding to the half of the reference voltage potential, as a global measurement reference. In the case of Arduino with 4.4 to 5.25 V serving as working voltage when plugging only to the USB, 4.096 V is a convenient and logical reference voltage choice. When this reference is chosen, positive WE potentials correspond to the range from 2.048 to 4.096 V and negative to the range from GND to 2.048 V, the latter potential thus being the “virtual ground”. With this reference and a 12 bit DAC (4096 analog signal output levels), the digital resolution of the device equals to 1 mV/level.

Although Arduino bears an internal reference voltage, its use for accurate measurements is strongly discouraged. For the sake of accuracy, the reference used by the controller should be derived from the same source as the analog reference, thus assuring impetuous self-elimination of measurement errors due to concordance of fluctuations of measured potential values together with the reference point values. Hence, it is of great importance to use all resistors of the same type to guaranty that their thermal coefficients of resistance could be considered equal in the practical sense; 0.1% tolerance resistors are recommended and listed in the Bill of Materials (Supporting Information, SI). In fact, less precise resistors can also be successfully used, although in this case additional calibration values may be required in the code sketch to provide correct absolute output results (e.g., the set WE potential may be multiplied by an experimentally pre-determined coefficient before sending it to the DAC in order to achieve concordance with the real output WE potential; or pre-measured actual shunt resistor value may be used instead of its nominal resistance.

It is important to mention that breadboard assembly of the device should be realized with shortest possible connection wires to reduce electromagnetic noise. For mass-assembly in a student practicum, we recommend purchasing several sets of standard breadboard connection wires (pre-terminated with pins) with different lengths and making wire kits in accordance with a certain color code (a specific color for each length).

As Arduino is powered from the computer USB port, plugging the PC into a grounded plug or operating on battery is required. **Fig.1** demonstrates the schematic of the proposed device and its recommended arrangement on a breadboard.

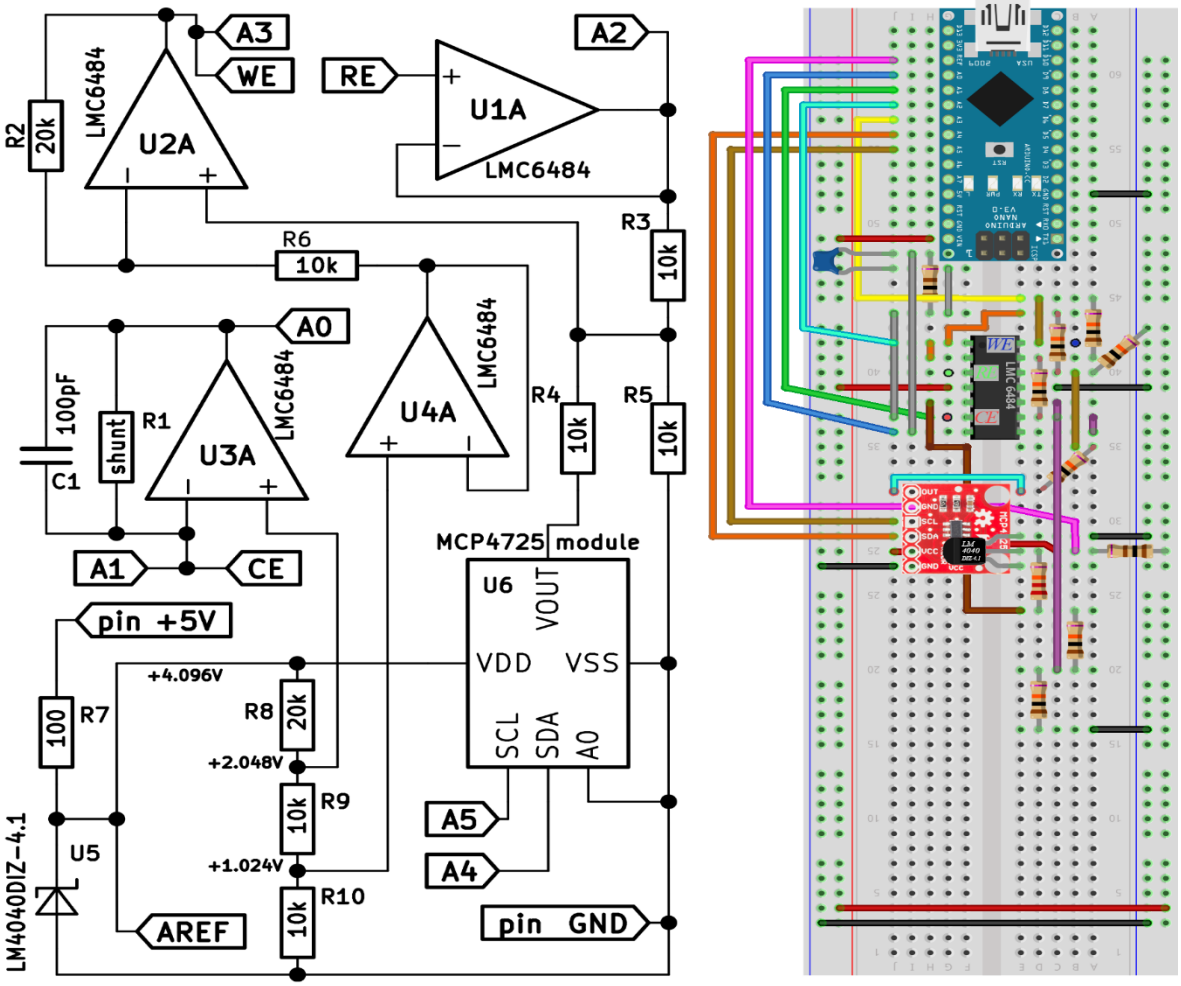

WE — working electrode
RE — reference electrode
CE — counter electrode
A0 to A5 - Arduino input pins
pin +5V - Arduino VDD pin

U1A to U4A: LMC6484 — operational amplifiers from 1 to 4
U5: LM4040DIZ-4.1 — reference voltage source
U6 —- MCP4725 module digital to analog converter
AREF - Arduino Analog Reference input
pin GND - Arduino VSS (ground) pin

Fig.1. Design schematic and breadboard arrangement

4.3. Hardware design considerations

In the LMC6484 chip, four operational amplifiers (OA) are conveniently assembled into one unit. PDIP package allows direct mounting it to a breadboard. The same applies to LM4040 voltage reference in its through-hole variant. MCP4725 does not have a PDIP version and is complicated for soldering due to its small size, thus a Sparkfun Electronics breakout board, adapted for breadboard implementation, is recommended. The Arduino used in the present design is Arduino Nano 5 V version. In order to simplify parts ordering, their reference numbers in Digi-Key supplier catalog are provided in the Bill of Materials **(Table 1).**

Table 1. Bill of materials

Component	**Parameter**	**Digi-Key part number/comment**
LMC6484	-	LMC6484IN/NOPB-ND
LM4040	-	LM4040AIZ-4.1/NOPB-ND
MCP4725		1568-1047-ND
R_1	From 100 Ohm to 10 kOhm.	Current measurement range selection resistor. 100ADTR-ND (100 Ohm) A105942CT-ND (1kOhm) A105970CT-ND (10kOhm)
R_2, R_8	20 kOhm	A105929CT-ND
R_3 to R_6, R_9, R_{10}	10 kOhm	A105970CT-ND
R_7	100 Ohm	100ADTR-ND
C_1	100 pF	490-16217-1-ND

Functions of all IC (Integrated Circuits) in the design schematic are summarized in the **Table 2.**

Table 2. Integrated circuits functions explication

IC name	IC function	Comments and explanations
U1A	Reference electrode potential follower	Reference electrode has very high internal resistance (hundreds of thousands kOhm to several MOhm). Although, when averaged with the DAC signal on the resistor divider formed by R3/R4, the RE electrode signal does have to be low impedance, otherwise it would not keep the currents required to flow through the resistors. The follower produces a low-impedance signal with the same potential as the original high-impedance one.
U2A	Summing amplifier, generating on the WE the sum of RE and DAC potentials	In a typical summing amplifier schematic, the «-» input is linked through a resistor to the ground. In the proposed design, however, ¼ of the reference voltage potential (i.e. 1024 mV) is used as a summation reference. This allows outputting the sum of the signals, referred to ½ of the reference voltage as zero point.
U3A	Transimpedance amplifier, realizing current measurement	A classical OA current measurement block. ½ of the reference voltage is used as the local reference, allowing bidirectional current measurement. Current measurement theoretic full range is defined by R1 shunt value according to the formula Range (mA) = 2048/R1(Ohm).
U4A	¼ reference voltage follower	¼ reference voltage, used as local reference in the OA2 summator, is required to be low impedance due to the use of the R6/R2 divider. The OA4 follows this potential.
U5 LM4040 voltage reference	Precision voltage reference	LM4040 provides the main reference voltage source with 0.1% precision and 4096 mV potential versus GND, which is used as DAC feed and reference, Arduino reference and, after resistor dividers, as 2048 and 1024 mV reference sources for the analog schematic.
U6 CP4725 DAC	Digital to analog converter	Digital to analog converter is used as a source of program-controllable analog potential with 12 bit resolution.

4.4. Important variables, startup and calibration

At the startup, initial checks and calibration of the device are required in order to get correct readings. First of all, it is important to ensure that correct analog inputs are used. In the presented sketch, $\mathbf{A_0}$ is chosen for the measurement of current, $\mathbf{A_1}$ for the CE potential, $\mathbf{A_2}$ for the RE potential, $\mathbf{A_3}$ for the WE potential. These analog pins can be changed if necessary, although with corresponding correction in the sketch.

In principle, the potential of the CE is always maintained constant and should not necessarily be measured. However, in a practical device under load, it can fluctuate and hence it was decided to use the real measured value in the program.

All readings of current and potential are sampled several times and averaged in order to reduce the stochastic noise. The **avernum** variable gives the number of readings to be averaged for all measurement points. The values between 5 and 20 are recommended with 10 being the optimum for most cases. As sampling and averaging requires processor time, high **avernum** values result in limited scanning speed in LSV and CV measurements. At **avernum** = 10, the maximum scanning speed of 150 mV/s is achievable.

The **potref** variable corresponds to the expected value of the CE potential versus GND in mV, i.e., the virtual ground potential vs ground. For a 4096 mV voltage reference, this value should be close to 2048. We recommend measuring the actual voltage on the CE without load and introducing it as the value of **potref** in the sketch.

4.5. Software uploading, operation and method parameters

Measurement software includes two interacting components – a program in the Arduino IDE language for the microcontroller and Python frontend PC application.

4.5.1. Arduino IDE program

4.5.1.1. Uploading

The program that should be uploaded into the Arduino board (the so-called «sketch») is designed to perform low-level interactions with the device through a COM port. Official Adafruit MCP4725 library should be installed with the help of the standard Arduino IDE library installation wizard («Tools» - «Manage libraries») prior to sketch uploading. **Arduino Nano** board with **Atmega 328P** processor should be selected from «Tools» – «Board» and «Tools» – «Processor» menus, respectively. If an error takes place during uploading, we recommend trying **Atmega 328P old bootloader** option in the «Processor» menu, which can be adequate for some old board version.

4.5.1.2. Operation

The Arduino sketch can be used without the PC application (for instance, for testing purposes), by typing commands in the «Send» field in the «Serial monitor» mode of Arduino IDE.

The sketch supports two main modes: fixed potential and potential sweep. The commands to start operation in a certain mode, arriving from the COM port, should be constructed in the following format: «N, Ss, Vs, E_i, E_f>», where N is the number of the mode: **1 for voltammetry**, and **2 for chronoamperometry**.

For mode 1, **Ss** corresponds to scanning speed in mV/s, **Vs** to number of void samples, discarded before the actual measurement starts, $\mathbf{E_i}$ to initial potential in mV, $\mathbf{E_f}$ to final potential in mV. Thus, scanning occurs with given speed from the given starting potential to the given final potential. First samples can be rejected in order to let the system stabilize at the applied potential before the data recording starts.

In mode 2, **N** and **Vs** keep their context, **S** stands for the time in seconds during which the potential should be maintained, while $\mathbf{E_i}$ for the potential to be set. $\mathbf{E_f}$ is not used and can be omitted from the command string. The end of the command string, meaning sending it to be executed, is stated by «>» symbol.

Command string examples:

«*1, 10, 5, -1000, 1000>» - rising sweep from -1000 mV to 1000 mV with 10 mV/s speed and 5 discarded samples.

«2, 50, 20, 500>» - constant potential of +500mV during 50 s, 20 first samples discarded.

It is worth mentioning that, although using **Vs** is a convenient way to discard noisy first values at method startup in the command string mode operated directly from Arduino IDE, we do not recommend using it when complex sequential methods are implemented due to gaps in data flow it causes. In the commands generated by the PC measurement application, non-zero **Vs** values are used exclusively in the chronoamperometry mode; in other modes, system «conditioning» at a given potential, initiated by a separate command, is instead applied before starting main method execution. This consideration is of especial importance for capacitance measurements, where omitting the first current points can drastically affect the final integral value.

4.5.2. PC measurement application

The application is written in Python. It communicates with the Arduino sketch using serial commands and allows programming more complex experimental presets. At the moment, four types of experiments are supported:

- Linear sweep voltammetry (LSV)
- Cyclic voltammetry (CV)
- Chronoamperometry (CA)
- Cell capacitance measurement (CC)

LSV and **CV** modes allow, in addition to the Arduino sketch parameters, to set supplementary specifications. For **LSV**, the following parameters can be specified:

- Start and stop potentials
- Potential stabilization time at startup

If the potential stabilization time is indicated, the start potential is applied to the WE for the indicated time in seconds before the execution of the scan begins. It is required in order to stabilize the measurement and avoid high capacitive currents at scanning startup. If zero time is set, the scan starts immediately.

For the **CV** mode, the following parameters are given:

- Start and stop potentials
- First and second vertex potentials
- Number of vertexes
- Potential stabilization time at startup

In CV mode, each scan corresponds to combination of two (rising + falling or falling + rising) passes, called cycles, thus the number of vertexes gives the number of direction changes.

Chronoamperometry is conducted simply by applying the requested potential during the requested period of time in accordance with the parameters of the mode 2 of the Arduino sketch. Potential in mV, time in seconds and number of void samples are given as parameters.

Capacitance measurement is accomplished by changing the WE potential from E_1 to E_2 and integrating the resulting current by time during the time period t. The resulting integral value (corresponding to the charge passed through the system) is then corrected to take into account the faradaic current C_f, measured as an average of last 100 current readings during the integration. The correction is performed by subtracting the corresponding faradaic charge component C_f t from the integral. The resulting corrected integral value is divided by the potential difference (E_2-E_1) to get the capacitance.

To avoid overloading the potentiostat and obtaining incorrect results, we always recommend connecting a resistor with the resistance equal to 2x shunt resistance, in series with the WE of the cell i.e., between the capacitive electrode of the cell and WE.

Before the measurement is started, the system is «conditioned», i.e. ,fully charged for a long enough time at WE potential E_1. After this, the potential of the capacitive electrode can also be considered equal to E_1, flowing capacitive current is negligible (although a faradaic current can be present). Then the WE potential is changed to E_2 and the capacitor starts to charge or discharge through the resistor R_s with momentary potential E_t following the Equation 1:

$$E_t = E_1 + (E_2 - E_1)\ (1 - e^{-})$$ Equation 1.

The R value in the Equation 1 is the total series resistance of the system, in most cases it can be considered close to the R_s resistance. However, the actual potential on the capacitive electrode is not measured directly due to the presence of the series resistor between the capacitive electrode and WE. Instead, momentary current is measured and used for capacitance calculation. The momentary current I_t is defined by Ohm's law according to the voltage drop on the resistor $(E_2-E_t)/R$ and is decreasing with time according to the same exponential law (Equation 2):

$$I_t = \frac{E_2 - E_1}{R} - \frac{(E_2 - E_1)\ (1 - e^{-})}{R}$$ Equation 2.

RC is called the time constant of the RC charging circuit. It is easy to see that after a time period equivalent to one RC, the capacitor acquires 63% of the applied potential difference E_2-E_1 (and capacitive current decreases by 63% as well). After 4RC, 98% charging is reached and thus the capacitor can be considered fully charged in the practical sense.

Initially, the capacitance can be determined by simply measuring the time required to reach a certain charging level, for instance 63%, or fitting the charge curve with the corresponding equation. However, due to the fact that in some cases the overall series resistance of the system R differs noticeably from the R_s, integration of the current value over time provides more precise way of measurement.

In the correction method, only the faradaic current C_f, measured at the end of integration (at potential E_2), is considered. The faradaic current, corresponding to the starting potential point E_1, is not taken into account. For accurate measurement, however, it is of utmost importance to guaranty that the faradaic current value does not change noticeably in the potential change region from E_1 to E_2. Ideally, the values of faradaic currents should be significantly lower compared with capacitive currents.

4.6. Experimental part

All chemicals, as well as 3 M KCl reference Ag/AgCl electrode BASMF2056, were purchased from Sigma Aldrich. Chemicals have been used without further purification. 3.18 mm thick, carbon cloth (CC) sheets and 0.6 mm thick platinum wire were supplied by Alfa Aesar.

4.6.1. Self-assembly reference electrodes

Although commercially available reference electrodes are recommended for use during the initial startup of the device, the Ag/AgCl DIY electrodes can be relatively easily prepared and used to further deepen the hands-on experience in the principles of electrochemistry. In addition, non-standard small-size electrodes required for some research purposes can also be successfully manufactured [7].

An Ag/AgCl reference electrode is essentially a silver wire covered by silver chloride and immersed into a solution with a stable chlorides concentration. Several similar procedures were proposed for the preparation of Ag/AgCl wire for electrodes [8,9,10] and all of them include 2 steps: i) cleaning the silver surface, often by short-time positive polarization and ii) formation of the AgCl layer on the silver surface, so we propose the modification of this procedure described below.

A glass Pasteur pipette was cut and a silver wire (0.25 mm in diameter) was placed in and fixed with a small piece of silicon rubber (see **Fig. 2**). Afterwards the electrode was wired to the potentiostat and polarized for 1 min at -2000 mV and 10 min at +1000 mV. During the positive polarization stage, the current was monotonously decreasing indicating the growth of the AgCl layer on the surface of the Ag wire. Finally, the electrode was filled with the 3 M solution of KCl containing 2% of agar-agar and left in the vertical position for 2 h for gelation of the liquid.

Testing of thus prepared electrodes versus a standard reference electrode typically gives values within the range of several mV. These electrodes can be used within a limited time (typically 2-3 weeks), after which the concentration of KCl decreases noticeably due to the diffusion and the reference potential becomes shifted.

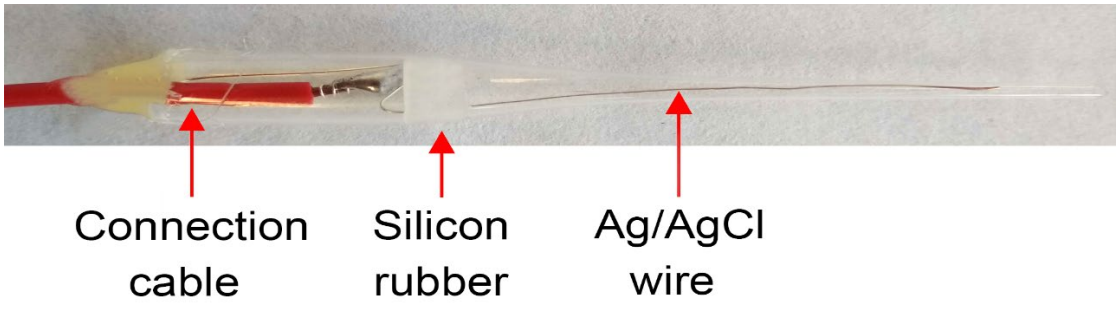

Fig. 2. The appearance of the DIY Ag /AgCl electrode

4.6.2. Resistor polarization test, voltammetry and chronoamperometry experiments

The potentiostat was initially tested with a dummy cell – a 20k resistor (the reference electrode short-circuited with the counter electrode, shunt resistor 10k). The obtained polarization curve is presented on the **Fig. 3**. The polarization curve is linear with the slope fairly fit with the resistor value. The reliability of the potentiostat for measuring of a real electrochemical system was first tested by recording a CV curve of Zobell solution: the mixture of potassium ferrocyanide (3.33 mM $K_4Fe(CN)_6$,), potassium ferricyanide (3.33 mM $K_3Fe(CN)_6$) and 0.1 M KCl [6]. 0.3 cm^2 Pt wire was used as working electrode, 0.8 cm^2 Pt wire as counter electrode. The comparison of CV curves, obtained with the proposed device and the high-end potentiostat Autolab PGSTAT204, respectively, is shown in the **Fig. 4**.

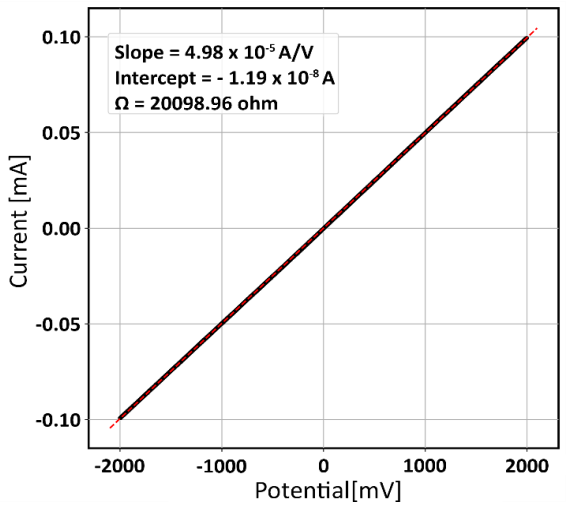

Fig. 3. Dummy cell test of the potentiostat

It can be easily noted that, albeit the curves obtained with the proposed potentiostat are noticeably noisier, the shape of the curves and the absolute values are in good correspondence.

Chronoamperomentry experiment preset was tested on the cell with 0.3 cm^2 Ti cathode and 0.8 cm^2 Pt wire anode immersed in 0.1N H_2SO_4. Cell currents were recorded at -200 mV, -300 mV and -400 mV vs Ag/AgCl for 120 s. The recorded graphs are presented in the **Fig. 5**.

Electrodes made of titanium and other so-called valve metals can be recommended for a practicum as an example of system with almost linear cathodic current versus potential response due to presence of highly resistive titanium oxide layer on the surface. A nearly-zero current in anodic mode on Ti can also be demonstrated to students. By contrast, on platinum cathodes, even small change of potential towards more negative typically result in drastic current increase and, consequently, require selection of a different shunt resistor in our potentiostat.

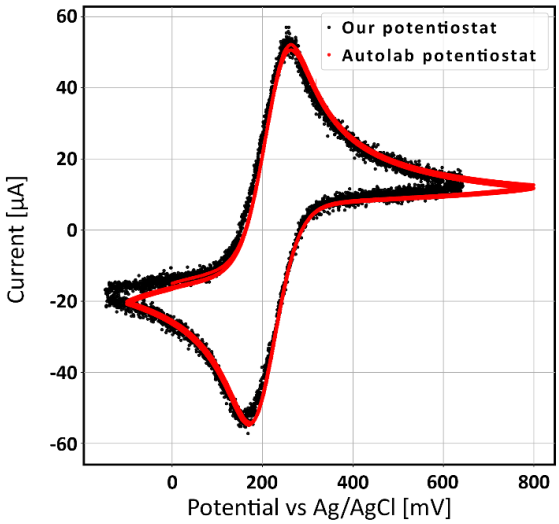

Fig. 4. CV curve in Zobell solution (black). The curve obtained with Autolab PGSTAT204 is shown for comparison (red)

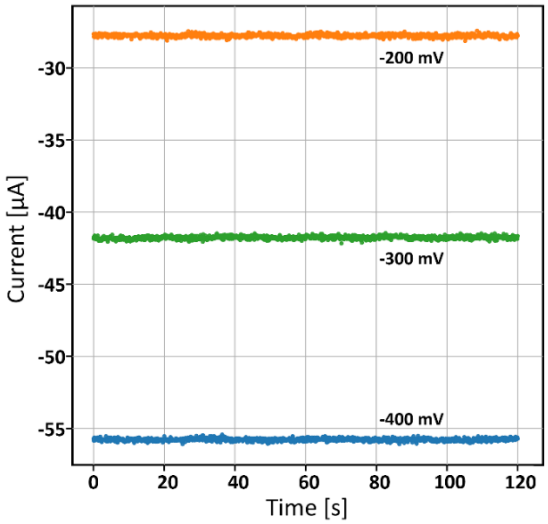

Fig.5. Chronoamperometry graph recorded with 0.1 N H_2SO_4 solution on Ti cathode at three different potentials versus Ag/AgCl.

4.6.3. Capacitance measurements

In the standard electrochemical practice, mF-range capacitances, typical for small scale carbon felt electrodes, are usually determined from LSW or CV scans accomplished at different scanning rates, galvanostatic charge-discharge method or by means of impedance spectroscopy [11]. Nevertheless, stable potential scanning with high capacitive loads requires the potential scanning speed to be perfectly uniform, while galvanostatic mode is difficult to conduct with low processor speed due to

necessity to organize the measurement of potentials and currents with extremely high sampling rate in order to manage highly stable regulation of current based on a digital feedback loop. Hence, both methods lay well beyond the digital capabilities of the proposed simple potentiostat design (although the given analog schematic allows such modification without any changes). By contrast, the impedance spectroscopy would require serious modifications of both digital and analog parts of the schematic.

The suggested measurement approach, based on integration of charge-discharge curves of a cell, connected in series with a current limiting resistor, is described in details in the section **5.2.** This approach allows overcoming the limitations within the basic Arduino 8-bit controller framework and measure capacitances in the range from hundreds µF to hundreds mF (with the appropriate selection of shunt resistor and series resistor) with a simple low-cost device.

To examine the basic viability of the capacitance measurement technique preset, the capacitance of a standard 940 µF aluminum electrolytic capacitor UKL0J102KPD was tested. The RE was short-circuited with the CE. 10 kΩ shunt resistor and 20 kΩ series resistor were used. The capacitor was kept at 0 mV for 60 s, then the potential stepped to 500 mV and the resulting current measured during 20 s. The same procedure was repeated with the Autolab potentiostat. The resulting curves and the fitting curve (according to Equation 2 in the SI, same coefficients for data obtained with our potentiostat and the Autolab values) are shown in **Fig. 6**. The measured capacitance, 906 µF, fits well within the ± 10% tolerance range of the capacitor.

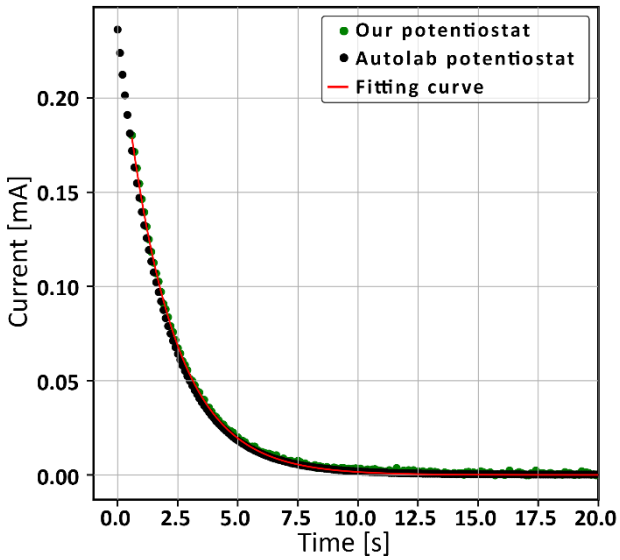

Fig. 6. Charging a capacitor through a 20 kΩ resistor

It is important to mention that for any standard electronic component capacitor, the own resistance is negligibly low. Hence, the R value appearing as the RC term in the equation for capacitor charging through a resistor, is known and is equal to 20 kΩ for the demonstrated case. Thus, the capacitance can easily be calculated without the need

for curve integration, just by fitting the curve through the corresponding equation or even (although with less precision) by measuring the time constant as time required for 63% current deterioration. The value calculated from the fitting curve provided oin Fig. 6 was exactly the same (906 μF) as the value obtained by the integration.

The situation, however, is complicated considerably when the capacitance of a real electrochemical system needs to be measured. Electric double layer capacitors are characterized by Equivalent Series Resistance (ESR) [11]. Typically, it is very low, lying in the range of mΩ to several Ω for supercapacitor electrodes. However, in some cases, for instance for electrodes coated with semiconducting layers or exhibiting pseudo-capacitive behavior, the ESR value can drastically alter the overall series resistance R in the RC term. Thus, although the RC term can easily be obtained by curve fitting, it does not allow calculating the capacitance in a general case. The integration approach, on the contrary, gives the actual charge received or lost by the system regardless of the speed of charge transfer and thus is not affected by the ESR value. For this reason, it was chosen as basis for the standard capacitance calculation method in the offered PC program.

Following the basic method validation on a standard capacitor, we successfully implemented the simple potentiostat design for measuring the capacitance of carbon cloth electrodes in 0.1 N Na_2SO_4 solution. The experimental setup was assembled in a classical way: a 50ml glass beaker equipped with stirring with immersed reference electrode and Pt spiral-wound from wire, corresponding to a geometric surface of 6 cm^2. Electrodes (3.18x3.18x50 mm) were cut out of the felt. Finally, 10 kΩ shunt resistor and 20 kΩ series resistor were used.

Preliminary CV scanning at very low speed (1 mV/s) shows flat (although quite noticeable) faradaic currents profile in the potential window from +200 mV to +700 mV vs Ag/AgCl, which was consequently chosen for the measurements. **Fig. 7** demonstrates the charging curves and the corresponding charge integral curves after faradaic current correction. With the intention to exhibit the applicability limitations, we have selected for demonstration the most complicated measurement case. The initial current (33 μA) exceeds the equilibrium faradaic current (26.7 μA) by 24% only, for which reason the data are quite noisy. However, even in this worst case, the capacitance value resulting from integration of data, obtained with our potentiostat, differs from the capacitance calculated from Autolab curve by only 4%. 134.3 μF and 139.9 μF capacitances, respectively, were obtained.

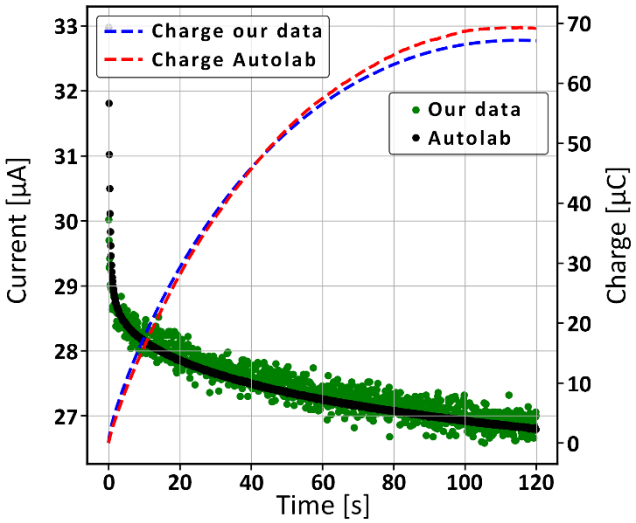

Fig. 7. Charging curves for a carbon felt electrode.

4.6.4. Effect of soldering on the performance of the device

Although the basic functionality of the proposed potentiostat can be built on the breadboard, soldering of the components on a solderable prototyping board undoubtedly increases the quality of data, drastically reducing the level of noise.

Figure Fig. 7 provides an example of a CV curve, obtained with a prototyping-board-based device on a platinum electrode in 0.1 N H_2SO_4. It can be noticed that the curve is smooth and the oxygen evolution peak is well resolved.

The Fig. 8 demonstrates a curve recorded during capacitance measurement of a large (10 cm^2) carbon felt electrode in 0.1 N Na_2SO_4, also using a soldered device. Nearly ideal charging curve can be observed.

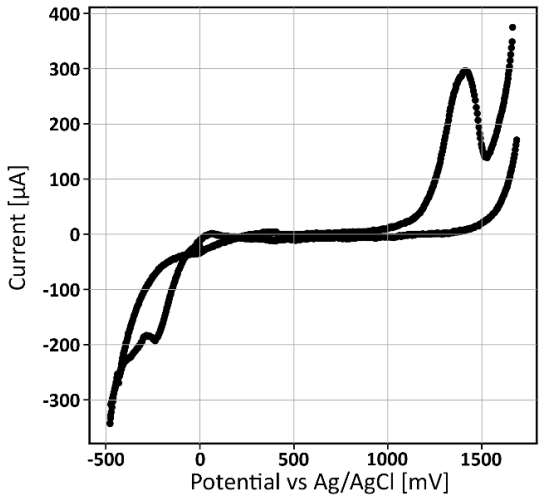

Fig. 7. CV curve on Pt electrodes. in 0.1 N H_2SO_4.

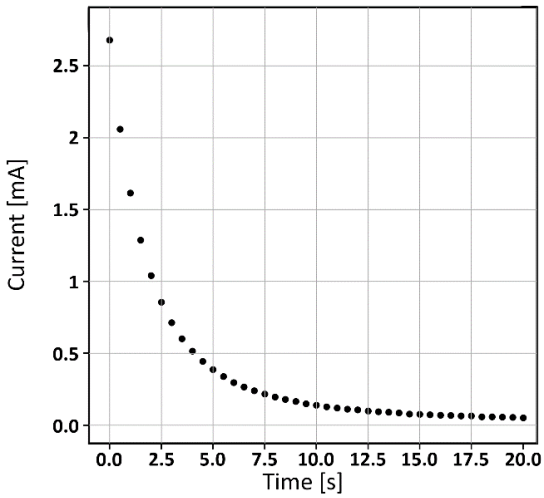

Fig. 8. Carbon felt electrode charging in 0.1 N Na_2SO_4.

4.7. Conclusions

A simple DIY potentiostat design has been proposed. It has been optimized for quick assembly by students without any special expertise in electronics.

It has been demonstrated that even in the simplest possible breadboard-based assembly, the device is capable of providing reasonable quality voltammetry and chronoamperometry data, well corresponding with the results obtained with the research class potentiostat used for comparison.

We also have shown that capacitance measurements, based on charging or discharging the capacitive cell through a serially connected resistor and integration of resulting curves, yield reliable values of capacitance. The minimum capacitance that can be measured with our device is in the range of 100 μF.

The device together with the proposed Arduino and PC software provides a convenient and efficient way to curry out electrochemical experiments in a student practicum or during demonstrations.

In addition, we share a method for quick fabrication of Ag/AgCl reference electrodes with gel KCl electrolyte that can be conveniently used with the proposed device and provide further immersion into hands-on chemistry.

4.8. GitHub repository links to the Arduino/PC software:

GitHub link to Arduino IDE and Python-based software for Windows/Linux:
https://github.com/ashavel/potentiostat

4.9. References for Chapter 4

1. Š. Kubínová, Jan Šlégr, 2015. ChemDuino: Adapting Arduino for Low-Cost Chemical Measurements in Lecture and Laboratory. Journal of Chemical Education 92, 1751–1753.

2. Grinias, J.P., Whitfield, J.T., Guetschow, E.D., Kennedy, R.T., 2016. An Inexpensive, Open-Source USB Arduino Data Acquisition Device for Chemical Instrumentation. J. Chem. Educ. 93, 1316–1319.

3. S. N. H. Umar et all. A Low Cost Potentiostat Device For Monitoring Aqueous Solution. MATEC Web Conf. Volume 217, 2018.

4. Li, Y., Melenbrink, E., Cordonier, G., Boggs, C., Khan, A., Kwembur, I.M., Nkhonjera, L., Bahati, D., Billinge, S., Haile, S., Kreuter, R., Crable, R., Mallouk, T., 2018. An Easily Fabricated Low-Cost Potentiostat Coupled with User-Friendly Software for Introducing

Students to Electrochemical Reactions and Electroanalytical Techniques. Journal of Chemical Education 95 (9), 1658-1661.

5. Meloni, G.N., 2016. Building a Microcontroller Based Potentiostat: A Inexpensive and Versatile Platform for Teaching Electrochemistry and Instrumentation. J. Chem. Educ. 93, 1320–1322.

6. Darrell Kirk Nordstrom. Thermochemical redox equilibria of ZoBell's solution. Geochimica et Cosmochimica Acta, Volume 41, Issue 12, 1977, 1835-1841.

7. East, G.A., del Valle, M.A., 2000. Easy-to-Make Ag/AgCl Reference Electrode. J. Chem. Educ. 77, 97.

8. Rootare, H.M., Powers, J.M., 1977. Preparation of Ag/AgCl electrodes. Journal of Biomedical Materials Research 11, 633–635.

9. Brewer, P.J., Leese, R.J., Brown, R.J.C., 2012. An improved approach for fabricating Ag/AgCl reference electrodes. Electrochimica Acta 71, 252–257.

10. Mohammed Shafeeq, K., Nair, S., Uma, Dr.G., Mukundan, Dr.T., 2019. Fabrication of Ag/AgCl electrode for detection of electric field in marine environment. IOP Conference Series: Materials Science and Engineering 561, 012054.

11. Vicentini R, Da Silva LM, Cecilio Junior EP, Alves TA, Nunes WG, Zanin H., 2019. How to Measure and Calculate Equivalent Series Resistance of Electric Double-Layer Capacitors. Molecules. 2019 Apr 12, 24(8), 1452.

4.10. Chapter 4 acknowledgements

The following third-party code/libraries have been used in the code of the Arduino IDE and PC programs:

https://github.com/adafruit/Adafruit_MCP4725 - the library for controlling the MCP4725 DAC.

https://gist.github.com/dwblair/97edd6b8bef565437f332d37db60f664 - code for parsing serial port messages.

UNIVERSITAT ROVIRA I VIRGILI
SEMI-AMORPHOUS CARBON NITRIDE FILMS DERIVED FROM SOLUBLE POLYMERIC PRECURSORS: TOWARDS MULTIFUNCTIONAL ELECTROCHEMICAL COATINGS WITH ENHANCED STABILITY
Oleg Dubov

Chapter 5

General conclusions and future work

The final chapter of this thesis presents a general overview of the main results, obtained in the course of the work, as well as the presentation of the most relevant general conclusions. The potential for the future research on the covered topics is also introduced.

5.1. General conclusions

A new class of ultra-nitrogen-rich polymers –linear imides of triazine and heterocyclic aminotriazole and aminotetrazole moieties– have been synthesized by means of condensation of cyanuric chloride with corresponding aminoheterocyclic precursors in the presence of DIPEA as strong non-nucleophilic base and then characterized. In addition, synthesis of polymeric product of 2-amino-4,6-dichloro-1,3,5-triazine self-condensation, azanediyl (2-chloro-1,3,5-triazine-4,6-diyl, has been achieved, also in the DIPEA presence. The last polymer can be viewed as partial structural analog of the first two products with triazinic amino-component.

All three polymers demonstrate excellent solubility in aprotic dipolar solvents in the form of corresponding salts with DIPEA. In contrast with previously developed nitrogen-rich polymeric precursors, new polymers exhibited decreased tendency of nitrogen loss during thermal decomposition, thus permitting the synthesis of carbon nitride films with nearly equal atomic content of carbon and nitrogen on various substrates by liquid coating methods followed by solvent drying and annealing.

Coatings obtained by this approach have been extensively characterized using elemental analysis, TGA, TEM, XRD, FTIR, STM, UV-Vis diffuse reflectance spectroscopy, contact angles measurement and potentiometric electrochemical methods. These analytical techniques allowed classifying the coatings as partially amorphous heptazinic carbon nitride, enriched with carbon. Structural similarity to vitreous carbon materials has been demonstrated.

Electrochemical characterization of the new coatings, performed by means of voltammetry and chronoamperometry in sulphuric acid solution, demonstrated outstanding long-term stability of materials in harsh anodic polarization conditions.

In the same time, low pyrolysis temperature, required for preparation of coatings, permitted to expect the viability of synthesis of composite materials, containing nanoparticles or molecular transition-metal-based precursors as structural/catalytic and catalytic components, respectively, with carbon nitride representing the oxidatively stable and mechanically robust coating matrix.

However, intrinsically non-porous nature of coatings obtained from organic solutions of precursors represented a problem from the point of view of synthesis of catalytically active materials, where developed surface is a prerequisite for efficient practical use.

To overcome this obstacle, a modified method for coating synthesis was developed. It was noticed that two azole-based precursor polymers possess remarkable solubility in aqueous ammonia, presumably in the form of corresponding ammonium salts. Then, pyrolysis of polymeric films, produced from aqueous solutions, resulted in formation of nanoporous carbon nitride coatings.

The catalytic coating concept has been verified using carbon nanoparticles as structural and micropore-forming component, and nickel nitrate as catalytic precursor. catalytically active Ni-loaded coatings have been obtained on the basis of poly(CYA-Cl-AMTAZ) precursor polymer on carbon cloth as electrode support and characterized by SEM and XPS spectroscopy.

Microscopy of the samples, although lacks resolution, allows assuming nanometer-sized intrinsic porosity. In samples with carbon nanoparticles filler content, nanoparticles-based secondary pores structure of the size of hundreds of nanometers has been observed. XPS results allow to classify catalytic centers of the materials as nitrogen-coordinated Ni, thus assuming deep interaction between the carbon nitride matrix and the metal.

Coated carbon cloth electrode exhibits outstanding catalytic activity in oxygen evolution reaction in alkaline media with overpotentials as low as 0.26 V and Tafel slope of 61.8 mV/dec –signaling the performance of the range, typical for catalytic efficacy of platinum-group metals and their oxides. The stability of coated electrodes was exceptional, with no degradation of oxygen evolution parameters after 1000 hours of electrolysis at 100 mA/cm^2.

Yet another result, obtained within the framework of the current thesis, is related to the assembly of easy and low-cost Arduino-based potentiostat device. Although initially proposed as a simple schematic for student practicum, the device in the soldered version demonstrated the ability to perform precise three-electrode potentiostatic measurements and was implemented for routine automated screening of carbon electrode properties. In addition, a simple and reliable approach to measurement of capacitances in purely potentiostatic mode has been demonstrated.

In electrochemical laboratory practice, the efficiency of massive screening of sample properties is often limited by the number of available high-end measurement units. In some applications, simple and cheap purpose-made potentiostat can serve as initial screening means, providing the quality of results, sufficient for pre-selection of efficient samples to be carefully studied on a research-grade potentiostat.

The precision and reproducibility, obtained with the proposed device, makes it suitable for industrial production of low-cost electrochemical measurement units based on the same schematic.

5.2. Future work

Previous studies have demonstrated the suppression of two-electron water oxidation with corresponding prevention of peroxide species and hydroxyl radical formation as intrinsic characteristic of carbon nitride matrices. Thus, the prolonged stability of the catalyst can presumably be related with this fact, although further studies are required in

order to elucidate the specific mechanisms governing catalytic activity and stability of new materials.

One more important topic of future research is related to fabrication of composite coatings comprising novel carbon nitride materials as binder for catalytic nanoparticles, composed of precious metals as well as transition metals phosphides, nitrides, oxides and still others. Composite coatings materials can combine the easiness of fabrication and high stability, typical for novel carbon nitrides, with high active surface and specific catalytic activity of nanoparticles.

Another important research field, not approached in the present thesis, is related to the possibility to control the mechanical properties and porosity of annealed carbon nitride films by means of alternating polymeric precursors, solvents and counter-cations in the precursor polymer solution. The present work demonstrates the formation of smooth non-porous flexible films when DIPEA salts of precursor polymers in DMAc are used; nanoporous sponge-like materials are formed in case of implementing ammonium salts of poly (CYA-Cl-AMTAZ) in water solutions. It remains apparent, however, that various other combinations of mechanical properties and porosity can be achieved. In this sense, the implementation of poly(CYA-Cl-AMCARTRIA) precursor with transition metals salts can be expected to result in interesting effects due to possible participation of –COOH groups in coordination interactions with MOF-like structures formation.

On the other hand, interesting results can be expected in application of new materials to the fabrication of micromechanical devices (MEMS). At present, vitreous carbon is extensively used to this end. Most typically, a corresponding MEMS part (e.g., microelectrode, mechanical actuator) is produced from a corresponding polymer resin and carbonized in order to achieve transformation to glassy carbon. Intensive shrinking and deformation of material in the course of carbonization represents a significant drawback, requiring careful pre-calculation of initial polymeric component proportions and impeding direct fabrication of mechanically precise microstructures.

Implementation of semi-amorphous carbon nitride as source material for MEMS component can result in a drastic modification of the fabrication approach. Carbon nitride materials are well-known to decompose when heated above 700 ºC. In particular, full decomposition below 670 ºC has been demonstrated for the new carbon nitride films obtained in this work. It is important to mention that pyrolytic decomposition does not affect the structure or composition of the material and thus can be compared to some extent with sublimation (although irreversible). This opens up a way to production of micro-sized components by direct ablation of pre-pyrolysed material with a UV laser. Widely available and cheap near-UV lasers (for instance, 405 nm laser diodes) of relatively low power (several watts) could be used for cutting carbon nitride layers with production of precisely shaped MEMS components.